The Synthesis, Characterisation and Functional Testing of Metal Oxide Thin Films

A thesis presented to University College London in partial fulfilment for the requirements of the Degree of Doctor of Philosophy

Alison Jennifer Cross

Supervised by Professor Ivan P. Parkin

Declaration

I, Alison Jennifer Cross, confirm that the work presented in this thesis is my own. Where information has been derived from other sources, I confirm that this has been indicated in the thesis.

Signed:

Acknowledgements

I must first acknowledge the work of others that is presented in this thesis. Chapter Two includes results of experiments carried out by Niall Logan at the Eastman Dental Institute under the supervision of Dr. Peter Brett and Dr. Laurent Bozec. The CoCrMo alloy substrates were kindly supplied by Corin Ltd and the work was supported by colleagues there, Simon N. Collins and Alison Traynor. I would also like to thank Niall for sharing his knowledge of stem cell research with me and for an enjoyable and productive collaboration. Thanks to Dr Sofia Elouali and Professor Andrew Mills for their help with NO_x testing.

Secondly, I would like to thank my supervisor Professor Ivan Parkin for giving me this opportunity and supporting me in my endeavours in and beyond the lab. Your encouragement, guidance and reassurance throughout my time at UCL has made my PhD an enjoyable and rewarding process. I would also like to thank my second supervisor, Professor Jawwad Darr, for his support throughout.

I have been lucky enough to have received the help of so many post-docs and members of staff at UCL who have always been generous with their time and patient enough to put up with my questions. In no particular order, my thanks go to Dr Steve Firth for help with Raman and SEM, Mr Kevin Reeves also for help with SEM, Dr Rob Palgrave for help with XPS and solid state chemistry, Mr Martin Vickers for help with XRD and Dr Russell Binions and Dr Chris Blackman for explaining to me all manner of CVD related queries. On a daily basis I have received invaluable help and advice from Dr Raul Quesada-Cabrera, Dr Andreas Kafizas, Dr Nathan Hollingsworth, Dr Caroline Knapp, Dr Kristopher Page and Dr Charlie Dunnill. I would also like to thank the many members of the Parkin, Carmalt and Hogarth groups at UCL, past and present for their friendship in the last three years.

Finally, my parents and grandparents have always provided unconditional love and support and been a source of inspiration to me throughout my life, thank you.

Table of Contents

Table of Figures

List of Abbreviations

AACVD – aerosol assisted chemical vapour deposition

Acac – acetylacetonate

ALD – atomic layer deposition

APCVD – atmospheric pressure chemical vapour deposition

aq – aqueous

BLB – black light blue

CoCrMo – cobalt chromium molybdenum alloy

CB – conduction band

CTA – conventional thermal annealing

CVD – chemical vapour deposition

DC – direct current

DCA – dichloroacetic acid

ddH_2O – doubly distilled water

DFT – density functional theory

DI - deionised

DOS – density of states

dp – decimal place

DRAM – dynamic random access memory

DSSC – dye-sensitised solar cell

ECM – extra cellular matrix

FEG – field emission gun

GIXRD – grazing incidence x-ray diffraction

GADDS – general area detector diffraction system

IR – infra-red

IPA – isopropyl alcohol

ISO – international organisation for standarisation

LPCVD – low pressure chemical vapour deposition

MO – molecular orbital

MOCVD – metal organic chemical vapour deposition

(h)MSC – (human) mesenchymal stem cells

MRSA - methicillin resistant staphylococcus aureus

PACVD – plasmon assisted chemical vapour deposition

PECVD – plasma enhanced chemical vapour deposition

PEG – polyethylene glycol

PSH – photoinduced superhydrophilicity

PV – photovoltaic

ReRAM – resistive switching random access memory

Rf – resorufin

RTA – rapid thermal annealing

Rz – resazurin

SEM – scanning electron microscopy

SHE – standard hydrogen electrode

TALH – titanium bis(ammonium lactate) dihydroxide

TAS – transient absorption spectroscopy

TTB – titanium tetrabutoxide

TTIP – titanium tetraisopropoxide

UV – ultra-violet

VB – valence band

XRD – X-ray diffraction

XPS – X-ray photoelectron spectroscopy

Abstract

This thesis is concerned with the deposition of titanium dioxide thin films using chemical vapour deposition (CVD). The work emphasises the influence of deposition parameters on the properties of the resultant film. The materials have been designed with a wide range of potential applications in mind, from air and water purification to energy production and medical implant devices. Where possible, tests have been conducted to assess the efficacy of the material for these applications.

The first chapter highlights a number of technologically important applications of titanium dioxide in order to demonstrate the motivation for research in this area. Some theoretical concepts are presented which are fundamental to understanding the behaviour of titanium dioxide. The principles behind chemical vapour deposition and the photocatalytic tests used in this work are discussed.

The second chapter focusses on the use of three different metal substrates in TiO_2 CVD. Firstly, the phase of TiO_2 deposited on steel substrates was investigated. It was shown that the grade of steel had little influence with predominantly anatase films being formed in the vast majority of areas analysed. Since each grade of steel has different mechanical properties and is used in different applications, this work demonstrates that the photocatalytic properties of anatase films can be endowed to a large range of products. Secondly, TiO_2 was shown to be adherent to a flexible substrate, namely aluminium foil. It was demonstrated from XPS analysis that aluminium ions did not diffuse into the TiO_2, which remained photocatalytically active. A photocatalyst on a lightweight, flexible substrate offers several advantages over glass which has been the most frequently employed substrate to date. Thirdly, titanium dioxide was coated onto an alloy of cobalt, chromium and molybdenum, CoCrMo. The alloy is of interest for biomedical implants but suffers from poor biocompatability. By coating its surface with TiO_2, it was shown to enhance osteogenic differentiation.

Chapter three investigates nitrogen doped titanium dioxide for its potential as a visible light photocatalyst. A novel synthetic strategy was employed in which the amount of oxygen precursor was varied to determine if this would affect the position of the nitrogen in the titanium dioxide crystal structure. Differences were observed in the nitrogen XPS signal, the absorption profile, surface morphology and photocatalytic activity under both UV and visible irradiation. Visible light activity was observed for a sample made with lower amounts of oxygen precursor under UV and visible light.

Finally, brookite, a rare, metastable form of titanium dioxide, was formed by atmospheric pressure chemical vapour deposition, APCVD. A brief literature review discusses the potential applications and some of the previously employed synthetic routes to brookite formation. Three sets of conditions are reported for the first known synthesis of brookite by atmospheric pressure chemical vapour deposition. A possible mechanism for brookite formation is hypothesised.

This work concludes with a summary of the key findings from the experimental work and possible avenues for further research.

CHAPTER ONE

INTRODUCTION

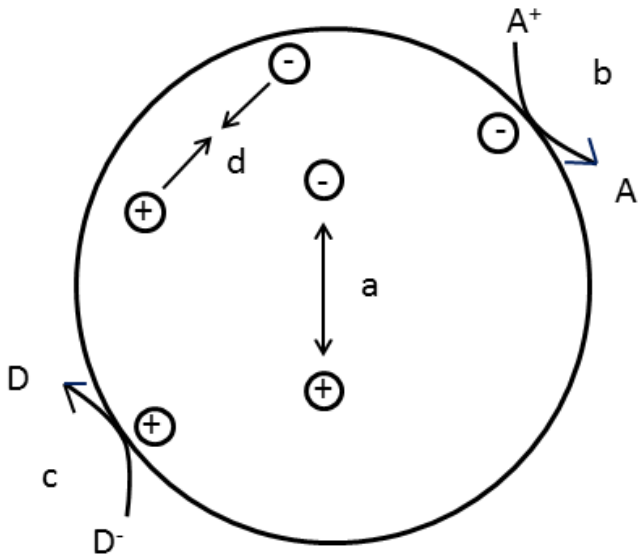

Chapter 1: Introduction

Abstract

This chapter outlines the fundamental reason for the scientific and technological interest in titanium dioxide by discussing the current and potential future uses of the material. Background to some of the basic theoretical concepts surrounding semiconductors and photocatalysis that must be understood by the laboratory chemist are explained. Chemical vapour deposition (CVD) is the synthetic method employed throughout this work and thus an introduction to this technique is given. The underpinning mechanism of three photocatalytic tests that were used is explained.

1.1 Applications and properties of TiO_2

Titanium dioxide, TiO_2, is one of the most common and intensively investigated semiconductor materials. It has been used since the beginning of the 20^{th} century in a powdered form as a pigment. The high refractive index of visible light by TiO_2 particles gives a brilliant white, opaque colour. This property is used in a wide variety of applications in which a white colour is desirable, from paints, cosmetics, milk and other food products, toothpaste and even in cigarettes to give white coloured ash. TiO_2 is biologically inert and is therefore safe to use in food and drug applications.

Whilst reflecting visible light, higher energy UV light is absorbed by TiO_2. This gives rise to another extremely useful application as a sun screen. TiO_2 particles in skin creams can absorb the damaging UV sunlight to protect skin.[1]

Due to the high dielectric constant of TiO_2, it has been investigated for its use as a transistor gate dielectric for integrated circuitry as a possible alternative to SiO_2.[2] Thin films can be used as media for electronic data storage. The high dielectric constant makes it suitable as a capacitor dielectric layer in dynamic random access memory (DRAM) and resistive switching RAM (ReRAM). DRAM is still used as the main memory in every computer and tablet device.[3]

The conductivity of titania thin films can be altered by the presence of certain gases. This can be exploited in gas sensors. When a gas, such as ethanol, binds to the surface of titania, electrons are injected into the crystal lattice resulting in an increase of conductivity.[4] This response is detectable in the range required for alcohol breath analysers.[5]

These applications rely on the physical properties and whilst use as a pigment and whitener accounts for over 4 million tonnes of TiO_2 annually, it is by exploiting the photocatalytic properties where TiO_2 appears to have the greatest potential. Interest in the photocatalytic applications of TiO_2 has expanded greatly in recent decades. Research efforts have sought to use TiO_2 to address some of the most

pressing environmental and societal concerns such as sustainable energy and pollution control.

In 1972, Fujishima and Honda demonstrated the ability of TiO_2 to split water into hydrogen and oxygen.[6] Hydrogen is seen by many as a possible future fuel, as an alternative to fossil fuels, being both renewable and clean to burn.

Another strategy for using TiO_2 to harness solar energy is the dye-sensitised solar cell (DSSC) pioneered by Grätzel.[7] In this method a film of immobilised titania particles are used as a photoanode in a circuit to produce an electrical current directly.

The reduction of carbon dioxide, CO_2, could potentially provide a feedstock of carbon based small molecules and/or fuels and simultaneously utilise a currently problematic waste product from burning of fossil fuels. TiO_2 photocatalysis has been shown to produce formaldehyde and methanol from CO_2 bubbled through water.[8]

One of the major harmful emissions products of vehicles is nitrogen dioxide, NO_2, which can lead to acid rain. It has been shown that TiO_2 under UV illumination can break down nitrogen dioxide into less harmful by-products. This topic is discussed further in section 1.5.3.

Many organic molecules have been shown to be destroyed by TiO_2 through photocatalysis. Some of these molecules are waste products from industrial processes whilst others can be present in a number of environments such as oils and fatty acids. Liquids, semi-solids and solids have been demonstrated to degrade by the photocatalytic action of TiO_2, however there is a trend observed that only small molecule weight molecules (e.g. glycerol trioleate and octadecane) will be completely removed and photomineralised to CO_2, whereas solids such as stearic acid and polyethylene glycol (PEG) will only be partially removed and that smaller molecules may be formed from their degradation.[9] Fortunately, TiO_2 is stable in various media and hence can be used for both air and water purification.

Thin films of TiO_2 have been of interest for self-cleaning windscreens on vehicles for many years.[10] With a thickness of around 60 nm on glass, TiO_2 films have

been shown to be sufficiently transparent (particles must be less than 30 nm to prevent scattering of visible light), resistant to abrasion and have the ability to breakdown organic contaminants which reduces the cleaning requirements and improves visibility for drivers of vehicles. Water which comes into contact with irradiated titania forms sheets of water on the surface rather than droplets (see discussion on superhydrophilicity in 1.2 section.[11] This combination of properties is also useful for applications in outdoor tiles and paints. It has also been shown that titania on glass gives anti-fogging properties which can be utilised in car windscreens and mirrors and also on lenses in glasses, in particular those used in safety goggles for sport such as skiing and scuba diving where fogging of the lens is a particular problem.[12]

Furthermore TiO_2 is capable of destroying bacteria[13] and viruses[14], fungi[15] and potentially even so-called super bugs such as MRSA (methicillin resistant staphylococcus aureus).[16] Photocatalytic disinfection has the advantage of being a low cost sterilisation method and avoids the use of antibiotics, to which bacteria can develop resistance, or chemical disinfectants which can be toxic.

Titania particles have been investigated for their ability to kill cancerous cells.[17] Irradiation of particles in tumours in mice showed that no viable cells were found after 10 minutes irradiation. This was not observed when only particles with no irradiation were used or when the cells were irradiated in the absence of the titania particles. The authors noted the difficultly in access of irradiation to tumours within the body but highlighted the potential for application in cancers of the skin, oral cavity, trachea and bladder.

Whilst titanium dioxide has many advantageous properties, it does also have limitations. The barrier to commercialisation of many products is the inability of TiO_2 to efficiently use sunlight to drive reactions due to the non-absorption of visible light. The reliance on the presence of UV light can make photocatalytic reactions infeasible in some environments where the use of a UV light could be damaging to skin and eyes, e.g. for the sterilisation of surfaces in hospitals. This problem is discussed further in Chapter three. Another major drawback, from the perspective of self-cleaning windows, is the inability to breakdown inorganic

materials such as NaCl. This is a particular problem in coastal areas. In this scenario, the superhydrophilicity of titania surface, in fact worsens the build-up of salt deposits since the sheeting effect means that water dries more quickly and is not able wash away the inorganic material.

These examples of the current and potential uses of TiO_2 are intended to give the reader an appreciation of the breadth of applications in order to demonstrate the motivation for greater understanding of the synthesis and properties of titania. However reviews are available in the literature with a more thorough discussion of the state of the art. The following section describes in greater detail how the physical and chemical properties of TiO_2 are exploited to these ends.

1.2 Band structure and photoreactivity of TiO_2

In order to fully understand the principle of "photocatalysis", it is necessary to first understand the basics of band theory. A solid containing many atoms is described as having 'energy bands'. Molecular orbital (MO) theory used to describe bonding in molecules can be extended to solids. In the solid state, every atom in the structure contributes an individual orbital, all of which have such a small separation in energy it can be considered as a continuous band of energy levels.[18] Figure 1 shows the separation of molecular orbitals decreases with an increasing number of atoms to the extent that an infinite number of atoms produces a band with molecular orbitals with an infinitesimally small energy gap between them.

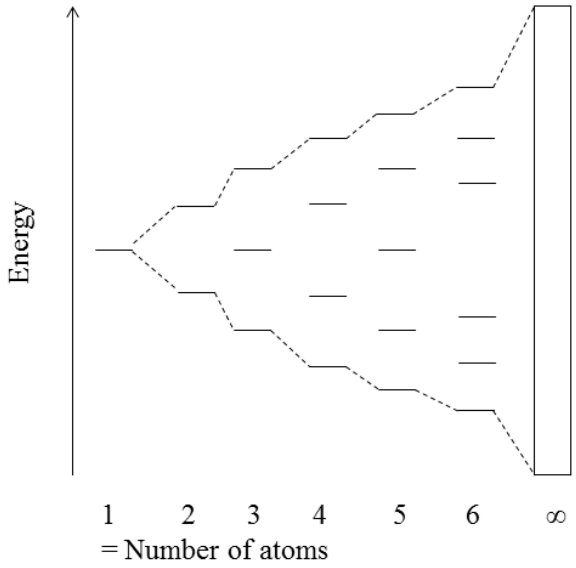

Figure 1 Formation of an energy band from many atoms. Adapted from reference [19].

A band such as that depicted in Figure 1 can be formed by the interaction of *s*, *p* or *d* orbitals. When more than one band is present, for example an *s* and a *p* band, they may be close in energy and overlap or be separated by an energy region for which no molecular orbitals exist.[20] This is termed as a band gap. When considering metals and semiconductors, the higher energy band is known as the conduction band, (CB) and lower energy band is the valence band, (VB).

Titanium dioxide has a band gap of an intermediate size and thus is classed as a semiconducting material. This means that conductivity can be induced by promoting electrons from the filled valance band to the partially filled conduction band. In order to achieve this, energy must be supplied to the electrons that is equal to or greater than the band gap energy. This energy could be supplied in the form of heat or light. Titanium dioxide is an intrinsic n-type semiconductor. As in the case with several other high oxidation state *d*-metal oxides, TiO_2 will often have a slight deviation in its stoichiometry due to a small deficit of oxygen atoms. The electrons which would have been localised on the lattice oxygen atoms form a donor band slightly below the conduction band.[21] The term “n-type” is used to denote that the predominant charge carriers are negative, i.e. electrons.

Photocatalysis either makes use of electrons in the conduction band of TiO_2 that have been promoted by light or the positively charged hole that remains in the valence band subsequent to electron promotion. These electrons and holes can be harnessed to take part in useful chemical reactions. This can only take place when holes are sufficiently oxidative and the electrons sufficiently reductive in relation to the redox potentials of the reaction in question. For example, the water splitting reaction can be considered as two separate reactions which involve the holes and electrons. The reduction of water to hydrogen has a standard potential of 0 V (Equation 1) and the water oxidation has an standard potential of +1.23 eV (Equation 2).[22]

$$2H^+ + 2e^- \rightarrow H_2 \quad (0\ V)$$

Equation 1

$$O_2 + 4H^+ + 4e^- \rightarrow 2H_2O \ (+1.23\ V)$$

Equation 2

Figure 2 illustrates how the electron and holes in photoexcited TiO_2 provide sufficient energy for the water splitting reaction.[23]

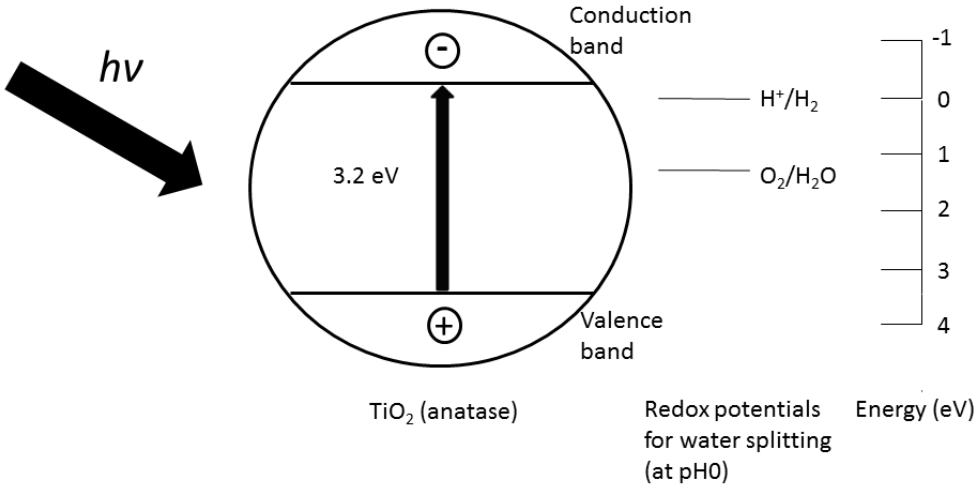

Figure 2 Potentials of electrons and holes in photoexcited TiO_2 and water splitting.

From Figure 2 it can be seen that the electrons of the photoexcited titania (anatase) particle are sufficiently reducing relative to proton reduction i.e. the bottom of the conduction band lies above the reduction potential for hydrogen. Indeed the holes are sufficiently oxidising for water oxidation to occur leading to overall water splitting.

Another photoinduced phenomenon was reported by Wang et al. in 1997.[24] A review by O'Carp et al. explains this phenomenon of photoinduced superhydrophilicity (PSH) as occuring when photogenerated electrons reduce Ti(IV) to Ti(III) which can then act as a hole trapping site.[25] These holes then serve to weaken the Ti-O bonds resulting in liberation of oxygen, creating oxygen vacancies. The oxygen vacancies are able to dissociate water upon adsorption to the titania giving hydroxyl anions on the surface. The increased hydrogen bonding interaction between the surface and water lead to enhanced wettability. The effect is reversible, the titania surface will become more hydrophobic if left in the dark for several days, due to re-oxidation by air. Water on a superhydrophilic surface spreads across it, forming a sheet rather than individual droplets. This assists in removing dirt from the surface of TiO_2 and hence is advantageous to self-cleaning applications and is complimentary to the degradation of organic contaminants by the oxidising holes.[11]

In photoexcited TiO_2, not all of the electrons and holes that are generated upon irradiation are available to be used in reactions. Recombination of the electrons and holes can compete with oxidative and reductive processes and reduce the efficiency of these photocatalytic reactions. Photoconductivity measurements of TiO_2 have been explained by the competing rates of photogeneration of electrons, trapping and scavenging.[26]

Figure 3 illustrates the possible pathways of photogenerated electrons and holes after irradiation.

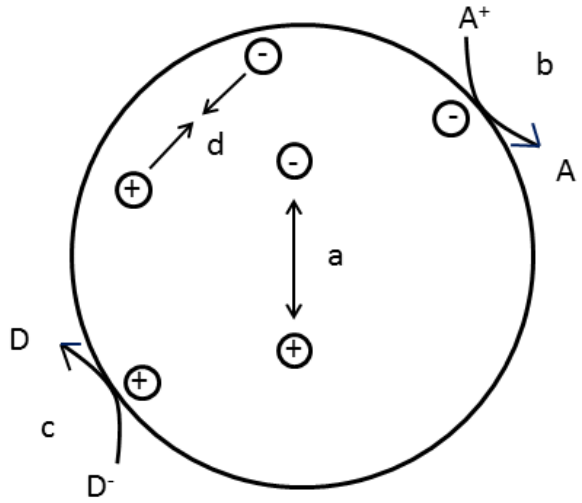

Figure 3 Electron and hole pathways within a particle, adapted from reference [27].

After the photoexcitation, (a), the electrons may reduce an electron acceptor A (b), the holes may oxidise an electron donor D (c) or alternatively the electrons and holes may recombine, (d).

One of the key aims of semiconductor photocatalyst synthesis is to produce materials with minimal electron-hole recombination and maximum conductivity. There are many factors which affect recombination and conductivity such as structural defects including grain boundaries and impurities (dopants), crystallite size[28], crystallinity and crystal structure. An understanding of how synthetic conditions affect these properties is crucial for engineering highly active photocatalysts.

1.3 Polymorphs of Titania

Titanium dioxide has three crystalline phases which occur in nature. They are rutile, anatase and brookite. They differ from each other in the arrangement of atoms in space. The structure of the atoms in the unit cell for each polymorph is shown in Figure 4.

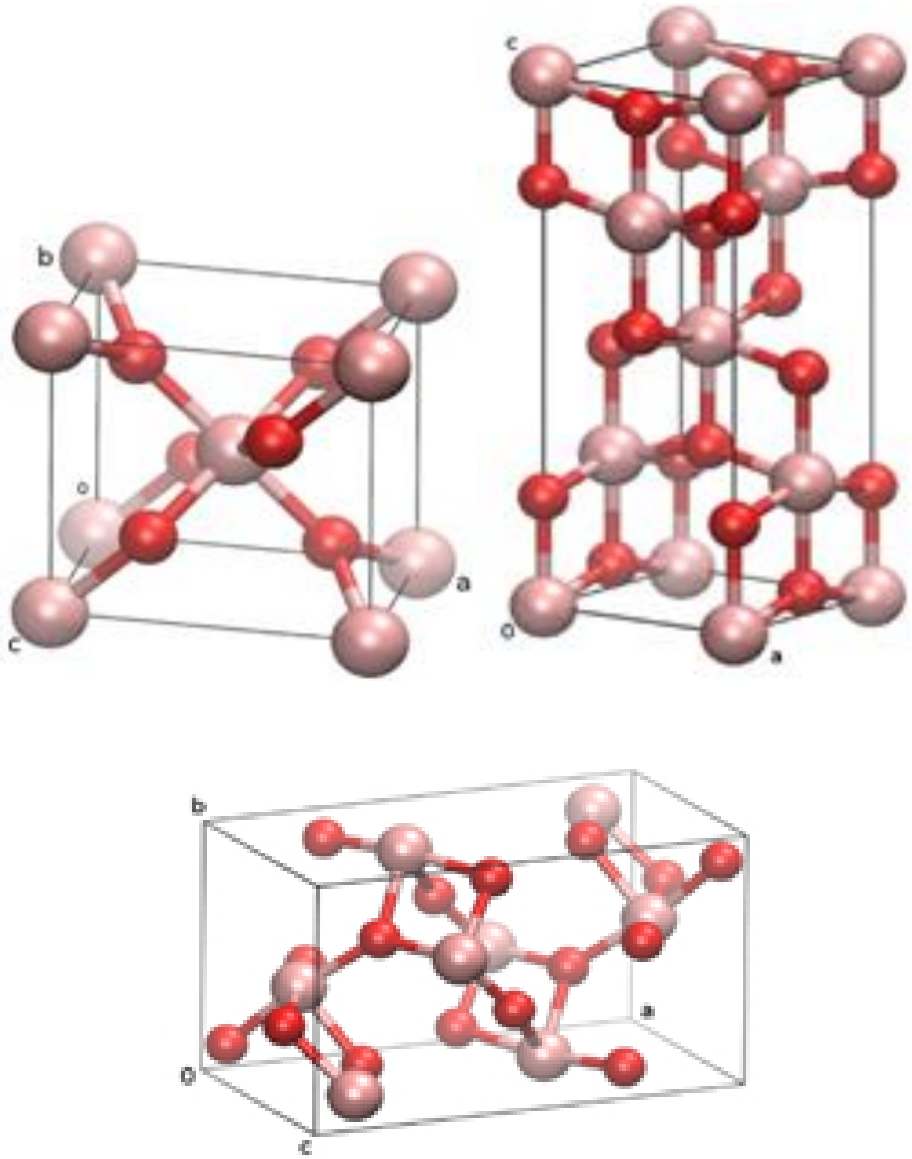

Figure 4 Unit cell diagrams of rutile (top left), anatase (top right) and brookite (bottom). Titanium atoms are shown in pink and oxygen atoms are shown in red. Reproduced, with permission from reference [29].

As can be seen in Figure 4, rutile and anatase both have a tetragonal unit cell (cell lengths a = b ≠ c and cell angles α = β = γ = 90 °). Brookite is orthorhombic (cell lengths a ≠ b ≠ c and cell angles α = β = γ = 90 °). The unit cell parameters for rutile a = 4.49 Å and c = 2.96 Å. For anatase a = 3.79 Å and c = 9.51 Å.[30] Brookite has the largest unit cell with parameters a = 9.18 Å b = 5.44 Å and c = 5.15Å.[31]

The crystal phase affects the properties and reactivity in a number of ways. Each polymorph has a slightly different band gap. The band gaps have been determined to be 3.03 eV, 3.14 eV and 3.24 eV for rutile, brookite and anatase respectively.[32] The position of the valence band has been reported to be insensitive to the crystal structure whereas the flat band potential does differ. The flat band potentials have been reported as -0.12 V, -0.03 V and 0.06 V for anatase, brookite and rutile respectively.[32] This has consequences for the type of reactions which each polymorph may participate in. Unlike anatase and brookite, the rutile conduction band electrons lie below the reduction potential for hydrogen and therefore cannot be used in the reaction without the addition of a co-catalyst.[33] More recent publications, however, have challenged some of these findings, such as the report by Chen et al. who have determined the band gap of brookite to be 3.3 eV with a more negative conduction band potential than anatase.[34] Electron mobility is higher in anatase, which is why it is typically used in photocatalytic applications rather than rutile.[35]

Brookite is by far the least studied of the three phases, largely due to the difficulty in synthesising a pure phase material. It is also very difficult to obtain powdered brookite commercially which would significantly impact the number of researchers who are able to study brookite, given that they must have, or collaborate with, a synthetic laboratory. However, some investigations have suggested brookite is a more active photocatalyst than anatase although it is often difficult to separate the differences caused by particle size, morphology and surface area. A great deal more research is required into brookite to fully understand its properties. A search on Web of Knowledge in February 2014 revealed the stark contrast between research output relating to anatase and brookite. The number of results returned per year from key word searches of "brookite TiO_2" and "anatase TiO_2" are shown in Figure 5.

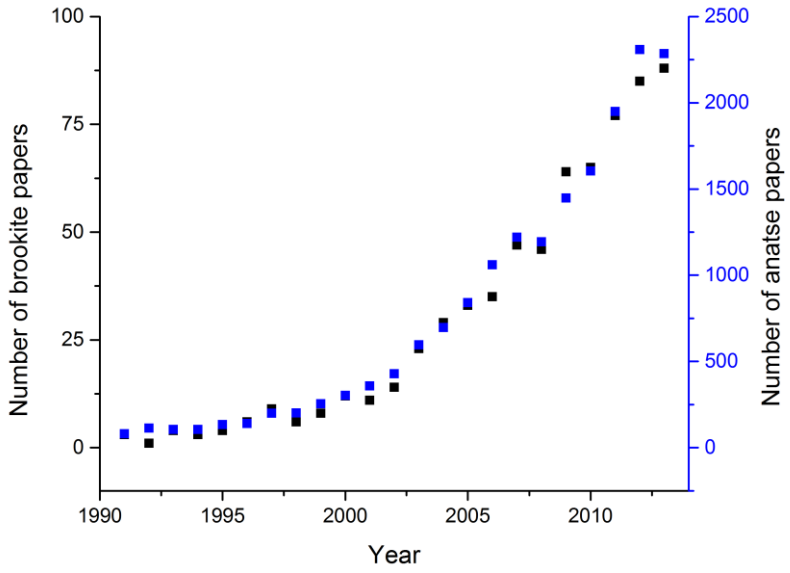

Figure 5 Number of papers published relating to anatase and brookite.

From Figure 5, it is clear to see that there is growing interest in both anatase and brookite, however the number of papers published relating to anatase is over an order of magnitude higher than the number relating to brookite. In fact over three times more papers relating to anatase were published in 2013 alone than have ever been published on brookite. Further discussion on the properties and application of brookite is given in Chapter 4.

The differences in properties of the titania polymorphs means that an understanding of how synthetic parameters influence phase formation is of critical importance.

1.4 Principles of Chemical Vapour Deposition

There are numerous ways to synthesise titanium dioxide. It can be formed as a single crystal, powder, colloidal solution or thin film. There are extensive reports in the literature regarding synthesis of nanoparticles, however this section

concentrates on the fabrication of thin films. For many industrial applications, films are advantageous as there is no need for separation of the titania from the products, which can be particularly challenging in the case of nanoparticles. Powder dispersions in liquids usually require stirring which could limit applications in the field. Furthermore, thin film coatings onto existing products can introduce a new functionality such as photocatalytic films in architectural glazing. The major limitation of films versus powders is the greatly decreased surface area leading to lower activities. From this, arises the challenge to maximise the photocatalytic activity to overcome the problem of limited surface area.

Thin films can be made by sol-gel,[36] spin coating,[37] sputtering,[38] CVD,[39] ALD[40] and spray pyrolysis.[41] CVD synthesis is typically favoured in industry since it can be incorporated into continuous, high throughput methods currently used commercially, such as the production of float glass. Thus, any useful products to come from research using a laboratory CVD reactor can be more easily scaled to mass production. Sol-gel and spin coating, however, are batch processes which are not so scalable and usually result in a significant amount of wastage of reactants. CVD is a one-step process in which a crystalline film is produced directly without the need for a secondary annealing which is costly and time consuming. However, CVD does require specialist equipment which is not available to many researchers. Not all, but many processes, require either high temperature (several hundreds of degree Celsius) and/or vacuum equipment to provide a low pressure environment. Both of these conditions add extra cost to the manufacturing process and usually extra time to reach the desired conditions.

CVD is suitable for coating a large variety of substrates, which allows the properties of TiO_2 to be conferred to a range of products suitable for different applications. Examples included crystalline[42] and amorphous silica,[43] metals (nickel,[44] stainless steel[45]), ceramic[46] and carbon nanotubes.[47] The major limitation is the (usually) high temperature required which means coating polymers and plastics is challenging. The effect of metal substrates on the properties of titania films is discussed in more detail in Chapter two.

The basic concept of CVD involves passing gaseous precursors over a heated substrate, adsorption of the precursor molecules to the substrate surface, diffusion to a reaction site and either decomposition or reaction with another precursor. The gaseous by-products are removed from the reactor through an exhaust by the flow of an inert carrier gas. These steps are shown in Figure 6.

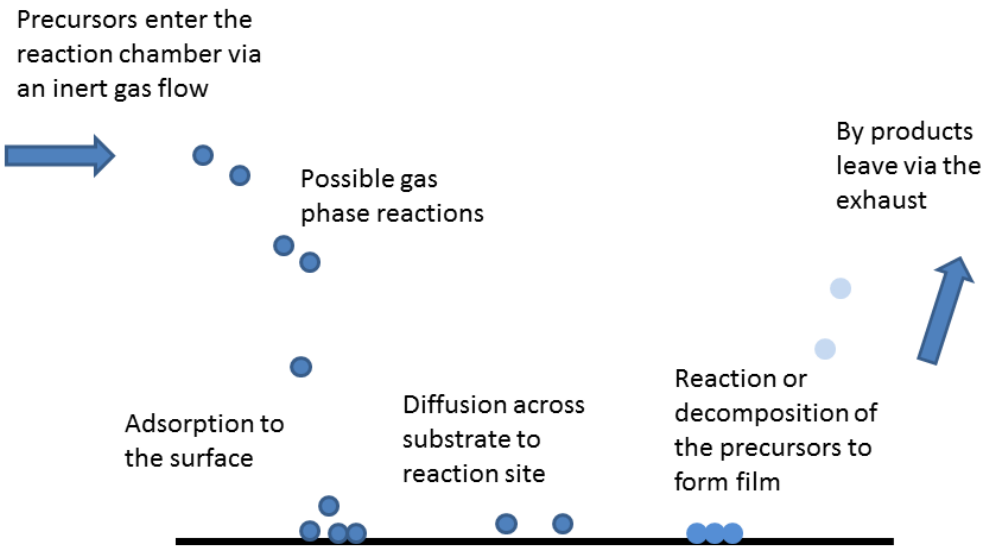

Figure 6 Basic steps in CVD process.

An ideal CVD precursor should be volatile, non-toxic, cheap, commercially available, easy to store and handle and have a clean decomposition pathway which results in high purity films.

There are many different precursors which have been used to deposit titanium dioxide. These include titanium chlorides, alkoxides, nitrates, keto-esters, amides, malonates as well as various combinations of these ligands around one metal centre.[48] Throughout this work, titanium tetrachloride ($TiCl_4$) and ethyl acetate ($CH_3COOCH_2CH_3$) are used as the titanium and oxygen source respectively. They meet all of these requirements except that $TiCl_4$ decomposes upon exposure to air and releases corrosive HCl fumes. However, this can be avoided by taking simple precautions such as transferring the liquid with a gas-tight syringe. $TiCl_4$ with ethyl acetate gives well adhered films with excellent optical properties. Ethyl

acetate, methanol, ethanol, isopropanol and water have all been investigated as an oxygen source for use with $TiCl_4$.[43, 49] It was found that the use of water gave hazy films, most likely due to excess gas phase reaction resulting in large particulates in the film.

There are many variations of CVD, AACVD aerosol assisted[50], LPCVD low pressure[51], MOCVD metal organic,[52] PACVD plasmon assisted,[53] and PECVD plasma enhanced chemical vapour deposition[54] to name but a few, all of which have successfully deposited titanium dioxide thin films. Each of these has their own advantages and disadvantages and are selected depending on the desired properties of the film, the properties of the precursors as well as time and cost considerations. AACVD, for example, allows the use of non-volatile precursors and inclusion of nanoparticles within a film.[55]

APCVD has the advantage of not requiring expensive high vacuum equipment and can be operated on a production line rather than batch production where a chamber would need to be evacuated. Other variations include hot wall reactors and vertical flow reactors.[56]

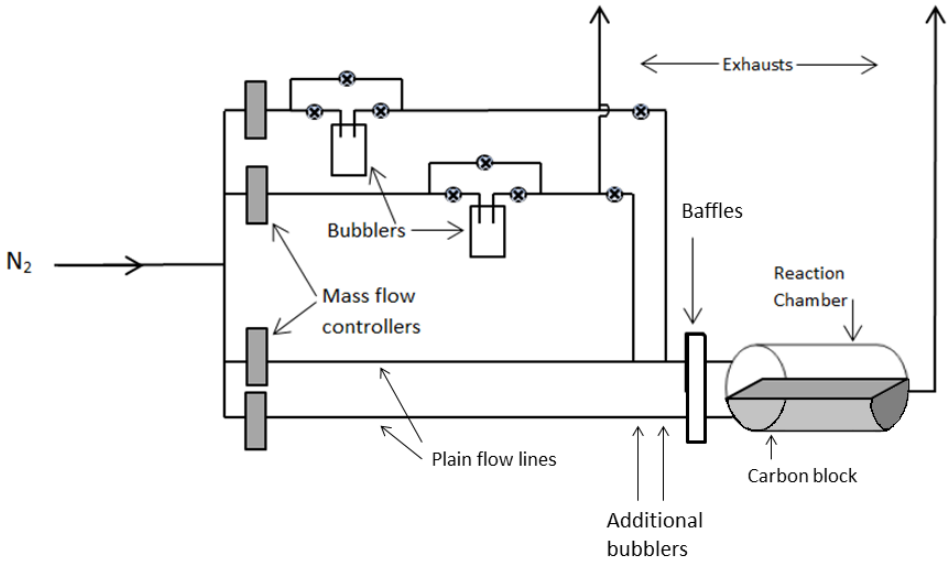

Figure 7 Schematic of chemical vapour deposition reactor.

Figure 7 shows a schematic of the CVD reactor which was used for every deposition reported in this work. Two further precursor bubblers are available but, for simplicity, are not shown in the diagram. They join a second plain flow at the position indicated by the arrows in Figure 7. The pipework is made of ¼ inch stainless steel pipes, which are surrounded by electrical heating tape, which can be controlled and monitored by thermocouples. During a deposition, the pipework is heated to over 100 °C to prevent condensation of the precursors in the pipes which can lead to blockages. The bubblers are also heated and can be controlled to give the vapour pressure desired for each precursor. If the precursor is required to be lower than room temperature, a thermostatic bath filled with 50:50 water:ethylene glycol can be placed around the exterior of the bubbler. The reaction chamber consists of a quartz tube with a half cylinder carbon block. The carbon block is heated by two Whatman heater cartridges. The sample to be coated is placed directly on top of the carbon block. A top plate may also be positioned 20 mm above the carbon block if required.

1.5 Background to Photocatalytic Tests

1.5.1 Stearic acid degradation

Stearic acid is widely employed as a model compound used to assess the photocatalytic ability of semiconductor materials. Stearic acid is a solid at room temperature and therefore simpler to handle compared to a liquid or gas. The basic principle of the test is that a thin layer of stearic acid is deposited onto a photocatalyst film (this can be done by drop casting, spin coating or dip coating the sample using a solution of stearic acid). There are a number of ways to quantify the amount of stearic acid on the photocatalyst including measuring the thickness of the layer using ellipsometery or observing the stearic acid on the surface by AFM.[57] The most commonly employed method is to use IR spectrometry and calculate the area under the peaks in the region of 2700-3000 cm^{-1} which corresponds to C-H stretching vibrations. There is a peak at 2958 cm^{-1}

due asymmetric in-plane C-H stretch in the CH_3 group and peaks at 2923 cm^{-1} and 2853 cm^{-1} due to asymmetric and symmetric, respectively, in-plane C-H stretching in the CH_2 groups.[58] The sample is then irradiated, leading to oxidation of the stearic acid by photogenerated holes or by hydroxyl radicals formed by the reaction of a hole with water.[59] The change in amount of stearic acid present is monitored at regular time intervals. The overall mineralisation process can be summarised as shown in Equation 3.

$$CH_3(CH_2)_{16}COOH + 26O_2 \xrightarrow{TiO_2 + h\nu} 18CO_2 + 18H_2O$$

Equation 3 Mineralisation of stearic acid.

Conveniently, both visible and UV light sources are suitable for this test as stearic acid is stable under illumination in this energy region (in the absence of a photocatalyst) and does not absorb any light in this region which simplifies any necessary quantum yield calculations.

A variation of this method, involves monitoring the evolution of CO_2 as a result of the photodegradation of the stearic acid.[58] In this instance, the sample must be contained within a gas-tight IR cell. There are several ways in which CO_2 could be monitored. For most laboratories, measurement of the IR spectrum of CO_2 is straight forward. Alternatively gas chromatography could be used.

1.5.2 Degradation of intelligent ink

The so called “intelligent ink” test has been developed for simple, fast assessment of photocatalytic activity.[60] The basis of the ink formulation is the molecule resazurin (Rz), which is blue in colour. Partial reduction leads to the formation of resorufin (Rf) which is pink and further irradiation bleaches the dye to colourless products. The reaction scheme is given in Figure 8.

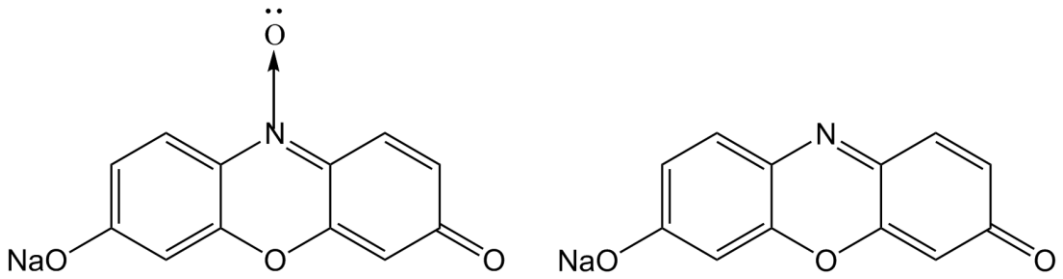

Resazurin (Rz)
Blue

Resorufin (Rz)
Pink

Figure 8 Structure of intelligent ink and its reduced form.

A qualitative screening assessment can be performed by monitoring the colour change during irradiation by eye. More quantitative data can be obtained using UV-vis spectrometry, or by extracting the colour values, using appropriate software, from a photographic image or scanned image of the sample.[61] The intelligent ink test is somewhat more sensitive than the stearic acid test but is not suitable for use with visible light irradiation. Given that it is blue, the ink absorbs visible light itself meaning that the amount of photons to reach the photocatalyst would be unknown making formal quantum yield calculations very challenging and hence fair comparison between samples tested on different dates or in different laboratories would be near impossible. A comparison for rates for stearic acid degradation and resazurin degradation on a set of TiO_2 films have shown a strong correlation although the intelligent ink test is complete within a matter of minutes rather than hours, as for stearic acid.[62]

1.5.3 NO_x testing

Nitric oxide (or nitrogen monoxide) is a harmful gas which is released into the atmosphere as a result of combustion in vehicle engines and power stations. It is known to play a role in acid rain formation and depletion of the ozone layer. It is

also formed as a waste product from several common industrial processes. For these reasons it has attracted the attention of researchers who have used photocatalysts to remove NO from the air by oxidising it to HNO_3. TiO_2 provides sufficiently oxidising holes for the conversion of NO to NO_3^- which has a redox potential of 0.96 V (vs SHE).[22] The reaction proceeds via a radical mechanism in two stages. Firstly oxidation to nitrous acid, and then to nitric acid as shown in Equation 4 and 5.[63]

$$4NO + O_2 + 2H_2O \rightarrow 4HNO_2$$

Equation 4

$$2HNO_2 + O_2 \rightarrow 2HNO_3$$

Equation 5

However, it has been shown that accumulation of HNO_3 on the surface of a photocatalyst in the presence of NO can lead to the undesirable formation of NO_2 which is toxic, as shown in Equation 6.

$$2HNO_3 + NO \rightarrow 3NO_2 + H_2O$$

Equation 6

In order for the reaction to be useful, the production of NO_2 should be low and the removal of NO high. This is why the difference between these two values, the overall NO_x removal, of a photocatalyst is often quoted. The photogenerated electrons react with oxygen to form superoxide radicals ($O_2^{\bullet -}$) and hydroperoxide radicals ($HO_2^{\bullet}$) which also assists the oxidation of NO.[64]

The popularity of the NO_x test has led to the development of an ISO standard test (number 22197-1). The laboratory procedure involves irradiation of photocatalyst material in a transparent, gas-tight transparent chamber. Humidified air (50%) and NO (1000 ppb) gas are flown over the sample to an analyser which monitors the

concentration of NO and NO_2. Prior to irradiation, the air and NO are exposed to the sample and usually a decrease in NO is observed as it adsorbs to the sample and the walls of the reaction chamber. Once the surfaces are saturated with adsorbed NO, the level of detected NO returns to the initial concentration. During irradiation of the sample, the levels of NO and NO_2 are constantly monitored. In the presence of an active photocatalyst the NO is oxidised and the concentration falls to a steady level within a matter of minutes. The concentration should remain constant during the experiment and then rise to the initial concentration once the light is switched off. On some occasions the concentration of NO rises somewhat during the experiment due to the HNO_3 blocking the active surface sites.[64]

A schematic for the gas flow systems is shown in Figure 9.

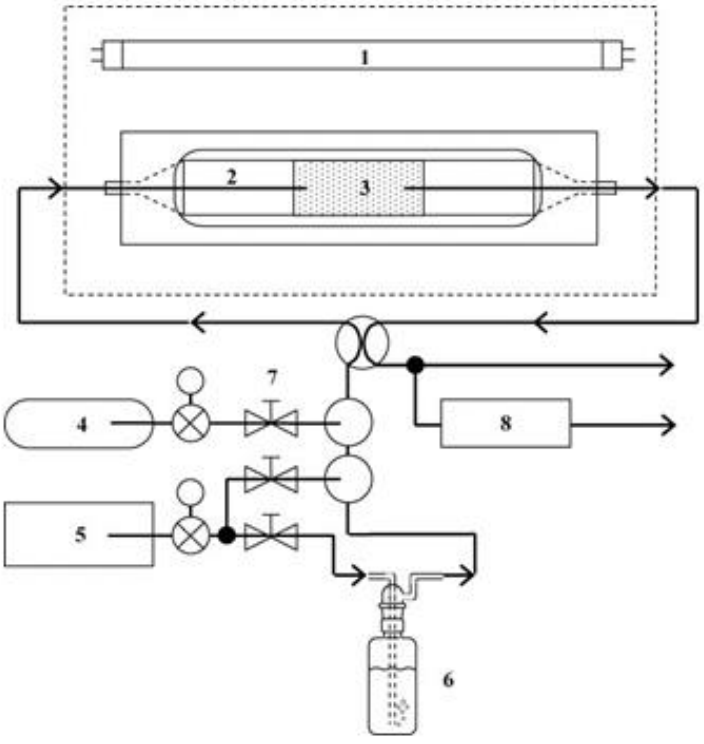

Figure 9 Schematic of NO_x testing rig. Reproduced with permission from reference [63].

Figure 9 (1) shows the position of the lamp, (2) is the glass cover on top of the reaction chamber, (3) is the sample to be tested, (4) is the NO supply, (5) is the air

supply, part of which is diverted through a Drechsel bottle (6). The mass flow controllers for the gases are indicated by (7). The flow of the dry and humidified air is monitored and kept at 50% humidity. The gas analyser is in position (8).

The design of a reaction chamber is shown in Figure 10.

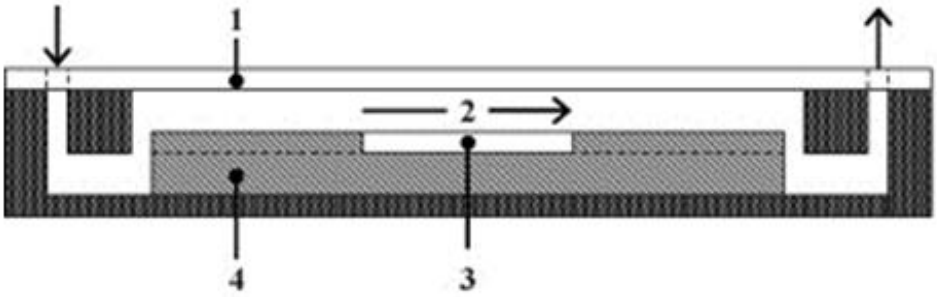

Figure 10 Diagram of the reaction chamber used in NO_x testing as viewed from the side. Reproduced with permission from reference [63].

In Figure 10 the entry and exit points for the gas flow are marked by the arrows. The glass cover is in position (1), (2) indicates the gas flow over the surface of a sample (3), which is placed on a height adjustable stage (4).

Both Figures 9 and 10 show the type of system used in subsequent chapters. An advantage of the NO_x test method is that activity of films on a non-transparent substrate can be quantitatively assessed. However, it requires specialist, dedicated equipment.

1.6 Summary

This chapter has introduced the applications and properties of TiO_2 and the principles of CVD and the photocatalytic tests used in this work. The next chapter presents results of CVD coatings on several types of metal substrate. Functional testing was carried out to demonstrate the utility of these coatings.

CHAPTER TWO

TiO_2 DEPOSITIONS ON METAL SUBSTRATES

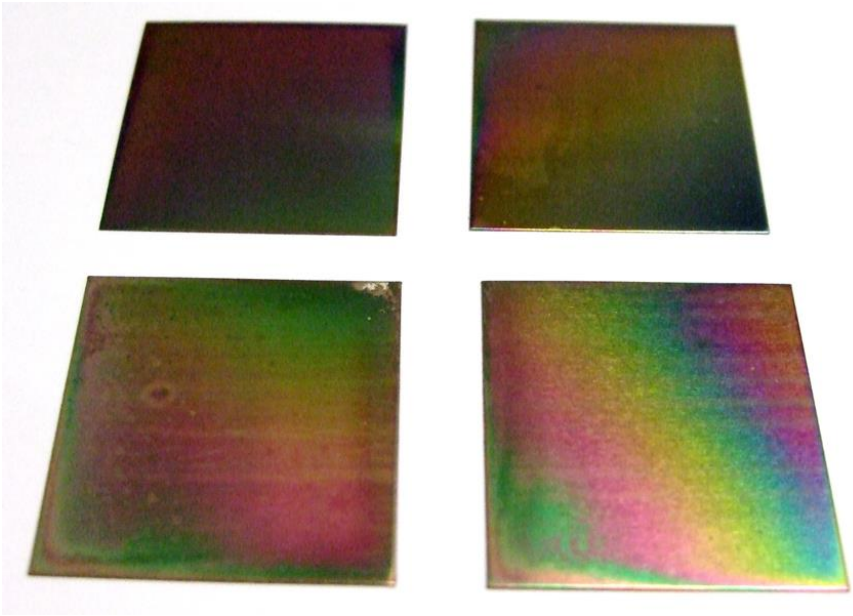

Chapter 2: TiO_2 deposition on metal substrates

Abstract

Much of the focus of TiO_2 thin films has concentrated on depositions on glass. This is largely due to the now commercial use of self-cleaning glass products such as Activ™, produced by Pilkington and Bioclean® by Saint Gobain. However an understanding of the properties of TiO_2 films deposited on metals is vital in expanding the applications of TiO_2 in new fields. This chapter investigates depositions on several different metallic substrates with a focus on understanding the phase and resultant properties. The first section investigates the phase of TiO_2 produced from chemical vapour deposition on various grades of steel. Secondly TiO_2 films on aluminium (kitchen) foil demonstrate the interesting property of being total flexible whilst remaining adherent and crack free. The third section was carried out in collaboration with the group of Dr. Peter Brett at the Eastman Dental Institute to investigate the properties of TiO_2 coated on an orthopaedic implant material, namely CoCrMo alloy. It is demonstrated that the TiO_2 coating gives improved and/or faster osteogenic differentiation of human mesenchymal stem cells i.e. trigger the pathway for the development of bone cells.

2.1 Introduction

Some of the important applications of TiO_2 films have been discussed in section 1.1. The most successful commercial thin films products currently, are coatings on glass for self-cleaning windows and architectural glass. Leaders in the glass industry offer products for commercial and domestic customers such the Activ glass range from Pilkington[65] and Bioclean from Saint Gobain.[66] As such, much of the literature on TiO_2 films focusses on glass substrates. Whilst there has been some interest in photocatalytic coatings on steel, the potential of metal substrates is somewhat underexploited. The work presented in this chapter comprises three studies using different metal substrates with different applications in mind. However, it may be that unexpected uses come to light in the future. For all three sections, TiO_2 thin films are deposited by atmospheric pressure chemical vapour deposition, a technique which is readily industrialised. The aim of this work is to provide further insight into how the synthetic conditions influence the phase and properties of the films and provide proof of principle of some novel applications.

2.1.1 Steel Substrates

Whilst there is some interest to develop steel with self-cleaning properties, there is perhaps less demand than for self-cleaning glass since dirt is less visible on a non-transparent substrate. However, one area of interest is the potential to use TiO_2 to degrade air-borne pollutants such as NO_x. Photocatalytic coatings on architectural steel, used in buildings in cities, where there are high levels of pollution from traffic, could contribute to removal of harmful emissions from the air. The idea that anti-bacterial properties of TiO_2 could be utilised on the surfaces of interior fixtures such as taps, push plates on doors and bed rails in hospitals is attractive. However, the issue of limited UV light indoors would need to be considered. Previous work has shown TiO_2 coatings on steel are effective in killing Escherichia coli bacteria under UVA irradiation.[45] A further use of TiO_2 on

steel is in photodiodes. A photodiode could potentially offer a simple, cost effective route to water splitting to provide hydrogen fuel. A schematic of a photodiode for water splitting is given in Figure 11.

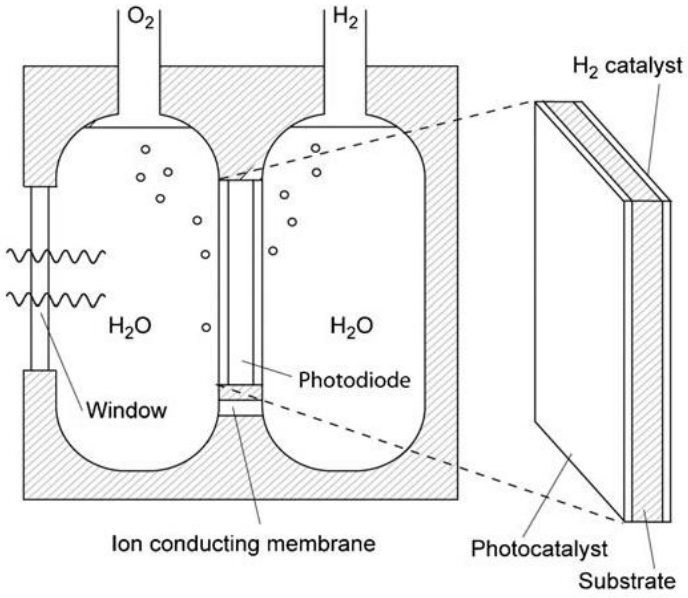

Figure 11 Schematic of photodiode reproduced with permission from reference [67].

Irradiation of the titania layer with light of energy equal to or greater than the band gap, results in photoexcited electrons in the conduction band and holes in the valence band. The electrons are able to travel through the steel substrate to a very thin layer of platinum co-catalyst where reduction of protons takes place to produce hydrogen gas. On the illuminated side, the holes are able to oxidise water for oxygen production. The spatial separation of the two reactions prevents the back reaction taking place and therefore improves the efficiency of the process. In a device, the two chambers are separated although ion exchange can take place via an ion conducting membrane. Water splitting by this process offers many advantages over photovoltaic (PV) and DSSC cells in that a hydrogen gas can be stored until required unlike electricity produced from a PV which is only available during daylight hours. It is also much simpler and therefore cheaper, DSSC cells can often be made of many layers and components, which is costly and often use rare and expensive elements such as indium. It has been shown that steel is a promising substrate compared to titanium metal for hydrogen production.[68]

As has been outlined above, there is considerable motivation for investigations into TiO_2 on steel. It is vitally important to understand how the synthetic parameters influence the properties of the TiO_2 film that is formed in order to be able to tailor the properties to a particular application.

Rutile is the most thermodynamically stable form, hence higher temperatures promote its formation. There are many other variables which can have an influence. Both steel and titanium metal have been reported to produce rutile thin films by APCVD from ethyl acetate and $TiCl_4$ at 600 °C.[68] It has been shown, for many CVD processes that the substrate plays an important role: for aerosol-assisted CVD with TTIP (titanium (IV) tetraisopropoxide) only rutile is formed on steel and titanium, whereas for glass either anatase, an anatase/rutile mixture or rutile is formed depending on the temperature.[69] It has also been demonstrated with LPCVD that both substrate and temperature are phase determining factors.[70, 71] Hitchman et al. suggested that the crystal structure and orientation of the substrate will direct the growth of TiO_2. Other researchers working with atmospheric pressure CVD have reported the importance of precursor selection.[72] Sheel et al. investigated two systems TTIP and $TiCl_4$ with ethyl acetate as the oxygen source. They observed with TTIP that when the steel substrate was heated to 450-550 °C anatase was produced and at 550-650 °C a mixture of anatase and rutile. With $TiCl_4$ and ethyl acetate no growth below 550 °C was observed and only rutile between 550-650 °C. Sheel et al. noted that anatase is observed with faster CVD growth rates. They offer this as an explanation for the $TiCl_4$ and ethyl acetate system producing only rutile since the formation of TiO_2 requires the reaction of two molecules rather than the intramolecular decomposition of just one molecule, as is the case for TTIP. They also argue that this supports the findings of Hitchman[70] where rutile is formed from titanium tetrabutoxide (TTB). The hydrolysis of TTB is slower that TTIP due to the increased length of the alkyl chain, hence rutile is favoured.

2.1.2 Aluminium and Other Flexible Substrates

A semiconductor on a flexible substrate has been investigated by many researchers. It offers the possibility to form flexible components of circuitry for wearable electronics and paper-like electronic displays. Thin films of amorphous TiO_2 on aluminium substrates have been investigated for use in ReRAM devices.[73] Aluminium foil is cheap and readily available hence its selection in this study. It is also lightweight, corrosion resistant (particularly in water) and has the ability to withstand high calcination temperatures either in service or during the manufacture of a device.

Aluminium could be a more suitable support for titania thin films used in water purification than glass (which is heavy and not easily shaped) and steel (which will corrode).

Aluminium can corrode in seawater due to attack from chloride ions, however a TiO_2 coating has been shown to effectively inhibit this corrosion.[74] Alloys of Al are used in machinery and aerospace but suffer from poor tribological properties but rutile can increase wear resistance and reduce the friction coefficient.[75]

A flexible photocatalyst and/or antibacterial surface offer intriguing possibilities for application in food and medical device packaging.

The shape-forming capabilities of foil with an adherent TiO_2 layer mean that the titania film could be deposited whilst flat, possibly incorporated as part of a roll-to-roll process for the manufacturing process of the aluminium foil and then subsequently formed into a variety of products with the photocatalyst layer already present.

Aluminium ions have been shown to diffuse in TiO_2 deposited on an aluminium alloy (97.95 % Al) by sol-gel followed by annealing up to 550 °C.[76] Aluminium was found throughout the 300 nm layer of titania at a maximum of 8%. A later report by Chen et al. showed that the presence of aluminium ions in a titania sol-gel film was detrimental to photocatalytic activity. Samples with three or fewer dip-coated titania layers showed deactivation after repeated cycles of benzamide

degradation.[77] However, samples with five or more layers, i.e. thicker coatings did not deactivate. A sample with six layers showed less than 80% of the amount of aluminium than in a sample with just one layer.

Yu et al. also showed poorer photocatalytic activity (degradation of acetone) of titania films formed by a reverse miscelle method on aluminium substrates compared with quartz and stainless steel substrates.[78] They observed the presence of aluminium ions in the titania films on the Al substrate and attributed the poor photocatalytic activity to the aluminium ions acting as a charge recombination centre.

In contrast, Mu et al. observed a higher rate of methyl orange degradation from titania nanoparticles immobilised on porous aluminium foil compared to a glass substrate.[79] They attribute this to the higher surface area and also suggest that aluminium acts as a trap and prevents electron-hole recombination allowing greater hole transfer across the interface. This report does not contain any analysis of the composition of the TiO_2 so it is possible that there is no diffusion of Al into the titania particles which are pre-formed prior to deposition by spin coating of a sol. The previously mentioned reports form the TiO_2 in-situ on the aluminium at high temperature which may allow the diffusion of Al ions into the titanium dioxide lattice.

TiO_2 films with photocatalytic properties have been deposited on flexible substrates such as polycarbonate.[80] Flexible titanium substrates have been investigated for use in solar cells.[81]

2.1.3 Cobalt Chromium Molybdenum Alloy Substrates

Our aging population has led to an increase in the number of joint replacements. In the United States, hip replacements have been predicted to rise by 174% between 2005 and 2030 and knee replacements to rise by 637% over the same time period.[82] The number of revision surgeries is also set to double by 2015 and 2026 for knee and hip implants respectively. These revision surgeries are

required after failure of an implant. One reason for the increase in frequency of implant failure is due to lengthening life spans which leads to patients out-living their implants. When a failure does occur this usually requires a retrieval operation and a new implant to be inserted, at considerable discomfort to the patient and cost to the healthcare provider.[83] This has led to an interest in the development of new materials which are more durable with longer service lifetime.

Titanium metal and its alloys are currently the materials of choice for orthopaedic and dental implants.[84] Titanium combines corrosion resistance with low toxicity and is also lightweight. However, studies of retrieved, failed implants have shown that those made from CoCrMo alloys have far less wear than titanium, to the extent that the use of titanium on articulating surfaces is no longer recommended for clinical use.[85] In addition to wear resistance, CoCrMo also has superior mechanical strength but lacks the biocompatibility of titanium based materials.

The success of an implant, in the short term, depends on its ability to fuse with existing bone without triggering an immune response. The term "osseointegration" is used to describe the anchorage or adhesion of the implant to the bone[86] and begins with the formation of bone cells on the surface followed by proliferation. The surface chemistry of the implant should be well understood in order to promote bone cell development, adhesion and growth. In the case of titanium, as with many metals under normal conditions (i.e. exposed to air) it forms a surface oxide layer of TiO_2. It is therefore this oxide layer which chemically interacts with the body rather than the pure metal. Given the known biocompatibility of titanium[87], in this work, it was hypothesised that by coating the CoCrMo with a titanium dioxide layer, it could mimic the surface chemistry of titanium. Other attempts to modify the surface of CoCrMo have been investigated, including diamond-like coatings,[88] acid etching,[89] titanium nitride coatings[90] and nanoscale topography,[91] but have either been largely unsuccessful or are unlikely to be commercially viable due to scale-up issues. Sol-gel titania coatings have also been investigated for improved cytocompatibility due to the reduced metal ion release.[92]

The work presented here is the first study using CVD to coat CoCrMo and investigate the osteogenic differentiation of human mesenchymal stem cells on this substrate.

2.2 Experimental

Atmospheric pressure CVD was used to deposit thin films of TiO_2 on various metal substrates. The details of the CVD reactor are given in section 1.4. The precursors used were titanium tetrachloride (99.9% ReagentPlus) and ethyl acetate (laboratory reagent grade) obtained from Sigma Aldrich and Fisher Scientific respectively and used without further purification. The steel and titanium substrates were obtained from Goodfellow. The aluminium foil (kitchen foil) was purchased at Sainsbury's and the CoCrMo alloy discs were kindly supplied by Corin Ltd (Cirencester, UK). The steel was supplied as 25 mm x 25 mm x 0.1 mm coupons. The aluminium foil was cut into squares of 25 mm x 25 mm and the thickness was measured with a micrometer to be approximately 0.01 mm. For all depositions, the metal substrates were placed upon a sheet of glass with a barrier layer of SiO_2 (supplied by Pilkington) acting as a tray and also to prevent deposition of TiO_2 directly onto the carbon block. Once the target temperature was reached, the system was left for a minimum of 45 minutes to equilibrate. A top plate was used for the deposition on steel but not on aluminium or CoCrMo discs.

Gold coating was achieved by sputtering a gold target (onto 316 grade steel and titanium metal) for 4 minutes at 35 mA using an Emscope SC500 sputter coater.

Raman spectroscopy was carried out using either a Renishaw inVia spectrometer with a 514 nm laser or Renishaw Ramascope spectrometer with a 633 nm laser. Where necessary, the percentage of anatase and rutile was determined by a previously reported method to deconvolute two selected rutile and anatase peaks.[93] This calibration method involved mixing commercial powders of pure anatase and pure rutile in a range of pre-determined ratios and measuring the

Raman pattern of each sample. From each pattern, the area of the rutile A1g (609 cm^{-1}) and the anatase Eg (637 cm^{-1}) peaks were calculated, chosen for their strong intensity and well defined shape over the region analysed. Since these peaks had partial overlap, CasaXPS software was used to deconvolute and give areas for each peak. The percentage ratio of the anatase peak area to the rutile peak area was calculated for each standard. A plot of anatase phase percentage vs. anatase peak ratio percentage yielded an almost linear relationship that plateaued at high concentrations. The data best fitted a slowly decaying exponential function, described as y = A1*exp(-x/t1) + y0, where A1 = -160.203, t1 = 97.772, y0 = 157.464, y = anatase area percentage ratio and x = actual anatase percentage.

XRD analysis was carried out using either Bruker D8 Discover diffractometer with a 2D GADDS detector or a Bruker D8 Discover diffractometer with a 1D Lynxeye detector. In both cases monochromated Cu Kα1 source was used.

SEM images were obtained from either a JEOL 6103 FEG (field emission gun) scanning electron microscope or JEOL JSM6700F FEG scanning electron microscope, without any conductive coating on the sample surface.

XPS analysis was performed using a Thermo Scientific K-Alpha surface analysis system with an Al Kα source and dual beam charge compensation system. A constant pass energy of 50 eV was used and a spot size analysis area of 400 μm in diameter. Where necessary, sputtering was used to remove surface material by bombardment with argon ions. Analysis of XPS data was carried out with Thermo Avantage software using the "smart" background function. The charge correction was performed by shifting the peak position of adventitious carbon 1s to 284.8 eV and applying the same shift to all other spectra recorded for that sample.

UV-vis reflectance/absorption spectra were recorded using either a PerkinElmer Lambda 950 spectrometer or a Filmetrics F20 thin film analyser instrument. Thickness calculations were performed using the Swanepoel method.[94] This method analyses the maxima and minima in the reflectance pattern to determine the thickness of titania films.

For the resazurin dye degradation test, the formulation used was 0.04 g of resazurin, 0.4 g of HEC (2-hydroxyethyl cellulose) and 3 g of glycerol made up to 40 ml with deionised (DI) water. The resazurin dye (sodium salt), HEC (typical M_v = 90,000) and glycerol (99.5%) were all obtained from Sigma Aldrich. The ink was sprayed onto the steel samples using an aerosol spray gun (SIP Emerald Spray Gun). In the case of the aluminium substrates, 100 µL (measured using a micropipette) of Rz ink was deposited onto each sample and spread out using the end of the pipette tip. A 365 nm lamp (Vilber-Lourmat 2 x 8 W bulbs) was used to irradiate the sample. The samples were pre-irradiated with 254 nm light for 1 hour prior to ink deposition.

The contact angles were determined using an FTA1000 instrument with FTA32 software to determine the droplet shape and contact angle. The drop volume was 5 µL DI water and a dispense rate of 2 µL/s. The sample was irradiated with 254 nm light for one hour prior to the contact angle measurement.

The NO_x testing was carried out using equipment described in section 1.5.3 which was built in house at Queen's University Belfast. The gas analyser was an Enviro Technology Services PLC T200 Chemiluminescence $NO/NO_2/NO_x$ Analyser. The concentration of NO and NO_2 were recorded once per minute for the duration of the experiment. The NO gas (48.3 ppm NO, 48.9 ppm total NO_x in N_2) was supplied by BOC. The irradiation source was a 352 nm lamp with BLB bulbs (Sankyo Denki). The irradiance at the height of the sample was measured as 2 mW/cm^{-2}. The samples were pre-irradiated with 352 nm lamp for 15 hours in a 50% humidity air flow

The functional testing of the coatings of the CoCrMo alloys were carried out by collaborators, specifically cell testing was carried out by Niall Logan of the Eastman Dental Institute. The detailed experimental procedure was supplied by the collaborators and is given for reference in Appendix One.

2.3 Results and Discussion

2.3.1 Study of the phase and other properties of TiO_2 produced on various grades of steel and other metal substrates

Four different grades of steel were studied SS304, SS304L, SS316 and SS316L. The 304 grade steel contains 18% nickel and 10% chromium, 316 grade steel contains 18% nickel, 10% chromium and 3% molybdenum. The letter 'L' denotes low carbon content, a maximum of 0.03% whereas 'straight' grades have a maximum of 0.08% carbon.[95] Onto each of the four steels, a thin film of TiO_2 was deposited by the decomposition of $TiCl_4$ and ethyl acetate at 500 °C with mass flow rates of 3×10^{-3} and 5×10^{-3} mol/min, respectively. The mass flow rates are calculated following a procedure reported elsewhere.[96] The flow rates and grade of steel were varied in the experiments whilst all other experimental variables, including deposition temperature (500 °C) and deposition time (1 min 15 s), plain line flow rates (6.95 L/min total of nitrogen) were kept constant. A second set of films on each type of steel were produced with low mass flow rates of 1.5×10^{-3} and 2.5×10^{-3} mol/min for $TiCl_4$ and ethyl acetate respectively. For each deposition, four coupons of identical steel were placed in the reactor. Titanium metal, gold coated titanium metal and gold coated 316 grade steel were also used as substrates. As before, the TiO_2 was deposited by the decomposition of $TiCl_4$ and ethyl acetate at 500 °C with mass flow rates of 3×10^{-3} and 5×10^{-3} mol/min, respectively. A photograph of a typical well-adhered coating is shown in Figure 12.

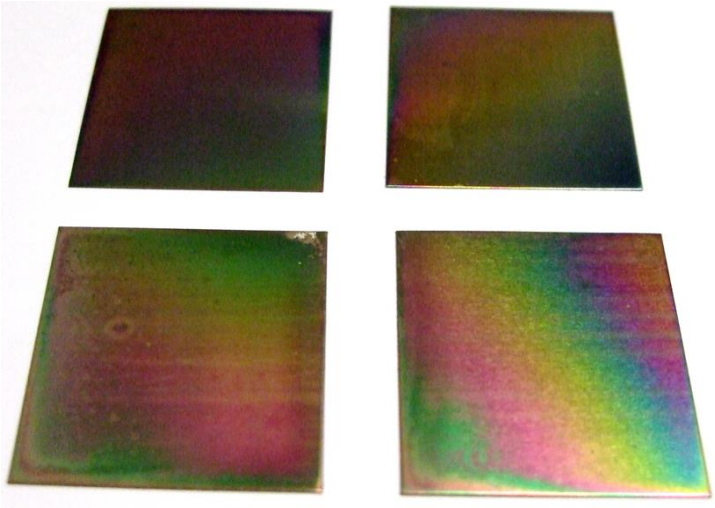

Figure 12 TiO_2 coating on steel substrates.

2.3.1.1 Raman and Thickness Analysis

Each coupon was characterised by Raman spectroscopy and where possible by UV-vis reflectance in order to determine the thickness by using the Swanepoel method of counting interference fringes.[94] Raman spectra were recorded at three arbitrary points on each coupon to identify the phase of TiO_2 present and the percentage of each phase. It has been shown previously that the relative intensities of anatase to rutile can be utilised as an accurate method to determine relative phases, as discussed in the experimental section 2.2.[93] Raman spectra are given in Figure 13 of a) a high percentage anatase (97%) b) low anatase content (40%). Spectrum a) comes from a sample produced using the set of high flow rates on 316L steel and the sample whose spectrum is shown in b) was produced also using the high set of flow rates but with 316 steel. These are chosen as representative spectra of high and low anatase content.

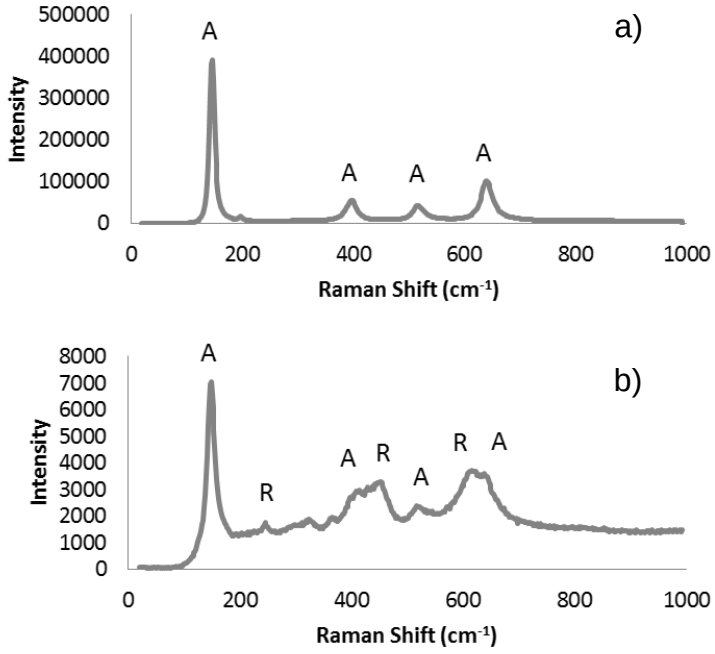

Figure 13 Raman spectra Top: 97% anatase Bottom: 40% anatase. A indicates anatase peaks and R for rutile peaks.

In some areas the Raman spectrum did not show TiO_2 (it is likely that some TiO_2 is present but it is too thin to be observed by this method) but instead oxides formed on the surface of the steel, predominantly hematite, α-Fe_2O_3.[97] However it is possible that there are other oxides present e.g. chromium oxides which are difficult to interpret given the strength of the hematite spectrum. In all other cases the remaining percentage can be assumed to be rutile. The median value for anatase percentages from each steel for both sets of flow rates are presented in Table 1.

	304L		304		316L		316	
	A %	T nm (range)	A %	T nm (range)	A %	T nm (range)	A %	T nm (range)
High flow rate	87	767	95	-	96	1540 (1478 - 1602)	79	825
Low flow rate	88	141 (110-172)	82	-	94	1020 (1062-977)	73	211 (124-262)

Table 1 A = Anatase percentage and T = thickness measurements for the different grades of steel deposited from $TiCl_4$ and ethyl acetate at flow rates of 3 x 10^{-3} and 5 x 10^{-3} mol/min, respectively and secondly using flow rates of 1.5 x 10^{-3} and 2.5 x 10^{-3} mol/min. All depositions were carried out at 500 °C. The range of thicknesses for each deposition is given in brackets. Where no range is given this is because only one measurement was obtained.

Average values are reported here since on some samples there was a difference in the phase percentage over the area of one coupon. For every type of steel there were areas which showed a minimum of 90% anatase. On two samples, 316 high flow rate and 316L low flow rate, there was one area on one coupon which had less than 50% anatase, 42% and 40% respectively. However on the same coupons high anatase content (87% and 96%) were also observed in different areas. This variation in phase is not unusual for these systems and has been previously reported[98] and is likely to be caused by small variations in temperature and precursor concentration due to depletion of reactants across the reactor zone and also the increase in precursor temperature as it moves across the reactor. Many other works in this area assigned a phase based on one analysis point only but these observations highlight the importance of multiple analysis points.

The UV-vis reflectance spectrum was recorded for each sample in order to establish the thickness of the TiO_2 film using the Swanepoel method of analysing interference fringes[94]. A representative UV-vis reflectance spectrum for TiO_2 deposited on 316L steel from $TiCl_4$ and ethyl acetate using flow rates of 1.5 x 10^{-3} mol/min and 2.5 x 10^{-3} mol/min respectively, is shown in Figure 14. This was

used to calculate a thickness of 1062 nm, however the average value for the coupons in the set is shown in Table 1.

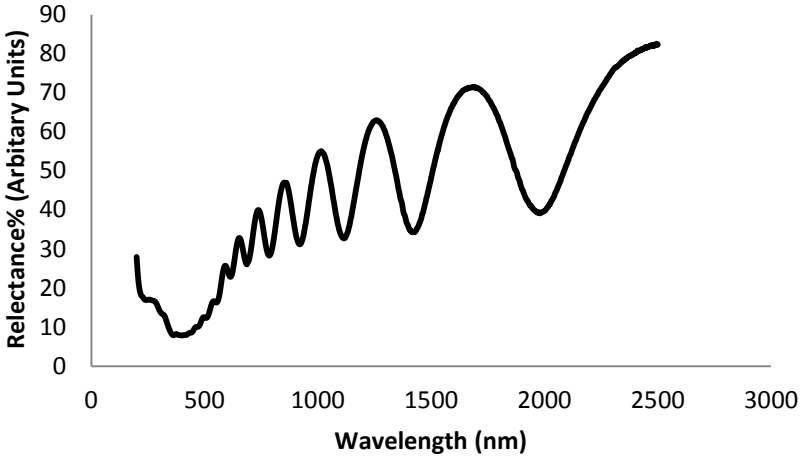

Figure 14 A representative UV-vis spectrum of a film deposited on 316L from $TiCl_4$ and ethyl acetate using flow rates of 1.5 x 10^{-3} mol/min and 2.5 x 10^{-3} mol/min respectively.

For films deposited on 304 steel at the high set of flow rates, it was not possible to obtain a UV-vis spectrum as the film had cracked and partially delaminated from the steel, primarily due to the film being too thick to withstand the change in thermal expansion during the heating before and cooling after the CVD process. This has been observed in the past for film thicknesses in excess of 1600 nm so the thickness of these particular films can be estimated to be somewhere close to this value. The films deposited on 304 steel at low flow rates were too thin to be analysed by UV-vis. This generally occurs for films thinner than 100 nm hence we may assume the thickness of these films to be under 100 nm. The variation in film thickness across any one coupon is estimated to be around 10% based on the colour of the interference fringes. Although it is possible to make thinner or thicker films in order to obtain thickness measurements, this would have required alteration of the flow rate meaning that comparisons with the other samples would not have been valid. The analysis techniques employed here mean that it is not possible to confidently correlate the thickness with phase since the analysis area for the thickness measurements is much larger than the analysis area for Raman (i.e centimetres vs micrometers) so the thickness is averaged over a large area

which may have different phases within it. However it is noted that both a thick (1602 nm) and one of the thinnest films (262 nm) have greater than 81% anatase in every area tested. A possible approach for a future study into variation of phase with thickness is suggested in Chapter 5.

The data presented in Table 1 may suggest that there are differences in deposition rate on the different steels, however there is not sufficient thickness data to arrive at this conclusion as one would require thickness data from samples with identical reaction conditions (i.e. identical points in the reactor) which is not available. Additionally missing data (from samples either too thin or too thick, as mentioned above) could alter the average.

The vast majority of the coupons have predominantly anatase phase TiO_2, with many which are almost the pure phase. There appears to be no direct correlation with the percentage of anatase observed and the different types of steel, suggesting that this method is suitable for depositing anatase on a range of substrates. This would allow tailoring of the properties of the steel, varying the composition i.e. grade to suit a particular application and retain the ability to deposit a photocatalytically active film. These results contrast with the findings reported by Sheel et al. who reported no growth of TiO_2 below 550 °C with $TiCl_4$ and ethyl acetate on 304L grade steel, and only rutile at higher temperatures. Sheel does not report the use of a top plate above the substrate, hence the reactor volume would in effect be much larger leading to a 'dilution' of the precursors. Additionally the total flow used by Sheel is higher (11 L/min) compared to this work (8.25 L/min) which would also have the effect of diluting the precursors. This is a possible factor which could lead to a slower reaction promoting rutile.

Previous work suggests that 304 and 316 steels that have been heated up to 450 °C form an oxide layer composed of an iron oxide rich outer layer and a chromium oxide rich inner layer.[99] For steel containing Mo (304), it was shown that Mo was only found in the inner oxide region. This may explain why there is little correlation with the grade of steel and the phase of TiO_2.

Where titanium metal, gold coated titanium metal and gold coated 316 steel were used as the substrate, predominantly anatase films were also observed. These

films were deposited using the high set of flow rates. Representative Raman spectra of each substrate is shown in Figure 15.

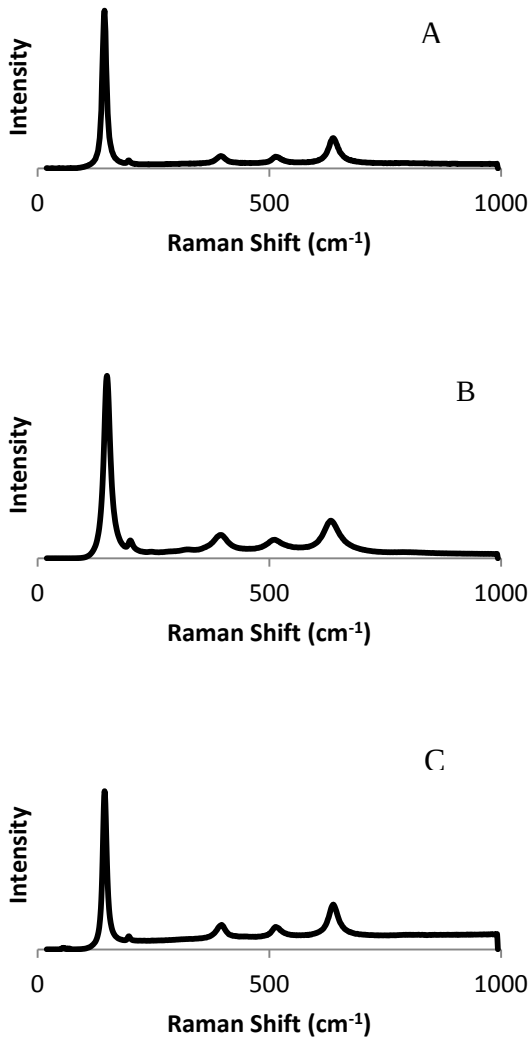

Figure 15 Raman spectra of a) TiO_2 on titanium metal b) TiO_2 on gold coated stainless steel and c) TiO_2 on gold coated titanium metal.

This demonstrates that there is no substrate selective phase deposition under these conditions. Even on titanium metal coupons where the phase native surface layer of TiO_2 may have been expected to exert a structural directing on the phase of the deposited TiO_2, no differences were observed.

2.3.1.2 Scanning Electron Microscopy

Scanning electron microscopy was used to image the morphology of the TiO_2 films formed by CVD. A sample (316L steel with low set of flow rates) was chosen which had areas of both high (96%) and low (40%) anatase composition (as identified by Raman analysis). Representative images are shown in Figure 16. Images were recorded at three different magnifications (x 60,000, x 35,000 and x 11,000) at both areas; those from the higher rutile area are in the left column and those with a greater proportion of anatase are in the right hand column.

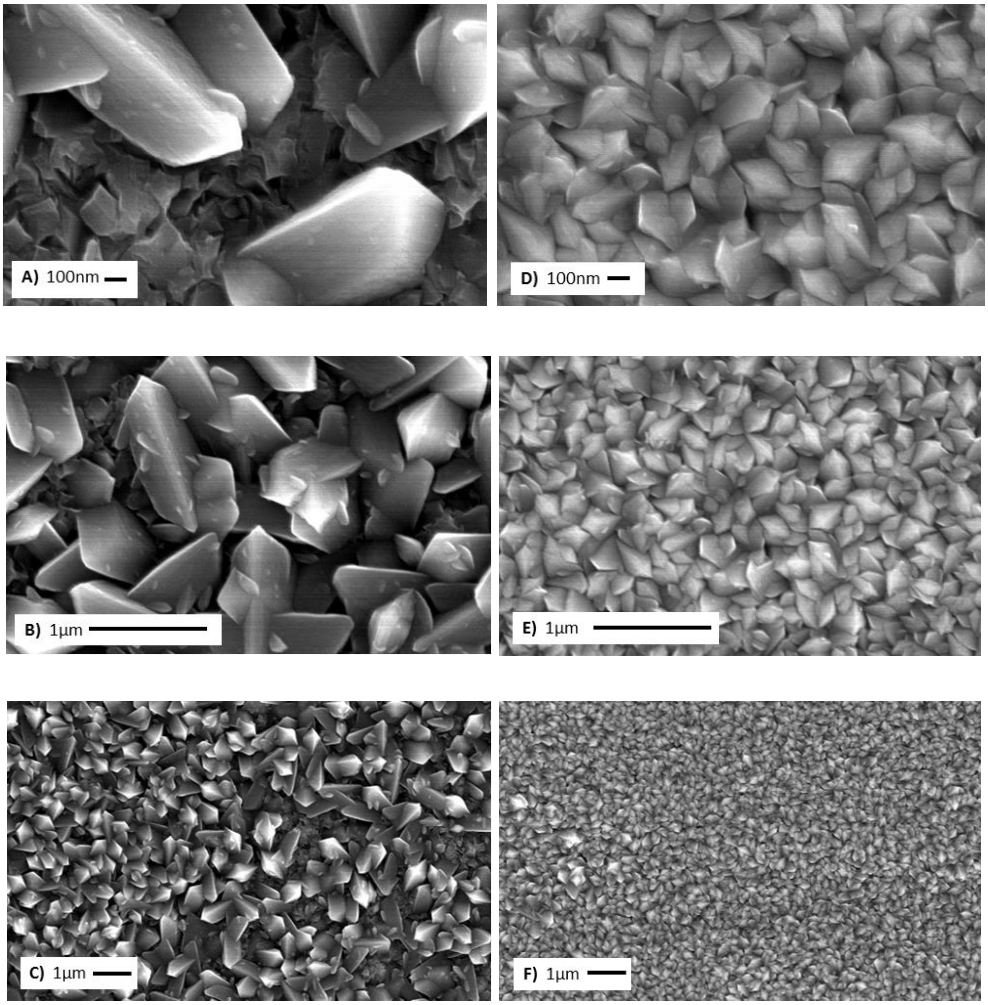

Figure 16 SEM images at three different magnifications of areas A and D were recorded at magnification at x 60,000, B and E are at x 35,000 and C and F are at x 11,000. A, B and C are at the area of low anatase content and D, E and F are at high anatase content.

There is a marked difference in particle size; the particles in predominantly anatase areas are significantly smaller than the particles in predominantly rutile areas. It can be clearly seen in image A and also in image B that there are also smaller particles present, which could account for the ca. 40% which is anatase. A smaller particle size correlates with faster nucleation. Previous findings suggested anatase growth is faster.[72] However, from the data presented here it is suggested that it is specifically anatase nucleation that is faster and thus there are more nucleation sites, yet when rutile does nucleate the growth of the crystallite itself is faster hence we see many small anatase particles and fewer but larger rutile particles. Furthermore previous work by APCVD on glass showed identical crystal habits and sizes for the large rutile and smaller anatase particles as seen here for the steel depositions.[98] The blocky or rod-like morphology often observed for rutile has previously been attributed to the presence of 4_2 screw axes along the *c* axis in rutile which promotes growth in this directly and leading to a morphology dominated by the 110 faces.[100]

SEM images were recorded for all other samples. A representative image for each type of sample is shown in Figure 17.

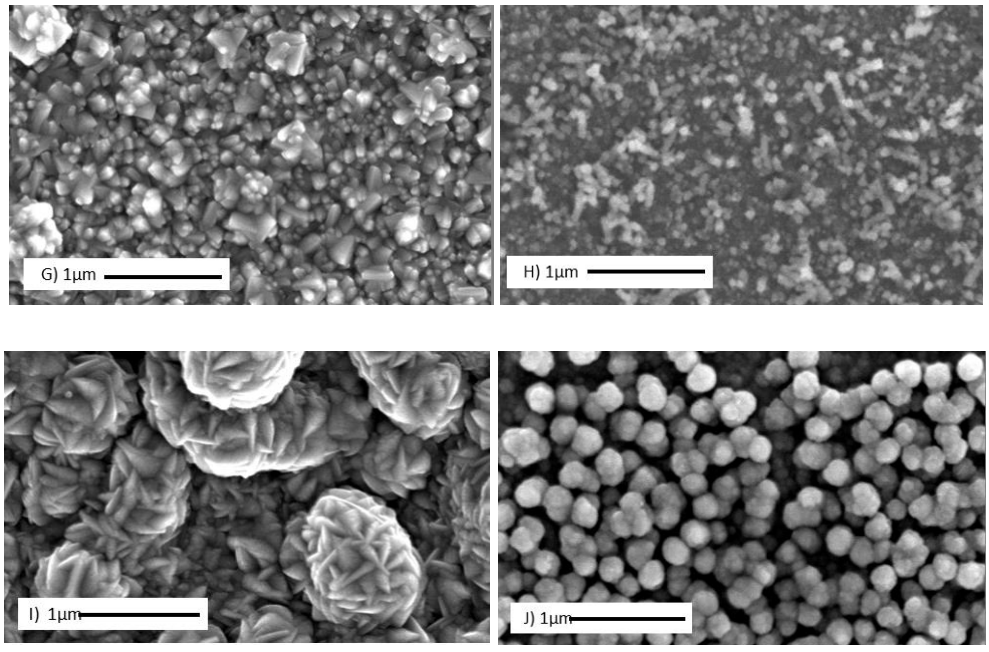

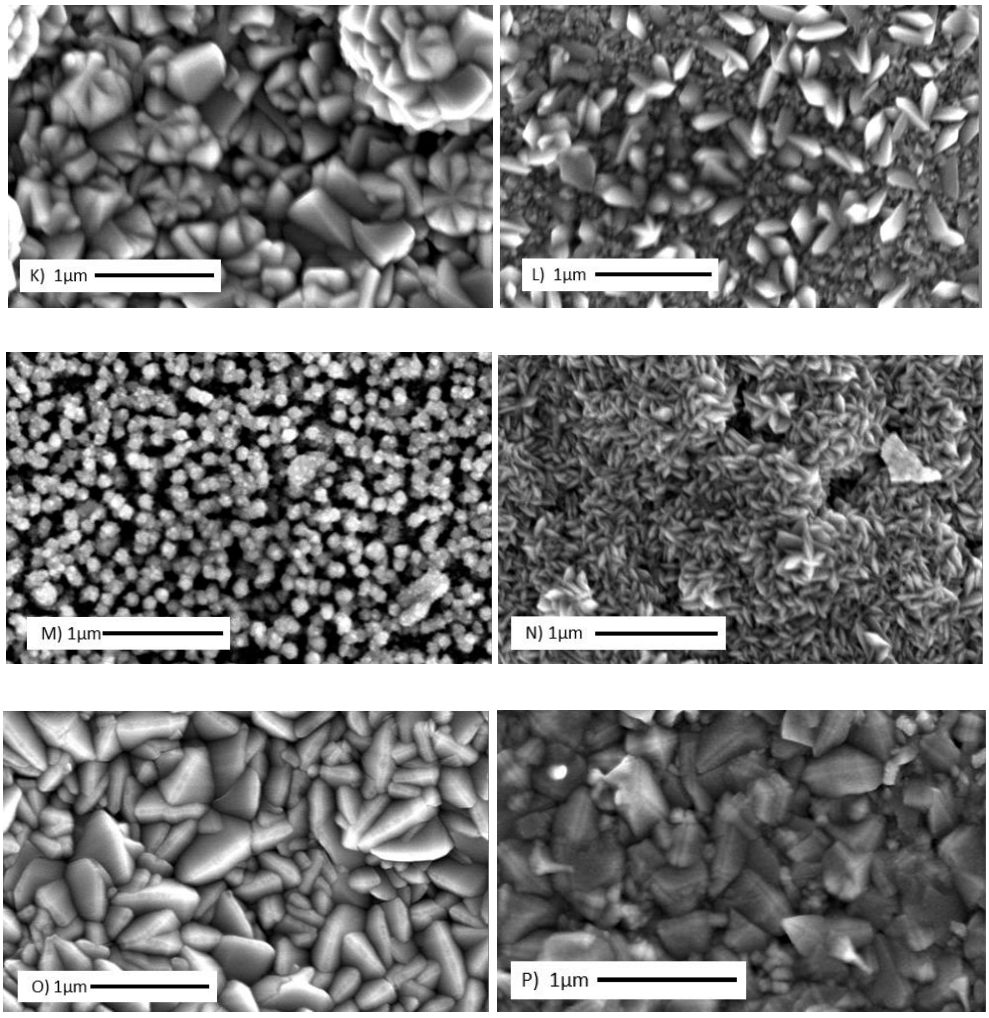

Figure 17 SEM images of TiO_2 films on different substrates G, I, K, M, N, O, P are all at high flow rates. H, J and L are at low flow rates. G and H are on 304L steel. I and J are on 304 steel. K is on 316L steel. L and M are on 316 steel. N is on Ti metal. O is on gold coated Ti metal and P is on gold coated 316 steel.

As can be seen from Figure 17, there are a range of morphologies observed for films consisting of high anatase, including "rose" type structures, rounded particles and rods. It is also observed again, that for lower anatase samples (i.e. one of two aforementioned samples with low, in this case, 42% anatase), 316 steel with high flow rates, image L also has a mixture of the rutile-like blocky structures with well-defined edges and sharp points as well as smaller (anatase) particles. Also of note is that the gold coated substrates appeared to give large more defined crystallites, showing there is some substrate selective morphology, however it is difficult to define all of the contributing factors such as variation in

thickness. These differences in morphology may lead to differences in photocatalytic activity.

2.3.1.3 X-ray Diffraction

X-ray diffraction was used to analyse each film, in approximately the centre of each coupon. Whilst it is possible to use the ratio of anatase peaks to rutile peaks to calculate the percentage anatase from XRD data for powders, it is significantly more difficult to do this with thin films due to preferred orientation effects. Figure 18 shows an XRD pattern of a film on steel which was shown by Raman to have relatively low anatase content (ca 60%). This specific sample was produced on 316 steel at the lower set of flow rates.

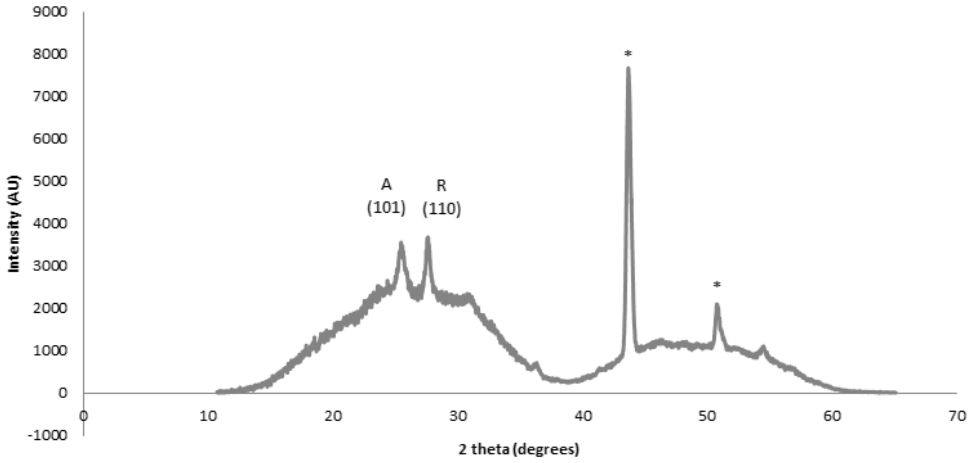

Figure 18 Steel with titania film. 'A' indicates anatase reflections, 'R' indicates rutile reflections and '*' are peaks due to the steel substrate.

The peaks are annotated to show whether they originate from anatase, rutile or the steel substrate. The broad background signal is due to the fluorescence from the iron in the underlying steel as shown in Figure 19 for a 316 steel sample heated to 500 °C in the CVD reactor. This XRD pattern is representative of all the other types of steel which had also been heated to 500 °C.

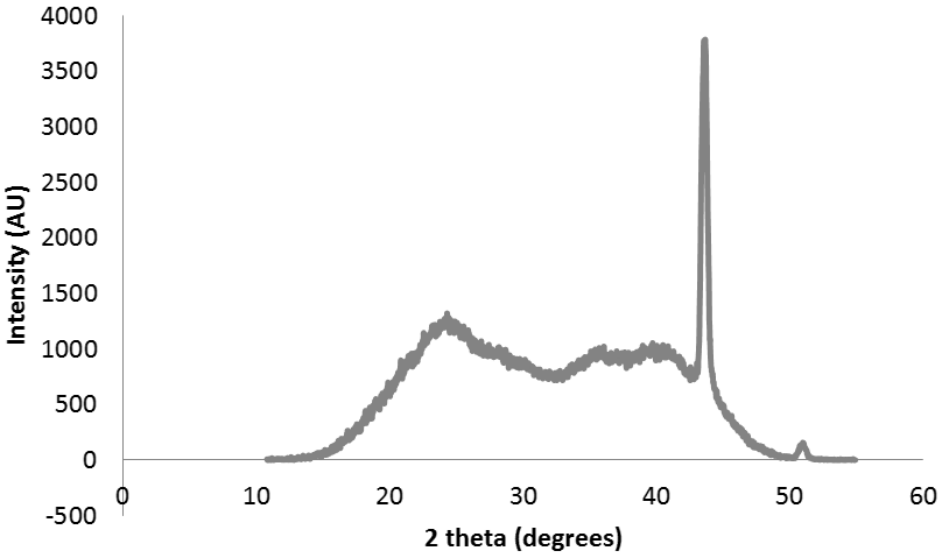

Figure 19 XRD pattern of steel heated to 500 °C.

2.3.1.4 Photocatalytic activity

Four samples with steel substrates were selected for photocatalytic testing, two with high anatase content (316L steel deposited with high flow rates) and two with lower anatase content (316 steel deposited with low flow rates). A resazurin based dye was spray coated onto the selected samples, a small piece of Saint Gobain Bioclean and untreated glass. Degradation of the dye is indicated by a colour change from blue to pink and then to colourless. All four samples on steel degraded the dye significantly faster than the Saint Gobain Bioclean standard which took several hours longer to totally remove all colour from the dye and untreated glass which did not show any change from the initial blue colour. Two samples which had 95% anatase degraded the dye from blue to pink in under 7 mins on average. The lower anatase content samples (67% and 71%) took around 4 mins to become pink. The change to colourless is much slower and hence more difficult to observe although it is possible to say that both high anatase content samples were completely colourless after 77 mins. The samples of 67% and 71% anatase required 51 and 32 mins respectively to become colourless. Unexpectedly, the higher rutile content sample degraded the dye approximately twice as fast as

the high anatase content samples. Whilst high anatase content would suggest higher photocatalytic activity, the high rutile samples were thinner (the two high anatase content films were 1478 nm and 1602 nm and the higher rutile content samples were 246 nm and 212 nm). These results may suggest that anatase and rutile are working together synergistically or that there are benefits from having a thinner film which outweigh high anatase content. It has previously been shown that thickness can affect photocatalytic activity.[67] It is also likely that difference in morphology, and therefore surface area would also affect photocatalytic activity. The ability to degrade organic material such as pollutants is a useful property for steel to possess particularly in construction industries for use as building materials and for vehicles.

2.3.1.5 Photoinduced Superhydrophilicity

As a further confirmation of photoreactivity, contact angles for samples which had been stored in the dark and samples which had been irradiated for 1 hour under 254 nm light were measured. For all depositions on steel substrates the irradiation caused superhydrophilicity i.e. the contact angle was less than 5°. Samples which had not been irradiated had contact angles ranging between 30° and 85°. The samples which had higher contact angles were noticed to be those with some delamination and did not correlate with the type of steel used as the substrate. Greater roughness is known to give more hydrophobic character. Delamination typically occurred with thicker films which may have had a rougher morphology leading to the higher contact angles. Photoinduced superhydrophilicity, PSH has been shown to improve self-cleaning properties since impurities can be more easily washed away. Along with the photocatalytic degradation of organic material, TiO_2 is an excellent candidate for self-cleaning surfaces.

2.3.1.6 Summary

It has been shown that high anatase content films may be produced from $TiCl_4$ and ethyl acetate at 500 °C by APCVD on 304, 304L, 316, 316L grade steel, titanium metal, titanium metal coated with gold and also steel (316 grade) coated with gold. We have demonstrated that under these conditions there is no substrate selective phase deposition, given that both anatase and rutile have been observed on the same substrate. This variation across a substrate is most likely due to small variation in reaction conditions at different points within the reactor due to changes in temperature and chemical depletion of the precursors. It is suggested that the reason for this contrast to previous literature (which reported that only rutile could form on stainless steel substrates from ethyl acetate and $TiCl_4$) is related to the flow dynamics of the individual reaction chamber. Predominantly anatase phase is produced in the vast majority of areas regardless of the grade of steel used as the substrate. These materials show promise for a range of applications including self-cleaning surfaces, water and air purification systems and water-splitting, based on the positive results of photocatalytic testing.

2.3.2 TiO_2 on flexible aluminium film

Titanium dioxide thin films were deposited onto squares (25 mm x 25 mm) of household aluminium foil using standard conditions of APCVD. Numerous samples were made and those which illustrate the important trends are discussed below. Delamination of the film from an aluminium substrate was never observed, unlike steel which is only fully adherent within a narrow range of carefully selected deposition parameters. Samples of titania on aluminium foil were revisited after three years of storage in standard laboratory conditions with no loss of quality or adhesion. This, again, is in contrast to steel, which slowly oxidises over time (presumably through small scale cracks in the film) and can lead to gradual delamination of the titania film.

2.3.2.1 Flexibility

The depositions on aluminium foil were carried out without a top plate in order to monitor the state of the foil through heating and cooling. Throughout the heating, equilibration (minimum of 45 mins at target temperature of 500 °C) and deposition stages, the aluminium foil remained flat however after the deposition and the carbon block was switched off the foil began to curl up. In areas with a thin film of TiO_2 this was just curling slightly from the edges. However in areas of thicker film, the foil curled up so much so that it formed a tight coiled tube. Upon reaching room temperature, the samples could be removed from the reactor and uncurled to be flat without any cracking or delamination of the TiO_2 film. Photographs of a typical film are shown in Figure 20.

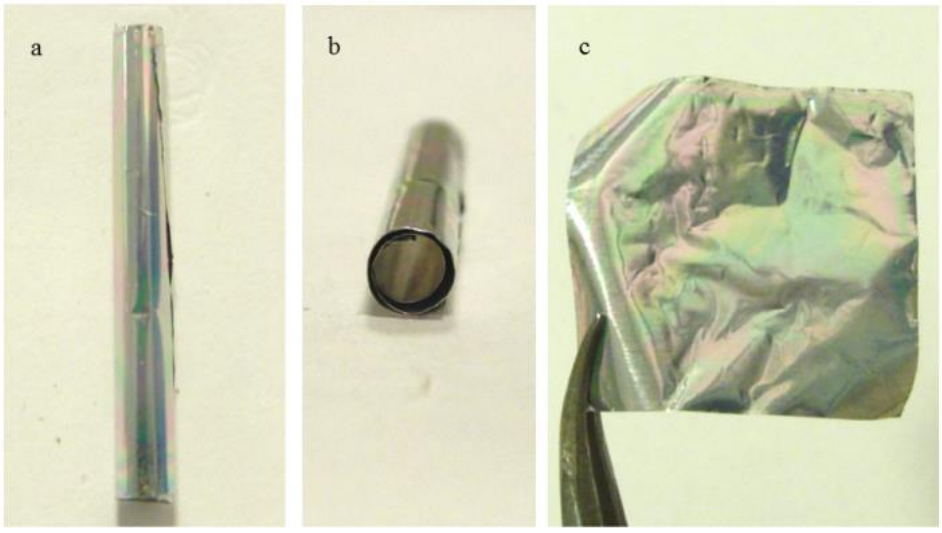

Figure 20 Titania on aluminium foil (25 mm x 25 mm) coiled into a tube a) top down view b) side view and c) uncurled and flattened.

In Figure 20c it is also possible to see the coloured interference fringes of the TiO_2 thin film. The flexibility of these films is a rather unusual property since flexing of the substrate would usually result in cracking, flaking and delamination of the titania film. Deposition of a moderately thick film on steel usually leads to delamination on cooling due to different expansion rates of the titanium dioxide and the foil. This can be prevented either by having a thinner film and also by

slow cooling of the carbon block, however, this is not necessary when the substrate is aluminium foil. Even with a deposition time of five minutes the same is observed. To investigate the robustness of the film, a sample was weighed using a four decimal place balance and then bent, folded and rolled into a small ball and then uncurled and flattened and weighed again. This procedure was repeated ten times with no loss of mass, indicating that the film is not flaking off or delaminating. This is also evident by visual inspection. In fact the robustness of the sample is only limited by the fragility of the foil itself and its tendency to rip or tear if not handled with care. It was hypothesised that the superior adhesion of the titanium dioxide to the aluminium substrate may be due to improved interaction of the two oxide materials, given that the surface of the aluminium substrate will be the oxide rather than metallic aluminium.

To further investigate the conditions which lead to flexible TiO_2, very thin steel coupons were purchased with a similar thickness to the aluminium foil, 0.01 mm. This also led to flexible TiO_2 which again, could be bent folded and rolled up without any delamination or flaking of the film. This would suggest the identity of the metal is not important but that it may be the thinness and foil nature of the substrate which gives the superior adhesion since, as previously mentioned, steel substrates that are thicker i.e. 0.1 mm do have a tendency to delaminate if cooled to quickly or if the titania film is too thick. The thinness of the substrate may allow greater deformation during cooling (i.e. curling up) which matches the contraction of the titania during cooling resulting in less stress in the film. The thicker substrate may not be able to deform to the same extent due to its own weight.

A typical film was chosen for detailed characterisation, referred to as sample TiO_2-Al. This film was deposited by the decomposition of $TiCl_4$ and ethyl acetate with mass flow rates of 3×10^{-3} and 5×10^{-3} mol/min, respectively, 6.95 L/min total of nitrogen, at 500 °C, for a deposition time of 2 minutes.

2.3.2.2 Thickness measurement

The thickness of the film was calculated as 615 nm, using the Swanepoel method. Due to difficulties in obtaining UV-vis spectra because of the reflectivity of the sample and not being flat, only one thickness measurement was possible, therefore it is difficult to assess the variation in thickness across a sample.

2.3.2.3 Raman Spectroscopy

Sample TiO_2-Al, was determined by Raman spectroscopy to be purely anatase phase as shown in Figure 21.

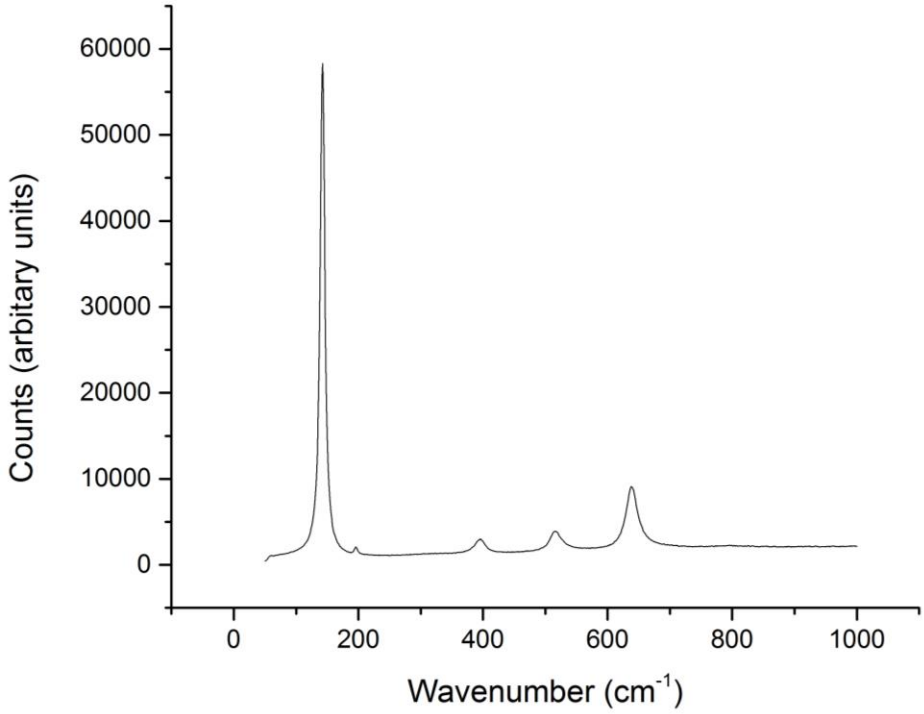

Figure 21 Raman spectrum of titanium dioxide on aluminium foil, TiO_2-Al.

The spectrum in Figure 21 shows peaks consistent with those reported for anatase in the literature.[101] No evidence of any other phase can be seen. The sample was analysed at several points and anatase was consistently present in all areas

tested. The TiO_2 on thin steel was also shown to be anatase. The anatase phase observed correlates with the findings presented in section 2.3.1 and adds further evidence to support the idea that the deposition conditions are more important than the nature of the substrate surface in determining crystalline phase.

2.3.2.4 X-ray Diffraction

The X-ray diffraction pattern for sample TiO_2-Al is shown in Figure 22.

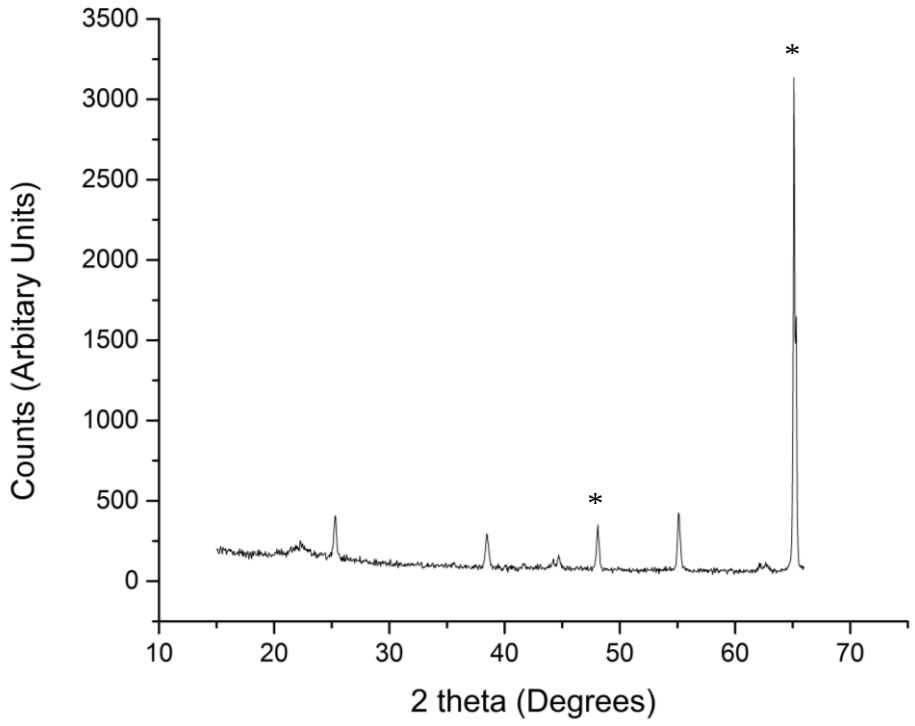

Figure 22 XRD data for sample TiO_2-Al, * indicates substrate peaks.

The peaks at 25.3°, 38.5°, 48.1° and 55.1° 2Θ at can be matched to a reference anatase XRD pattern (ICSD 44882). The peaks at 44.7° and 65.1° 2Θ (as indicated by '*') can be assigned to the aluminium substrate (ICSD 64700). This confirms the phase assignment from Raman data and also shows no other phase is present.

2.3.2.5 Scanning Electron Microscopy

The morphology of the surface was investigated by SEM, a typical image is given in Figure 23.

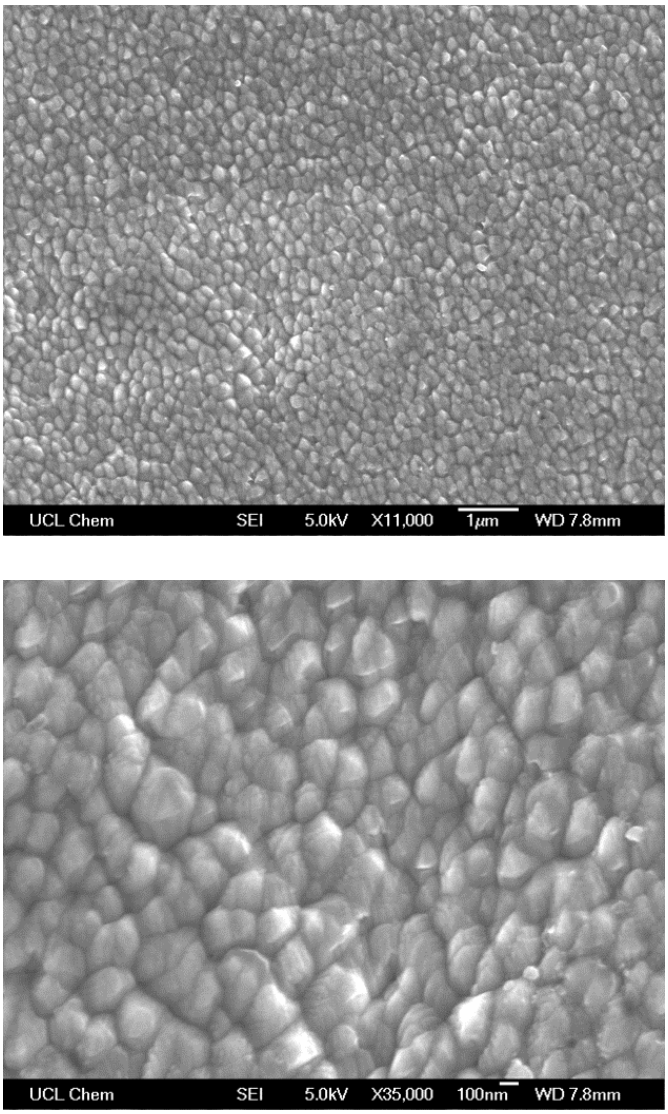

Figure 23 SEM images of sample TiO_2-Al.

These images show particles with a size of the order of 200 nm. This is similar to some of the anatase films deposited on steel that are detailed in section 2.3.1. These images also show that there are no cracks in the film at a micron level, although cracks could occasionally be found when moving the electron beam

around the sample that were typically many millimetres apart and measuring approximately 100 nm in width. This demonstrates that the film is well adhered at the submicron level.

2.3.2.6 X-Ray Photoelectron Spectroscopy

Analysis using XPS was carried out in order to determine if aluminium was present in the titania film. Depth profiling was used to ascertain if aluminium was present at deeper levels within the film, i.e. not just the surface. A high resolution scan of the energy region where a Al 2p signal would be expected at the deepest level of the depth profile (level 9) is shown in Figure 24.

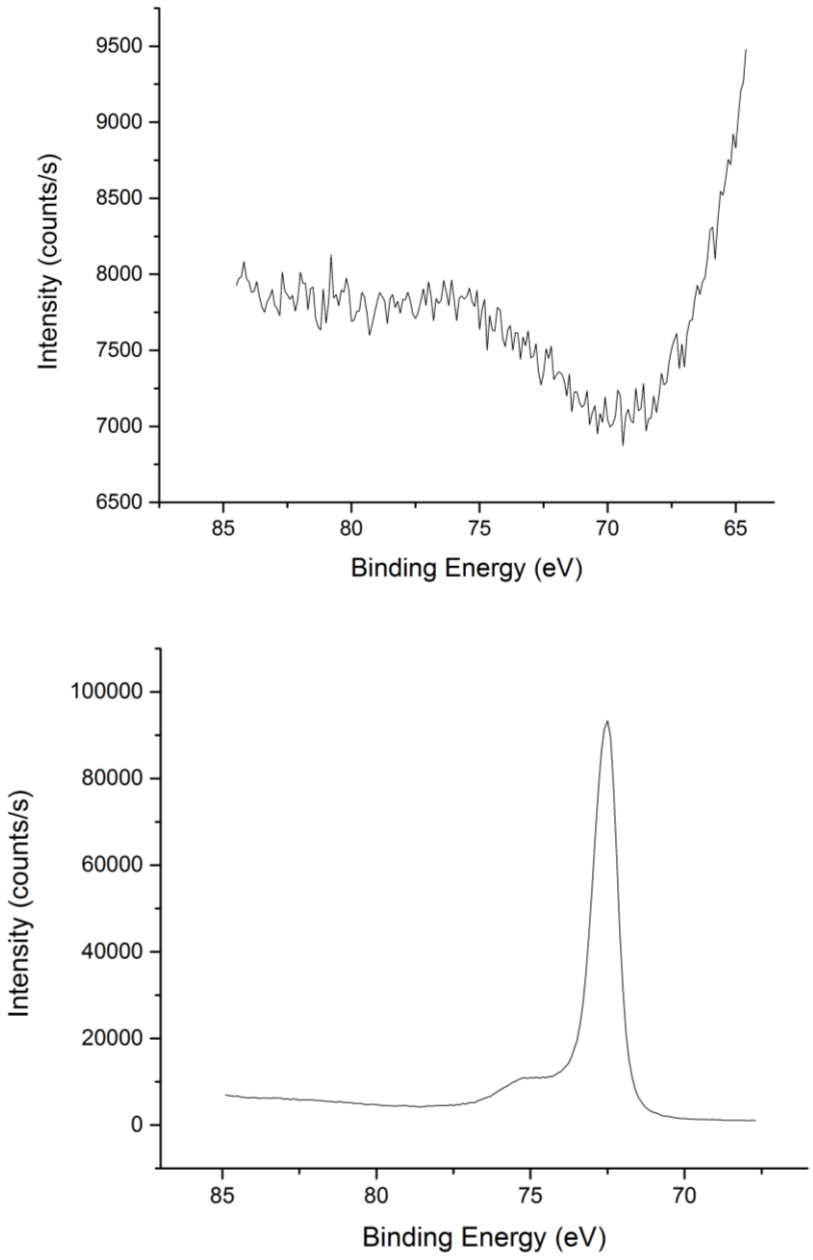

Figure 24 XPS aluminium 2p scan for sample TiO_2-Al (top) and uncoated aluminium foil (bottom).

The data above shows that there is no peak for aluminium for sample TiO_2-Al, above the detection limit of XPS (approximately 0.1%) indicating that aluminium ions have not diffused into the TiO_2 film at this level, however it is not possible to rule out that there may be Al^{3+} nearer the interface with the substrate. The data for uncoated aluminium foil, with a clear peak, is also shown for comparison. Diffusion of metal ions into CVD films is a known phenomenon [102] however

here, thickness (they report 156 nm) may be influential. Previous studies have shown that the presence of Al^{3+} ions in titania are detrimental to the photocatalytic activity. The absence of aluminium near the surface of this sample suggests that it is a promising candidate for an active photocatalyst.

2.3.2.7 Resazurin Ink Test

As a preliminary, qualitative test of photocatalytic activity, resazurin ink was deposited on the surface of sample TiO_2-Al, on a piece of uncoated aluminium as a blank and also a piece of Pilkington Activ glass for comparison of photocatalytic efficacy. Pilkington Activ glass has a thin layer of photocatalytically active crystalline TiO_2 and has been suggested in the literature as a suitable reference for photocatalytic films.[103] The samples were pre-irradiated with 254 nm light to clean the surface before ink deposition. The photographs in Figure 25 show the colour of the resazurin ink immediately after deposition, after 15 minutes irradiation with 365 nm light and after two hours irradiation.

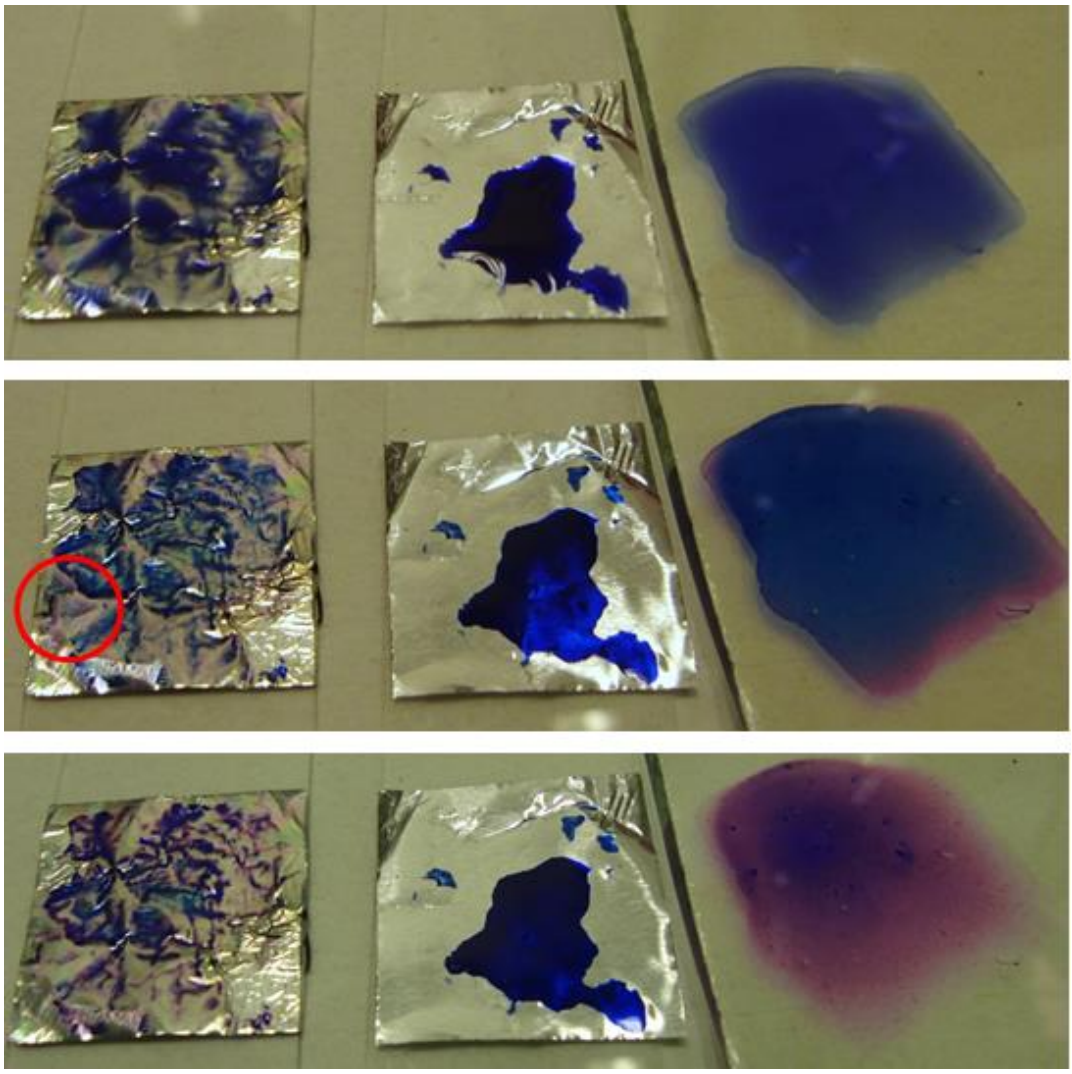

Figure 25 Resazurin ink on TiO_2-Al (left), uncoated aluminium foil (centre) and Activ glass (right) prior to irradiation (top), after 15 mins irradiation (middle) and 2 hours irradiation (bottom).

The ink was left to dry for over 1 hour after deposition onto the surfaces without any UV irradiation, i.e. a dark test. No colour change was observed after this time indicating that there are there were no reactive surface species present due to the pre-irradiation with 254 nm light. The central images clearly illustrate that the ink does not spread well on the uncoated foil substrate due to the hydrophobic nature of the surface. This means that the ink on the uncoated foil is much thicker than on the Activ glass. The coverage on the TiO_2 is, as expected, somewhat improved, however because the sample is not perfectly flat, small wells of ink were formed in the creases on the foil. The coloured interference fringes of the TiO_2 thin films

also add an additional challenge to monitoring any colour change. Despite this, it was still possible to observe the transition from blue to pink of the ink on sample TiO_2-Al. After 15 mins, the ink on Activ glass has begun to change colour at the edges where the ink is thinnest. There is also an observable colour change on the TiO_2 coated foil. Although it is more clearly seen by eye than photography, inspection of the area circled in red does show pinkish coloured when compared to the corresponding image above. After two hours the pink colour is easily discernable on the photograph. Bleaching of the resorufin is seen on the Activ glass but the colourless, transparent film is almost impossible to see on the TiO_2 coated foil. Crucially, there is no colour change on the uncoated aluminium foil, even in the three small spots of thinner ink. This demonstrates that the reduction of the dye is not possible without the photocatalytic action of TiO_2. The rate of reduction for the TiO_2 coated foil is comparable with the Activ glass although this test does not allow for precise evaluation. This is an interesting result as one may have expected diffusion of aluminium ions into the TiO_2 and hence the destruction of its photocatalytic properties. Although the comparison of activity to the Activ glass must be treated with caution since the ink deposition is not reproducible or well controlled, this purely qualitative test provides evidence that the TiO_2 coated aluminium is indeed photocatalytically active and that the rate is competitive with that of Activ and thus worthy of further investigation.

2.3.2.8 NO_x Test

A second more quantitative photocatalytic test was used, the destruction of NO_x gas. For this a titania thin film sample of 10 cm x 5 cm on aluminium foil was produced and a modified ISO standard test was performed and compared to the results obtained with a 10 cm x 5 cm piece of uncoated aluminium foil. The results are shown in Figure 26.

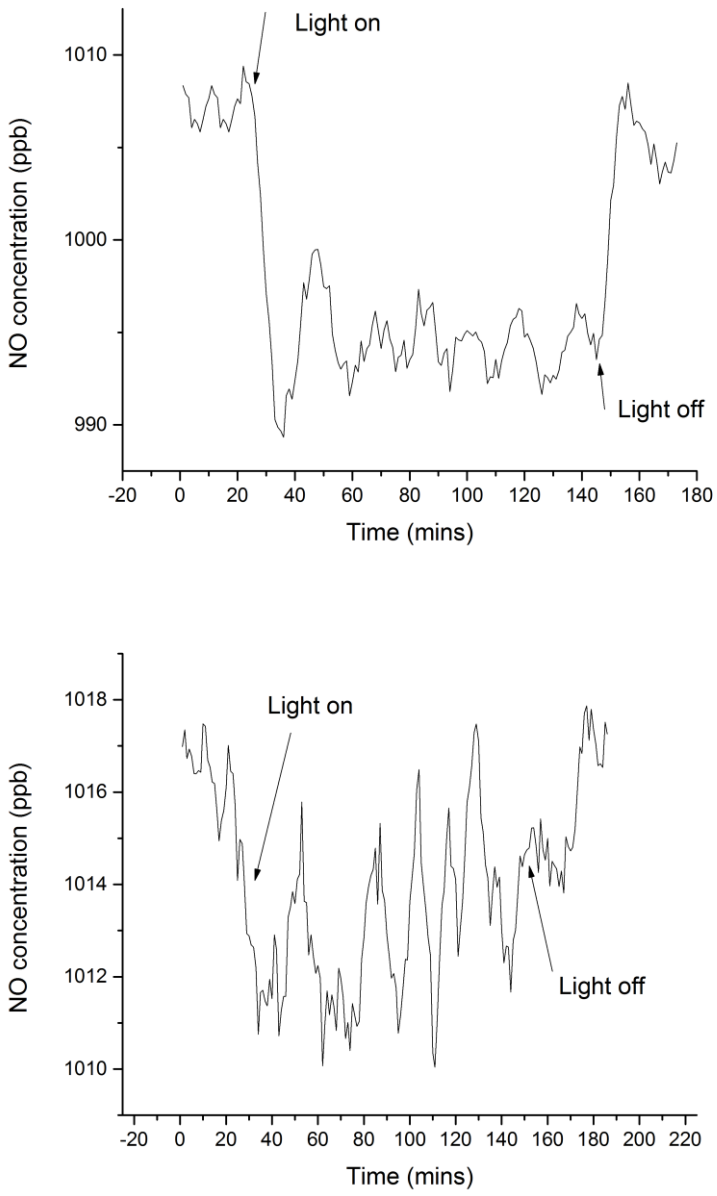

Figure 26 Change in NO concentration during irradiation of TiO_2 coated aluminium foil (top) and uncoated aluminium foil (bottom).

It is clear to see that there is a slight decrease in the concentration of NO when the sample of TiO_2 coated aluminium foil is illuminated. When the light is switched off the concentration of NO returns to the same level as prior to irradiation of the sample. However this level of response is very small when compared to an industry standard titania thin film on glass, i.e. Pilkington Activ. The percentage of NO removal was calculated to be 1.24%, 19.20% and 0.27% for the titania

coated aluminium, Activ glass and uncoated foil respectively. This large difference in activity between the titania coated aluminium and the Activ is in contrast with the Rz ink test which showed comparable activity. One possible reason could be that different samples were used in the NO_x and ink test which may have had some differing property that was not measured, however they were both pure anatase phase as determined by Raman and deposited with similar synthetic parameters. The two tests work by a different mechanism, for the ink test the process is a reduction, however for NO_x the process is oxidative. Therefore the poorer comparative performance of the titania coated foil in the NO_x test may suggest it has fewer oxidising species on its surface.

Nonetheless in both tests, the titania coated foil showed a response to the irradiation indicating that it is photocatalytically active and the presence of the aluminium substrate is not prohibitive to use in self-cleaning and pollution management applications. The combination of these two tests provide an encouraging starting point but a more sensitive, quantitative test method is required in order to identify optimised properties, and thus deposition parameters, to generate highly active films.

2.3.2.9 Summary

It has been demonstrated that aluminium is a suitable substrate for titania CVD films. The titania coating is well adhered even after repeated bending and folding. XPS analysis has shown that aluminium ions have not diffused into the coating. Preliminary tests have shown that these films are photocatalytically active. The prospect of a flexible, lightweight and robust photocatalyst would be attractive to the construction, healthcare and packaging industries. The ability to curl up this material, in the same manner as kitchen aluminium foil would be convenient for storage and transport.

2.3.3 TiO_2 coatings for biomedical implants

It was found that using similar deposition conditions for the APCVD of TiO_2 on steel, led to well adhered films on the CoCrMo alloy, which displayed the characteristic coloured interference fringes. Similarly to steel, it was observed that titania films over a critical thickness led to flakiness and delamination from the substrate. Naturally, it became difficult to measure the thickness of a film which had delaminated but the thickest film that was measured and not delaminated was 1380 nm. The films could not be removed by scratching with a steel spatula but could be marked by a diamond pen.

Typically between 20 and 30 discs were coated in each deposition in rows of four. Optimum deposition conditions were identified by feedback from collaborators which gave highly active samples. The data for one particular batch with 22 discs that was identified as active, was characterised in detail. This film was deposited by the decomposition of $TiCl_4$ and ethyl acetate with mass flow rates of 8×10^{-3} and 5×10^{-3} mol/min, respectively, 4.6 L/min total of nitrogen, at 500 °C, for a deposition time of 45 seconds. The data for these 22 discs are presented in the subsequent sections and are denoted as sample TiO_2-CoCrMo.

2.3.3.1 Thickness

Using the optimum conditions, an investigation into the thickness and variation in thickness was carried out. It was shown using a deposition time of 45 seconds, the average approximate thickness was 550 nm but with a range from 316 nm up to 830 nm, as shown in Figure 27.

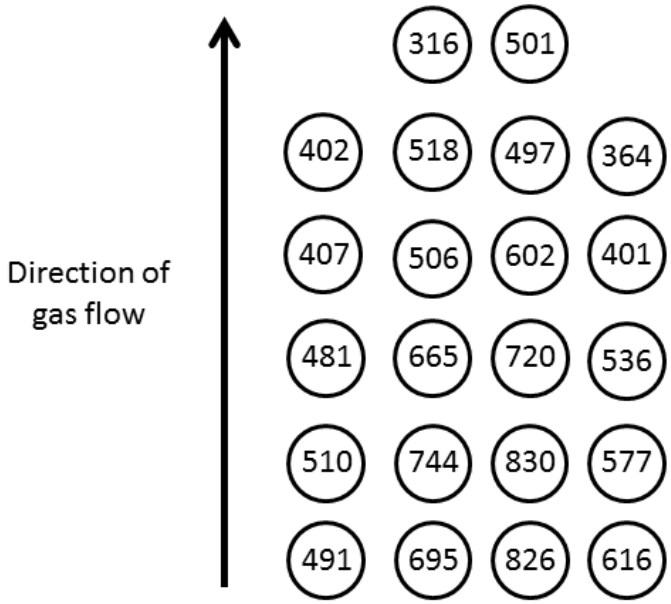

Figure 27 Thickness in nm for each disc, displayed as arranged within the reactor.

In general the central two rows (with respect to the direction of gas flow) had the thickest films, with thinner films nearer the walls of the reactor, likely due to slightly cooler substrate near the (cold) walls of the reactor. Also there was a general decrease in thickness towards the back of the reactor, presumable due to precursor depletion. One exception to this trend is that the front most row is slightly thinner than the second row which may be due to the precursors becoming hotter as they enter the reactor zone. These trends have previously been observed for horizontal, cold-wall CVD reactors.[104]These values were derived by measuring the UV-vis spectrum on a Filmetrics instrument and analysing the data using the Swanepoel method .

2.3.3.2 Raman Spectroscopy

A phase study was conducted, analysing the centre of every disc using Raman spectroscopy. It was found that in the vast majority of cases the phase was pure

anatase however a small amount of brookite was observed in one or two positions. Two representative spectra are given in Figure 28.

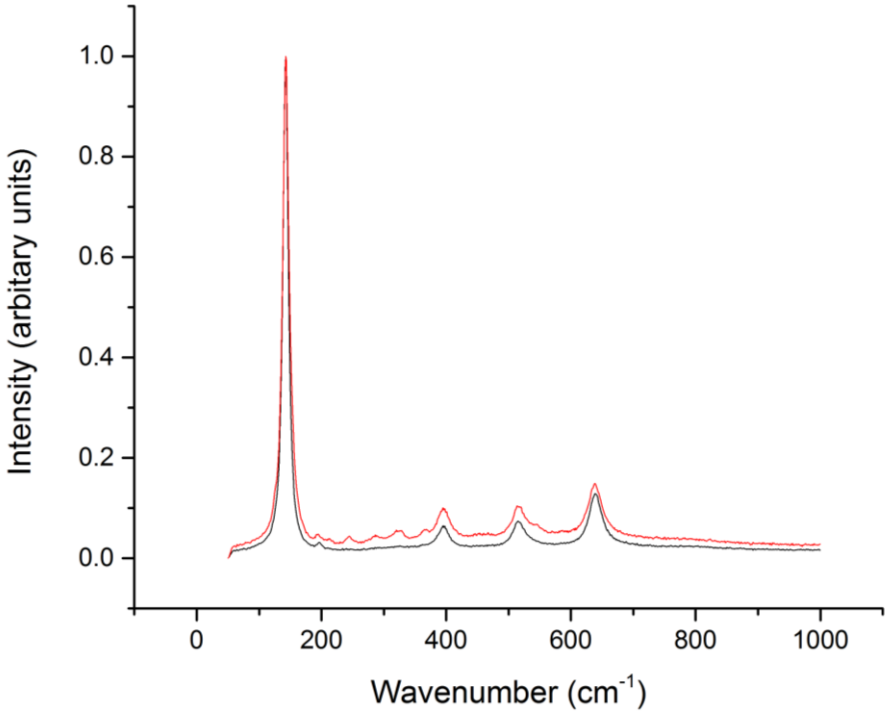

Figure 28 Raman spectra of pure titania coatings on CoCrMo discs.

The black trace shows pure anatase,[101] whereas the additional peaks in the 200-390 cm^{-1} region of the red trace indicate the presence of brookite.[105] The formation of brookite is covered in detail in Chapter 4. There was little consistency between runs regarding where on the substrate the brookite was observed. On one occasion, two discs from the front row showed some brookite yet a further deposition, with the same parameters, brookite formation was observed on two discs in the last row nearest to the exhaust. It was found that this relatively small amount of brookite did not affect the functionality of the films.

2.3.3.3 X-ray Diffraction

A thorough XRD study was conducted, by analysing all 22 discs from one deposition, in order to establish if there is any difference in the crystallinity in the

titania films deposited on discs from different positions within the reactor. A previous study has shown differences in preferred orientation in different areas of a similar CVD reactor.[104] The XRD diffraction patterns of discs 1-22 from sample TiO_2-CoCrMo are shown in Figure 29.

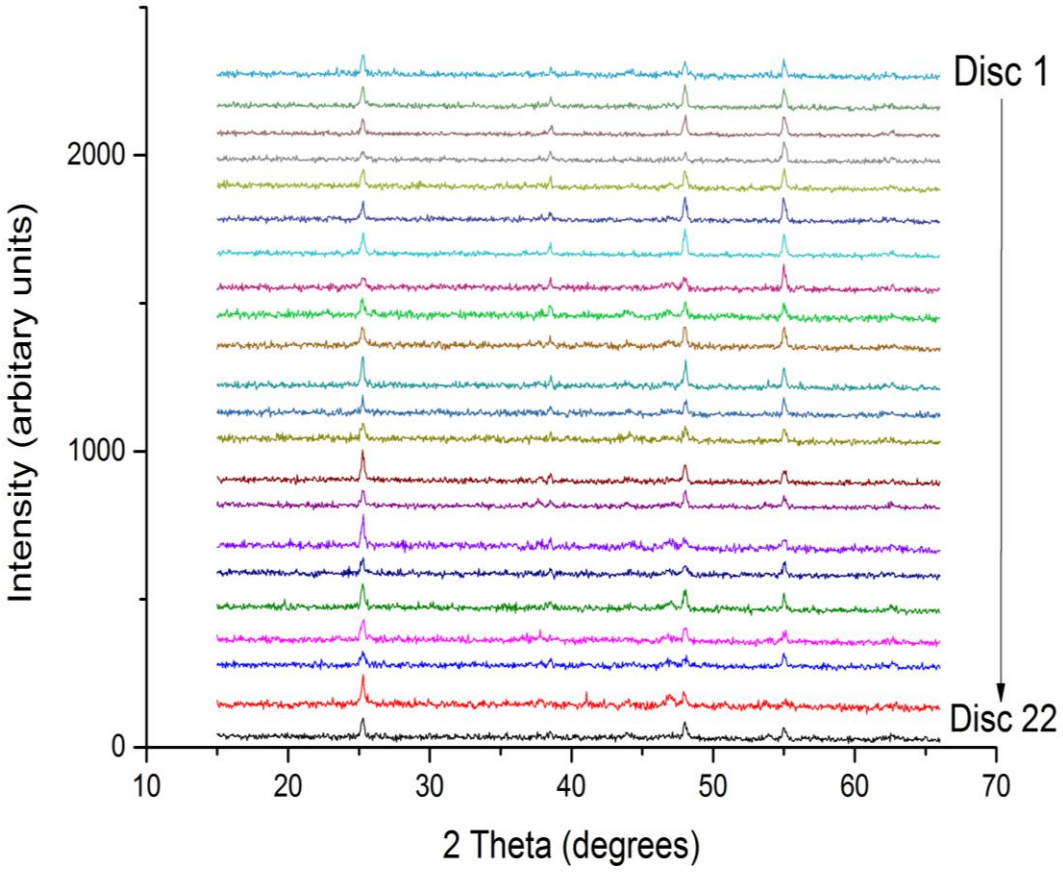

Figure 29 XRD data for sample TiO_2-CoCrMo discs 1 to 22.

All the peaks in every diffraction pattern in Figure 29 can be matched to anatase (ICSD 44882). There are some small differences in relative intensities of different reflections between the different discs but are not deemed to be significant and no clear trends in crystallinity are observable. This is in contrast to the aforementioned study, which reports a switch in the relative intensity of the (112) and (200) peaks from titania on a glass substrate. However in their experiment the deposition was carried out at 450 °C rather than 500 °C.[104] This could indicate that formation of a homogenously crystalline film is easier to obtain on CoCrMo than it is on glass.

2.3.3.4 X-ray Photoelectron Spectroscopy

Analysis of the composition of the surface and material close to the surface was carried out using XPS with depth profiling i.e. bombardment with argon ions to remove surface material. Two discs from sample TiO_2-CoCrMo were analysed along with an uncoated CoCrMo disc and an uncoated titanium disc. The two discs from sample TiO_2-CoCrMo gave practically identical data. A titanium 2p signal and oxygen 1s signal were observed on the surface and are shown in Figure 30 below.

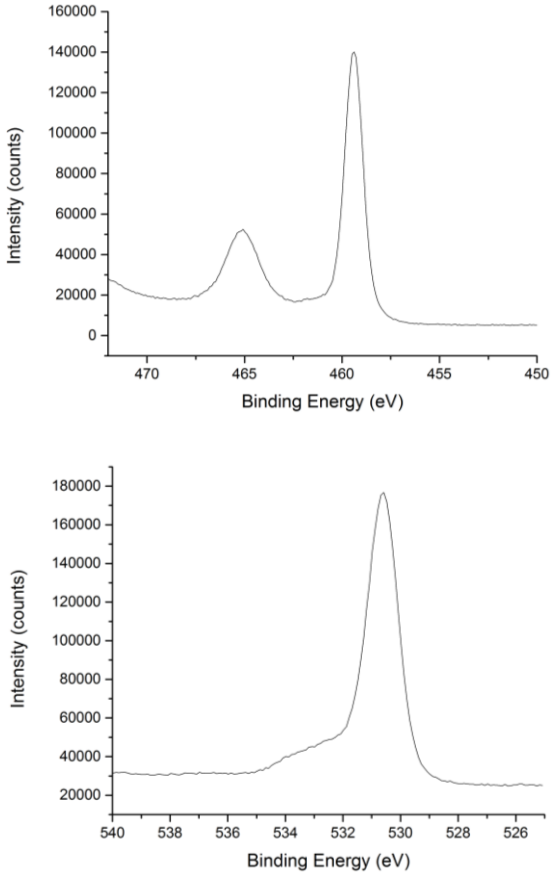

Figure 30 XPS spectrum of the titanium 2p region (top) and the oxygen 1s region (bottom) on the surface of TiO_2-CoCrMo.

The titanium $2p_{3/2}$ peak is positioned at 459.5 eV and the $2p_{1/2}$ peak is at 465.2 eV, giving a peak separation of 5.7 eV. These observations correlate well with literature reports of the titanium environment in TiO_2.[106] At lower etch levels a

slight shoulder at lower energy on the Ti 2p peak appeared indicating the formation of Ti^{3+}. This reduction of a small amount of the native elements is a well-known side effect of sputtering. The oxygen 1s peak occurs at 530.6 eV with a shoulder at higher binding energies which has been attributed, in the literature, to the oxygen in titanium dioxide and hydroxyls, chemisorbed oxygen or adsorbed water, respectively.[107] These data confirm the identity of the material as titanium dioxide.

No signals from cobalt or molybdenum were observed in either disc from sample TiO_2-CoCrMo at any etch level. However the high resolution scan of the energy region in which a chromium 2p signal would be expected, on first inspection, may appear to show a peak. High resolution scans in the chromium 2p region were also performed on the uncoated titanium and an uncoated CoCrMo disc. A similar signal was observed on the titanium disc but a very clear peak was identified on the CoCrMo disc. Since the titanium disc can be assumed to have no chromium present this, therefore, led to the conclusion that the apparent peak for the titanium disc and sample TiO_2-CoCrMo was in fact just noise. For comparison, these signals are shown in Figure 31.

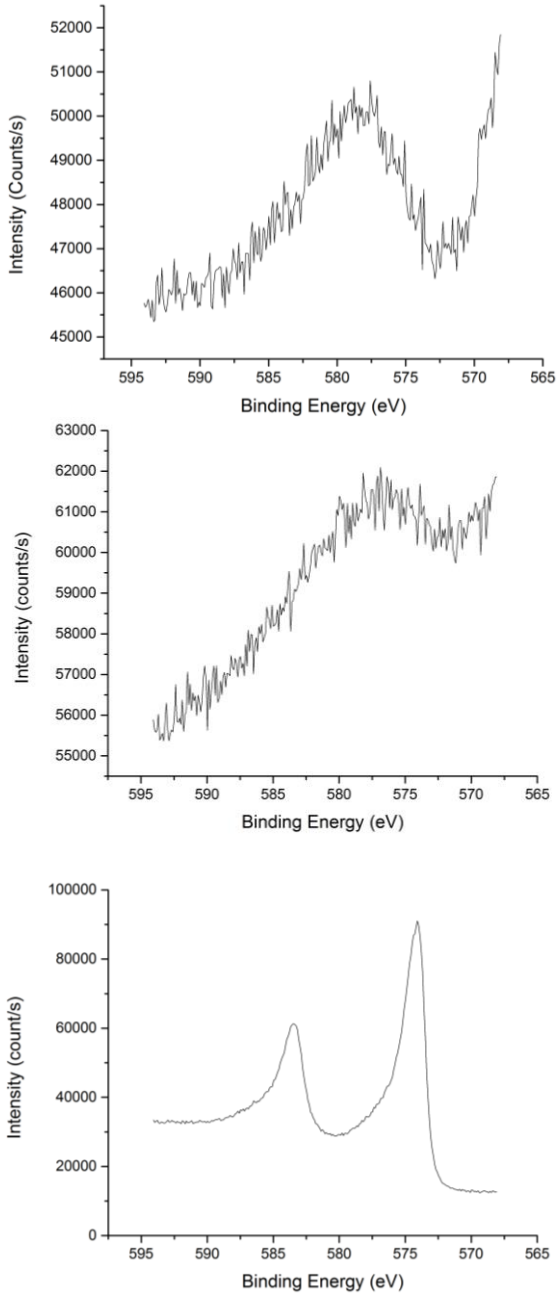

Figure 31 XPS spectra in the chromium 2p region for sample TiO_2-CoCrMo (top), uncoated Ti (middle) and uncoated CoCrMo disc (bottom).

The XPS data was also used to confirm the percentage of each alloying element against the manufacturer's specification. The manufacturer states the chromium content should be between 26-30% and the molybdenum content at 5-7% with the remainder as cobalt. The XPS data showed good agreement with chromium at 29.40 % and molybdenum at 7.51%.

2.3.3.5 Cell Morphology

The biocompatibility of the TiO_2 coated discs was assessed by studying the level of certain markers which are known to indicate the efficacy of an implant as a bone substitute. Human mesenchymal stem cells (hMSCs) are capable of developing into osteoblasts (bone cells), chondrocytes (cartilage cell), adipocytes (fat cells) or other specific cell types,[108] and are the first osteogenic cells recruited to this type of site in-vivo following implant surgery.[109] Osseointegration of an implant is determined by a number of factors such as shape, size and topology of the device, surface topography surface chemistry, as well as patient variables such as quantity and quality of bone and also surgical technique. The interface between the bone and metal surfaces should promote an environment which stimulates hMSCs to develop into osteoblasts therefore resulting in an interfacial layer of bone matrix of sufficient biomechanical strength.[110] In this work, hMSCs were used to assess the level of osteogenic differentiation occurring on a titanium, CoCrMo and TiO_2 coated CoCrMo surfaces. The specific markers studied were cytoskeletal structure, calcium deposition and formation of hydroxyapatite and type I collagen.

A cell's scaffold, or cytoskeleton, is in part, formed of F-actin proteins. In this study, F-actin proteins were labelled with a fluorescent marker and visualised using confocal laser microscopy. The F-actin fibres (their cytoskeletal shape) of MSC cells cultured on CoCrMo and TiO_2-CoCrMo surfaces were studied after one day and seven days, images are shown below in Figure 32.

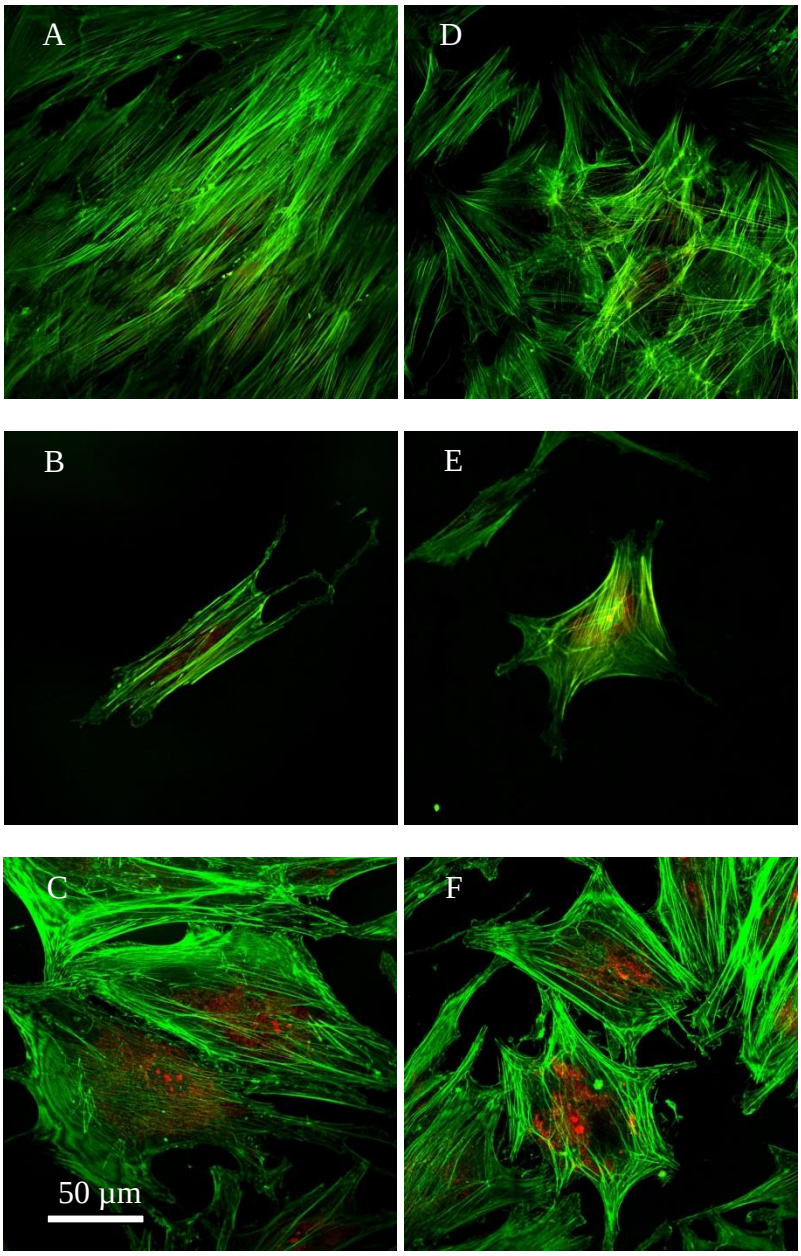

Figure 32 Fluorescent microscopy of F-actin fibres on CoCrMo surface (A-C) and TiO_2-CoCrMo surface (D-F). A, B, D and E are after one day, C and F are after seven days. A, D, C and F are of cell aggregates and B and E are single cells.

The F-actin proteins appear green and cell nuclei have been counter stained red as shown in the images in Figure 32. When comparing images A and D (cell aggregates after one day on CoCrMo and TiO_2-CoCrMo surfaces respectively) it is clear to see a difference in the cell shape. The cells in A appear to be more elongated and fibrous whereas the cells in D are more spread-out, spherical and criss-crossed. This is also apparent when comparing figures B and E, which show

individual cells after one day on CoCrMo and TiO_2-CoCrMo surfaces respectively This type of spherical, criss-crossed shape has been shown to be a characteristic of osteogenic differentiation of hMSCs.[111] After seven days, figures C and F, there does not appear to be any significant difference in the shapes of the cells. These results indicate that the TiO_2 coated CoCrMo samples accelerated the osteogenic response as evidenced by more rapid reorganisation of the cellular cytoskeleton. After seven days, the cells on both surfaces showed cells in the later stages of osteogenesis.

2.3.3.6 Hydroxyapatite and Collagen Formation

In addition to changes in shape during osteogenic differentiation, the cells also excrete extra-cellular matrix (ECM) which is rich in collagen and calcium. This mineralises into bone tissue, known as hydroxyapatite, which contains calcium phosphates as well as proteins and enzymes. Within the ECM, collagen can act as a scaffold for calcium nucleation. Here, collagen and hydroxyapatite were stained with fluorescent markers and studied with fluorescent microscopy. Again, hMSCs were cultured on CoCrMo, TiO_2-CoCrMo and titanium surfaces. The formation of type I collagen was studied after 7 days and 14 days and hydroxyapatite was monitored after 7, 14 and 21 days. The microscopy images of collagen formation after 7 days and hydroxyapatite formation after 21 days is shown in Figure 33.

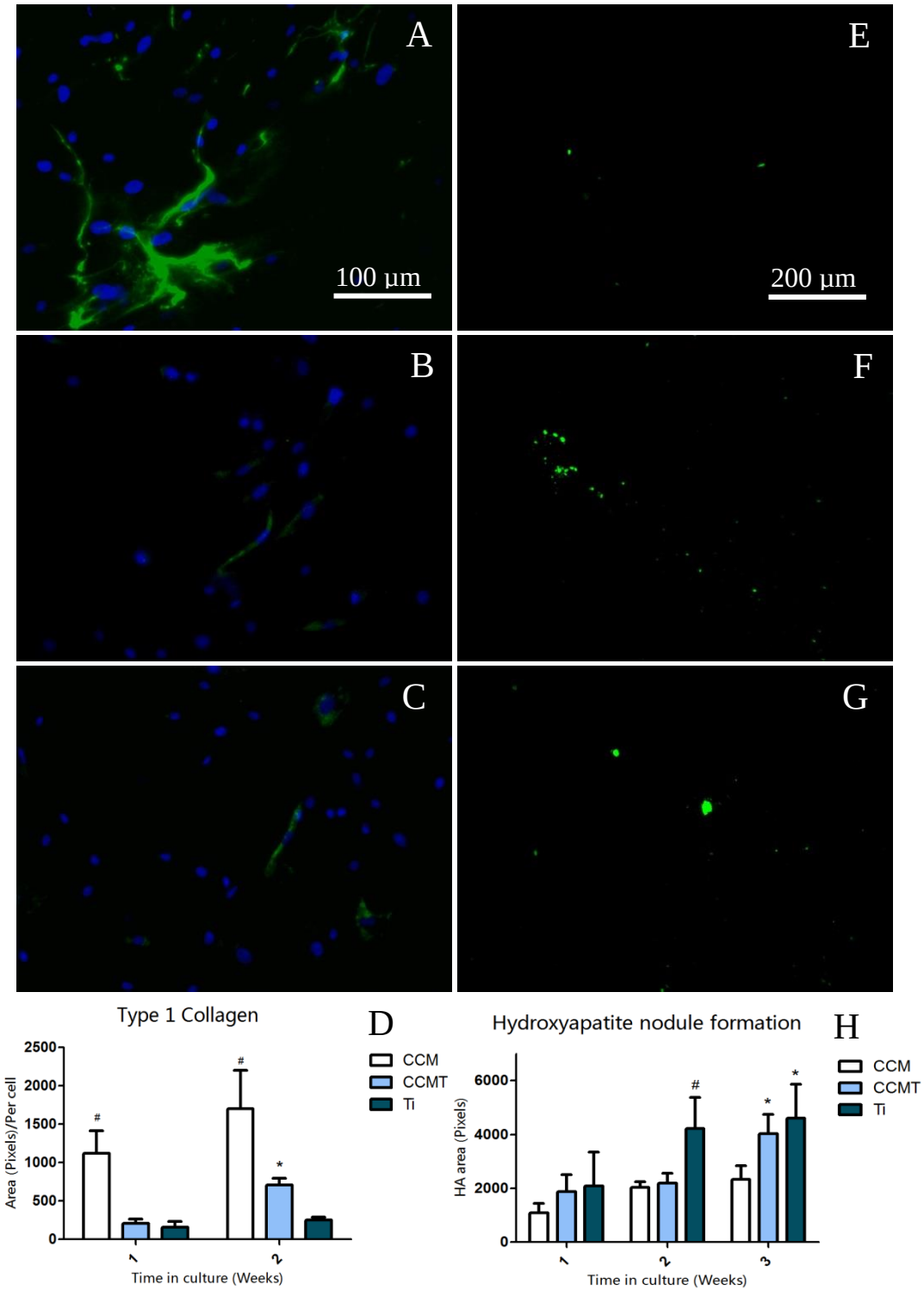

Figure 33 Fluorescent microscopy images of collagen (A-C) and of hydroxyapatite (E-G) on surfaces CoCrMo (A and E), TiO_2-CoCrMo (B and F) and titanium (C and G). D and H show the area of collagen and hydroxyapatite, respectively, for the three different surfaces. *indicates a statistically significant difference compared to CoCrMo. # indicates a statistically significant difference against the other two substrates ($p<0.05$).

These data show that type I collagen growth is more prevalent on CoCrMo surfaces than either TiO_2-CoCrMo or titanium (images A-C). The formation of hydroxyapatite appears to be similar on all three surfaces after one week, although CoCrMo does show the lowest amount. After two weeks the titanium surface shows significantly more hydroxyapatite relative to the other two surfaces and after three weeks both the TiO_2-CoCrMo and Ti surface show significantly more hydroxyapatite than the CoCrMo surface, and the performance of the TiO_2-CoCrMo surface has almost reached that of the titanium. These observations indicate that the formation of bone mineral on CoCrMo surface can be improved by the presence of the TiO_2 layer. The reduced formation of collagen on the TiO_2-CoCrMo and titanium surfaces has previously been identified as advantageous as over collagenous bone tissue can lead to mechanical weakness.[112]

2.3.3.7 Calcium Deposition

To further support the findings of the fluorescent microscopy techniques, the amount of calcium deposited per cell was also determined using a colourimetric assay. The results over three weeks for each of the three surfaces are shown in Figure 34.

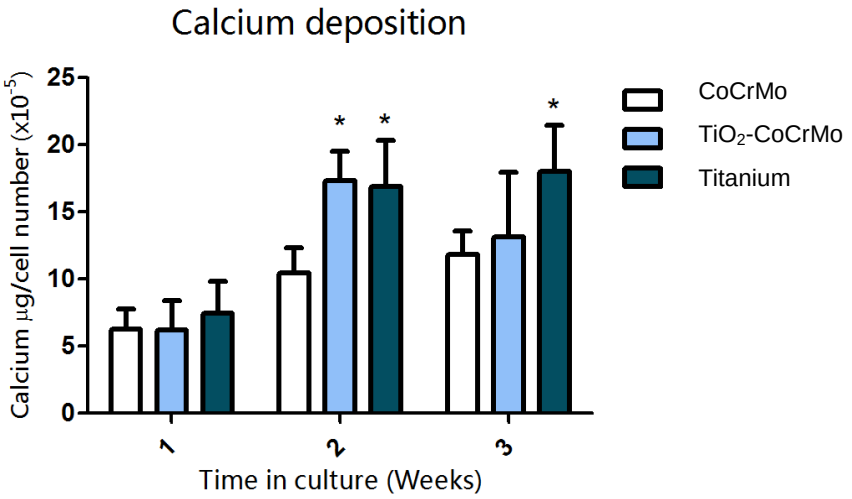

Figure 34 Calcium deposition per cell over a three week period on CoCrMo, TiO_2-CoCrMo and titanium surfaces.* indicates a statistically significant difference compared to CoCrMo ($p<0.05$).

The results in Figure 34 illustrate that the calcium deposition, required for the formation hydroxyapatite, is significantly enhanced on both the TiO_2-CoCrMo and titanium surfaces after two weeks. After three weeks the same trend is observed however the difference in calcium deposition between the CoCrMo and TiO_2-CoCrMo surfaces was determined to be statistically insignificant.

2.3.3.8 Summary

The combined results of these tests are indicative of improved and/or faster osteogenic differentiation of hMSCs on TiO_2 coated CoCrMo alloy compared to uncoated the CoCrMo substrate. This would suggest improved osseointegration however further in-vivo studies would be required in order to understand how these in-vitro experiments may translate into a clinical environment. Chemical vapour deposition has been identified as a suitable rapid, cost effective and scalable method of producing the TiO_2 coating with the required characteristics on the CoCrMo substrate. This strategy could also be considered for improving biocompatibility of other bio-inert implant materials.

2.4 Conclusions

The results presented in this chapter have demonstrated novel properties and applications of CVD TiO_2 films. Firstly, it was shown that, contrary to previous literature, anatase TiO_2 can be formed on various grades of steel and other metallic substrates from $TiCl_4$ and ethyl acetate precursors, eliminating the previously proposed theory of precursor control over crystalline phase. Secondly, TiO_2 was deposited on flexible aluminium foil and remained well adhered to the substrate after repeated bending and flexing of the aluminium foil. The photocatalytic properties may find potential applications in construction and packaging industries. Finally, TiO_2 films on CoCrMo alloys used in biomedical implants were shown to improve the osteogenic differentiation of mesenchymal stem cells relative to uncoated CoCrMo substrates. This demonstrates progress towards improving the biocompatibility of CoCrMo alloys allowing surgeons to take advantage of the better wear resistance of CoCrMo relative to titanium traditionally used for orthopaedic implants.

CHAPTER THREE

INFLUENCE OF DEPOSITION CONDITIONS ON NITROGEN DOPED TiO_2

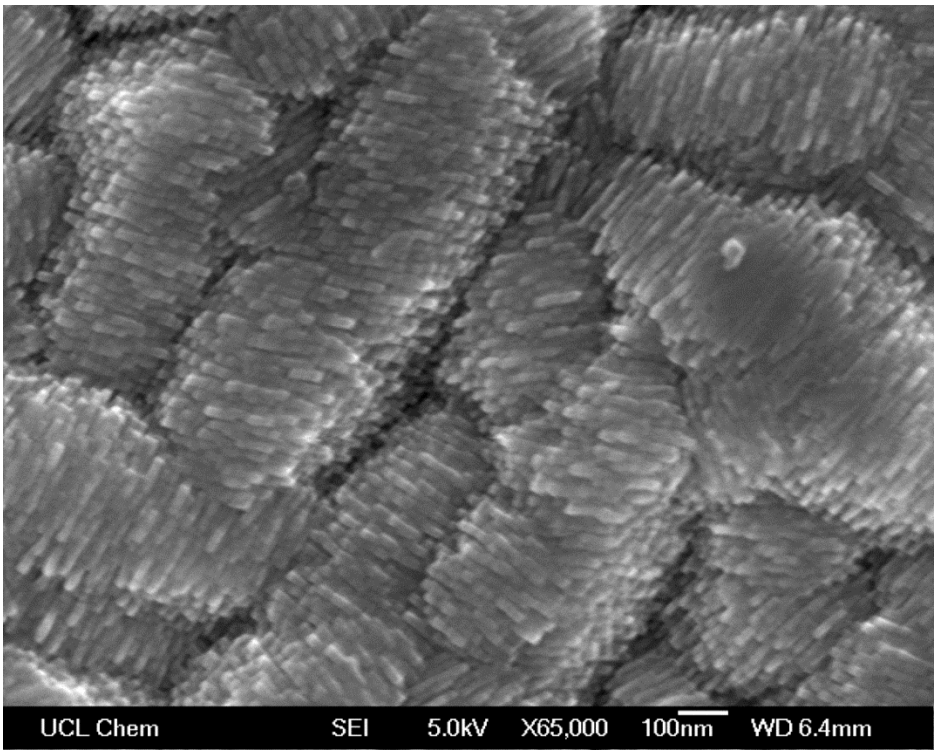

Chapter 3: Influence of Deposition Conditions on Nitrogen Doped TiO_2

Abstract

In order to use sunlight more efficiently to drive chemical reactions, researchers have sought to modify the band structure of TiO_2 to shift absorption from UV to visible light. Nitrogen doping of TiO_2 has been the subject of much debate in the field. Here, CVD is used to synthesise films with tert-butylamine as the nitrogen source and was kept at a constant flow rate for different samples. However, the amount of the oxygen source (ethyl acetate) for the depositions was varied in order to investigate the effect of this on the position of nitrogen within the crystal lattice and the consequences for the properties and photocatalytic activity of the resultant film. Differences were observed in the nitrogen XPS signal, UV-vis absorption profile, surface morphology and photocatalytic activity under both UV and visible irradiation. The sample made with low ethyl acetate conditions was found to be the most active for degradation of stearic acid.

3.1 Introduction

The prior chapters have covered many of the advantages and disadvantages of using TiO_2 as a photocatalyst. This chapter will outline the limitations of such a wide band gap for solar energy applications and summarise some of the strategies for band gap engineering that have been reported. Experimentally, this chapter focuses on results of characterisation and photocatalytic testing of nitrogen doped TiO_2 films, made by CVD, with differing amounts of ethyl acetate.

As discussed in Chapter 1 the band gap of anatase is 3.2 eV and that of rutile is 3.0 eV. The energy which is required to excite an electron from the valence band to the conduction band must equal or exceed the band gap energy. That is the equivalent of 388 nm and 413 nm light, which falls in the ultraviolet (UV) region of the electromagnetic spectrum. Given that UV light only accounts for approximately 5% of the solar spectrum,[113] as shown in Figure 35, the majority of sunlight incident on a TiO_2 particle is wasted. However if it were possible to alter the band structure of TiO_2 to make use of a greater proportion of the solar spectrum, titania based photocatalysis may become commercially viable technology for a great range of applications, including indoor uses.

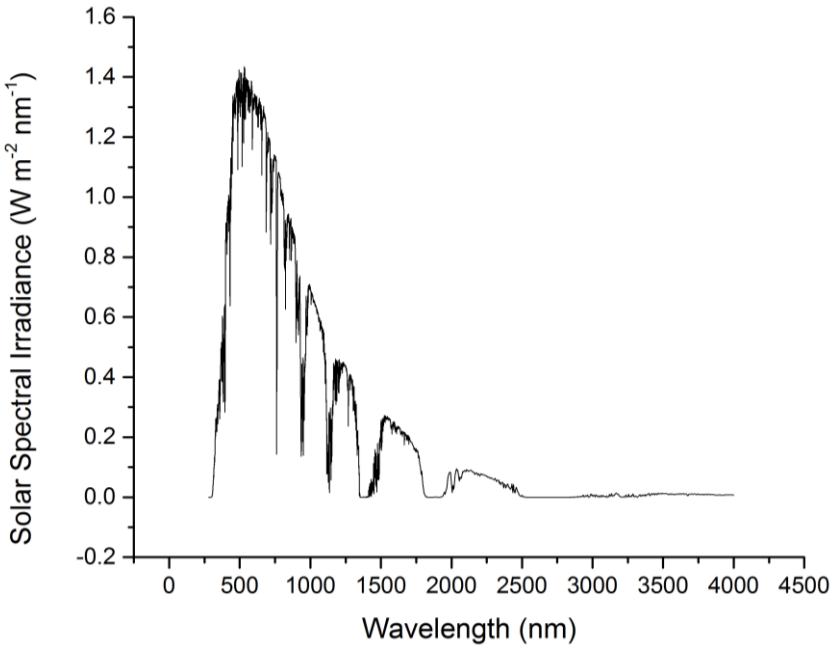

Figure 35 Spectrum of solar irradiance.

Many researchers have sought to modify titania to capture more visible light. One strategy is to partner TiO_2 with another material which itself inherently absorbs visible light and is able to transfer the energy to TiO_2. An entire research field has emerged, utilising the emergence of nanotechnology, with the goal of "sensitising" TiO_2 in this way. Some of the common strategies use a visible light absorbing dye,[114] quantum dots,[115] plasmonic metal nanoparticles[116, 117] and the formation of heterostructures of TiO_2 with other semiconductors.[118]

This work, however, is concerned with modification of TiO_2 itself by engineering the band gap to induce visible light absorption. The most commonly used strategy is the addition of dopants. Doping is a commonly used strategy to improve conductivity in semiconductors. This is the addition of a very small amount of another element with a different valency to the host. If the valency is higher than that of the host, this can result in additional electrons available for conduction. Since the charge carrier is negatively charged this is termed "n-type" doping. Whereas if the dopant has a lower valency, holes are formed in the lattice, giving rise to positive charge carriers, which is known as "p-type' doping. Figure 36 shows the mid-band states that are formed as a result of n- and p-type doping

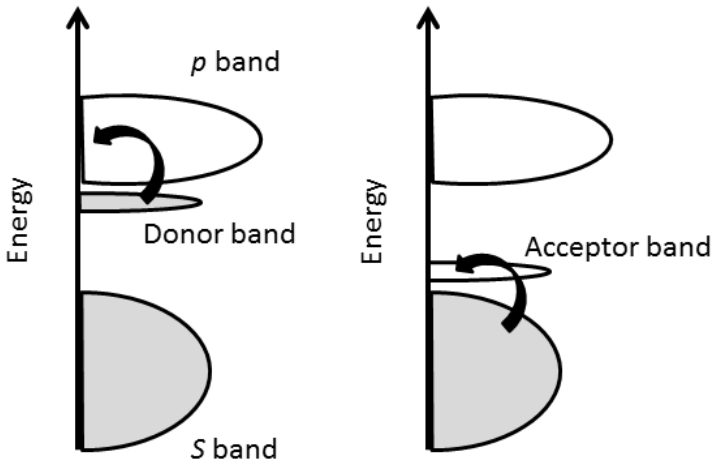

Figure 36 Density of states diagram for extrinsic doping, adapted from reference [18], n-type (left) and p-type (right).

A dopant may directly replace an atom in the crystal lattice, this is termed substitutional doping. Alternatively, the dopant atom can be positioned in the space between the atomic lattice sites. This is known as interstitial doping. A simplistic representation of these two types of doping is given in Figure 37.

Figure 37 Representation of substitutional and interstitial doping.

For TiO_2 the introduction of the mid-band gap states is designed to induce visible light absorption. Cationic, anionic and neutrally charged dopants are all possible. A cationic dopant generally replaces a titanium cation in the lattice structure whilst anionic dopants substitute oxygen. An uncharged atom can form an interstitial dopant, retaining the original stoichiometry of TiO_2.

Studies on the physical properties, such as conductivity, of metal doped TiO_2 have been reported since the 1960s,[119, 120] however very little work was done on the photocatalytic activity of these systems until the late 1990s. Manipulation of the band structure to yield visible light absorption is relatively facile. However, this can often result in poor photocatalytic activity in the UV due to faster electron-hole recombination.

Work by Anpo et al. has shown that for metal doping of TiO_2, the activity of the resultant photocatalyst is highly dependent on the synthetic method employed.[121] They have shown that metal ion bombardment with a sufficient accelerating voltage, leads to significant visible light absorption, photocatalytic activity in the visible and unimpaired UV activity. Yet when a lower acceleration voltage is used or wet chemical methods of dopant are introduced, visible light absorption is achieved but at the expense of poorer photocatalytic activity in the

UV and little or no activity in the visible. They have attributed this to the formation of metal oxide clusters, which enhance electron hole recombination. With their method of implantation of chromium, iron, vanadium, manganese or nickel, a titanium centre is directly substituted resulting in changes to the electronic structure but not the chemical properties of the surface.

In 2001, Asahi et al. published a seminal paper demonstrating the use of nitrogen as a dopant in TiO_2.[122] Density of states (DOS) calculations predicted that nitrogen would be the best dopant from a range of other (C, S, F, P) to substitute oxygen in the titania lattice. They reasoned that the nitrogen 2p states would mix with oxygen 2p to narrow the band gap. Experimentally, nitrogen was introduced to TiO_2 powder by treatment with a NH_3/Ar mixture at 600° C. XPS identified substitutional nitrogen at between 1 and 1.4 atomic %. Using photodecomposition of acetaldehyde to assess photocatalytic activity, Asahi et al. were able to observe visible light activity from the N-doped samples and activity in the UV which was comparable to un-doped TiO_2 powders.

This particular report stimulated a great deal of interest in N-TiO_2 with subsequent publications covering a range of different sources of nitrogen and different methods of doping including DC magnetron sputtering with a nitrogen containing plasma[123], hydrolysis of $Ti(SO_4)_2$ with ammonia[124], hydrolysis of $TiCl_4$ in the presence of a nitrogen containing base[125] and ball milling of P25 with hexethylenetetraamine,[126] and ALD with ammonia.[127] As contradictions in the photocatalytic activity of N-TiO_2 became apparent, different theories of the mechanism also appeared in the literature with debate surrounding the fundamental mechanism behind visible light absorption.

Di Valentin et al. have argued that the band gap is, in fact, not shifted (as proposed by Asahi) but a mid-band state is introduced between the valance and conduction band in substitutionally N-doped anatase.[128] Their DFT calculations show that this state lies 0.14 eV above the valence band of anatase resulting in red-shift (i.e. lower energy) in absorption. Later work by Di Valentin et al. theoretically calculated the mid-band state formed by interstitial nitrogen to be 0.73 eV above the valence band of anatase.[129] They suggested this state may

trap holes more strongly, reducing the ability to participate in oxidative reactions. They also proposed that oxygen vacancies will form more readily when interstitial nitrogen is present.

Serpone has provided evidence to suggest that it is not the dopant which causes the increase in visible light absorption but, in fact, oxygen vacancies that can be induced by the presence of the dopant.[130] He has argued that the computational studies that predicted narrowing of the band gap are unreliable and that if this were to happen such heavy doping would be required that a different material would be formed that no longer has the same properties of TiO_2.

Several groups have synthesised nitrogen doped TiO_2 films by CVD. The first report was by Lee et al. who used TTIP and nitrous oxide precursors, at 420 °C under reduced pressure.[131] The nitrogen was shown to be directly incorporated into the crystal lattice with a stoichiometry of $TiO_{1.58}N_{0.21}$. No photocatalytic or chemical properties were assessed by these researchers. Pradhan et al. also used low pressure MOCVD but with TTIP and ammonia precursors. Again there was no photocatalytic testing and limited investigation into the nitrogen environment.[132] The first investigation of photocatalytic activity in nitrogen doped TiO_2 films synthesised by CVD was by Yates et al.[133] These researchers used atmospheric pressure CVD with $TiCl_4$ and ammonia precursors. XPS investigations revealed nitrogen in the substitutional position at levels of between 1.5 and 5%. Absorption spectra indicated that the doped films had an extended absorption region extending into the visible, in agreement with the yellow colour of the films. Degradation of stearic acid was used to assess the photocatalytic activity under both visible and UV irradiation. The presence of nitrogen was shown to be detrimental to UV activity compared to un-doped TiO_2 films and little or no activity was observed under visible irradiation. This was attributed to differences in the morphology of the surface with less well defined crystallites on the sample synthesised in the presence of ammonia.

Work from the group of Parkin et al. has also demonstrated the detrimental effect of substitutional nitrogen when using an ammonia precursor.[93] A combinatorial APCVD approach was used in order to produce a range of different levels of

substitutional nitrogen ranging from 0-11 atomic %, which could then be simultaneously analysed using the intelligent ink method. Under UV irradiation it was found that the presence of nitrogen decreased the rate of photocatalytic activity and under visible light, the rate of change was not observable using this method. Further work by the same authors demonstrated the use of ammonia in combinatorial APCVD to produce both substitutional and interstitial nitrogen, by diluting the ammonia flow.[134] It was shown that films with interstitial nitrogen were slightly more active than un-doped TiO_2 under UV irradiation and had marginally better activity compared to predominantly substitutionally doped films under visible light irradiation. This is despite a greater visible shift in the absorption spectrum of the substitutionally doped samples.

Purely interstitial doping has been achieved via APCVD using tert-butylamine as a nitrogen source rather than ammonia.[135] These films degraded stearic acid under visible light irradiation whereas an un-doped titania control film showed negligible decrease. However no comparison of the activity of the doped and un-doped films under UV irradiation was reported.

In this work, a novel synthetic approach was used in order to investigate the influence of deposition parameters on the overall level of nitrogen doping and ratio of substitutional to interstitial nitrogen. The amount of nitrogen precursor was kept constant whilst the amount of oxygen precursor was varied. This not only affected the nitrogen content but also the absorption spectra and morphology which appears to have consequences for the photocatalytic activity.

3.2 Experimental Methods

The chemical precursors were purchased and used without further purification, $TiCl_4$ (ReagentPlus, 99.9%) was obtained from Sigma Aldrich, ethyl acetate (laboratory reagent grade) from Fischer Scientific and tert-butylamine (99.5%) from Sigma Aldrich. Quartz substrates (25 x 25 x 1 mm) were obtained from Multilab. Float glass with a SiO_2 barrier layer was provided by Pilkington. The

glass was cleaned with water and detergent, acetone and isopropanol followed by drying in an oven prior to use. The films were deposited using the APCVD reactor which was described in detail in the introduction section. The conditions for each deposition are shown in Table 2.

Sample	Mass Flow (mol/min)			Ti:O:N precursor ratio	Deposition time (mins)	Substrate Temperature (°C)
	$TiCl_4$	Ethyl Acetate	tert-butyl-amine			
Un-doped TiO_2	0.006	0.0033	0	1.8:1:0	14	500
N-TiO_2-1	0.006	0.0130	0.0013	4.6:10:1	14	500
N-TiO_2-2	0.006	0.0103	0.0013	4.6:7.9:1	14	500

Table 2 Deposition parameters for un-doped TiO_2, N-TiO_2-1 and N-TiO_2-2.

Note that when the nitrogen precursor, tert-butylamine was present, a higher mass flow of ethyl acetate was required to achieve the anatase phase (see Chapter 4 for further discussion). In order to prevent delamination of the films, the temperature of the carbon block after the deposition was cooled at a rate of 1°C/min. The films were analysed using XRD, XPS, SEM, UV-vis and Filmetrics and Raman instruments whose details are given in section 2.2. The parameters for the XRD measurements were: 15-66° 2Θ scan range, 0.05° per step, 2 secs per step with a tube angle of 1°. Stearic acid was used as a model organic contaminant to test the photocatalytic activity of the samples. Prior to coating with stearic acid the samples were irradiated with a 365 nm light in humidified air for 12 hours. A solution of 0.05 M stearic acid in chloroform was prepared and used as a stock solution. The samples were held by a dip-coating machine, which was built in-house, to submerge the samples in the stearic acid solution and withdraw it from the solution at a fixed rate of 120 m min^{-1}. This was to ensure an even and reproducible coating on each sample. The stearic acid on the back of the sample was removed by wiping with a chloroform soaked tissue. Each sample was then attached to an aluminium sample holder which had a circular hole of 1 cm

diameter in the centre. The amount of stearic acid was measured by placing the sample holder in a PerkinElmer FTIR SpectrumRX1 spectrometer. The IR beam passes through the substrate, the TiO_2 and the stearic acid coating. The amount of stearic acid present is proportional to the area of the peaks in the IR region 2820-2970 cm^{-1} determined by the Spectrum software. This initial reading is recorded at time zero, t0. The samples are then irradiated with either UV 365 nm light or filtered visible light and further IR measurement recorded at various time intervals. For the UV tests a Uvitec lamp with 2 x 8 W black light bulbs was used. The power of the lamp was recorded using a UPV UVX radiometer as 1 mW cm^{-2}. The distance between the lamp and the samples was 1 cm. For the visible light tests a white lamp (GE lighting 2D fluorescent GR10q 835 white 28 W) was used. To ensure no UV light was able to reach the samples, a sheet of UV absorbing Optivex glass and an additional sheet of float glass was placed directly underneath the lamp.

3.3 Results and Discussion

The samples of un-doped TiO_2 were off-white and all samples that had been exposed to the tert-butylamine were yellow in colour. In all cases the substrate was fully covered with no visible cracks or delamination. For each sample, a small section of the glass was cut to be photocatalytically tested and characterised in detail.

The values for the thickness of each film, determined using the Swanepoel method, were 5.7, 7.6 and 6.3 μm for un-doped TiO_2, N-TiO_2-1 and N-TiO_2-2, respectively.

3.3.1 Raman Spectroscopy

Raman spectra were recorded at three different positions (to check homogeneity of the phase) on each sample. For both doped and un-doped samples the phase was determined to be purely anatase at all of the positions tested, regardless of the presence of a nitrogen dopant. It is important to verify that nitrogen in the material does not cause a change to crystallographic phase (see Chapter 4 for a further discussion how a dopant may induce a phase change). One representative spectrum is shown for each sample in Figure 38.

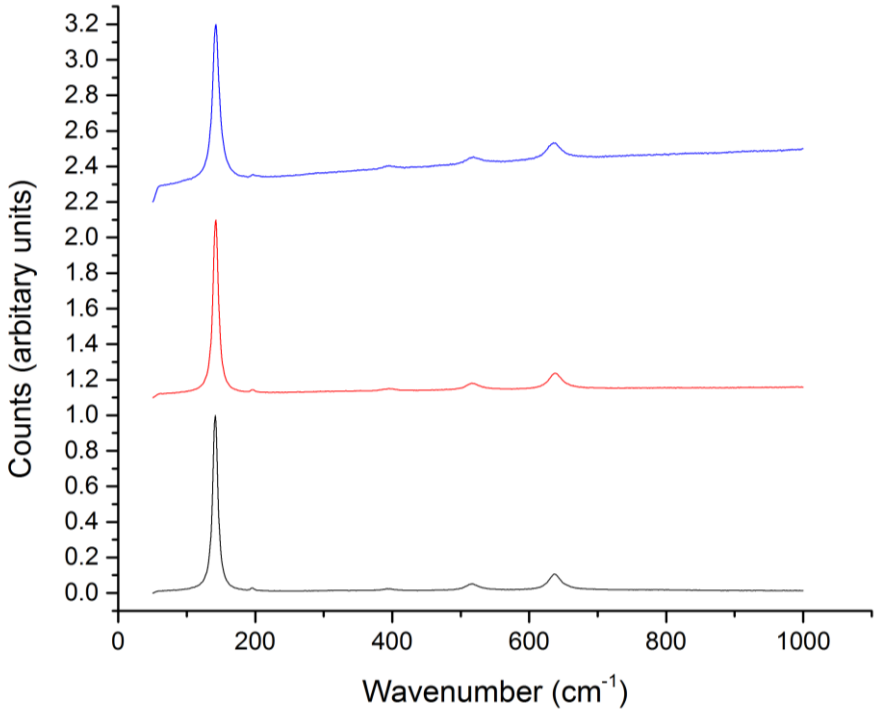

Figure 38 Raman spectrum of un-doped TiO_2(black), N-TiO_2-1(red) and N-TiO_2-2 (blue).

The peaks for un-doped TiO_2 occur at 141, 195, 396, 516 and 636 cm^{-1}, for N-TiO_2-1the peaks are at 142, 196, 398, 516 and 638 cm^{-1}; and for sample N-TiO_2-2 the peaks are at 142, 197, 397, 519 and 635 cm^{-1}. These are consistent with literature which reports observed peak positions for Raman modes at 144 (E_g), 197 (E_g), 399 (B_{1g}), 516 (A_{1g}, B_{1g}) and 639 cm^{-1} (E_g) for the Raman spectrum of anatase.[101]

3.3.2 X-ray Diffraction

The X-ray diffraction patterns were collected for all three samples and are shown in Figure 39.

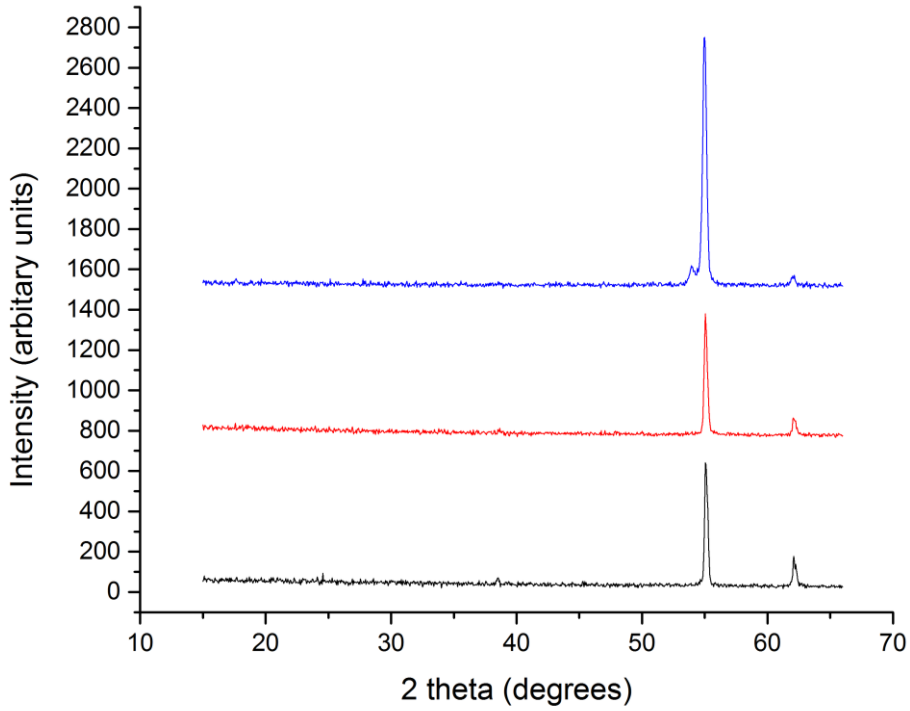

Figure 39 XRD patterns of un-doped TiO_2(black), N-TiO_2-1(red) and N-TiO_2-2 (blue).

Reflections at approximately 55 and 62° 2Θ are present for all three samples. These can be matched to anatase (211) and (213) reflections, respectively as reported in ICSD 44882. Sample N-TiO_2-2 also has a small additional signal at 53.9° which corresponds to the anatase *h,k,l* plane [105]. There are no indications in this data for the presence of rutile, brookite or TiN. Notably absent are the reflections at 25.3, 37.9, 48.1° and others, which would usually be expected for anatase. On first inspection, this would appear to be an indication of extreme preferential orientation of the film. However it has previously been observed, in this laboratory, that similar films do in fact have a weak signal at 25.3° when analysed using a diffraction analyser with a 2D detector, yet when using a 1D

detector (as is the case for the data presented here) these reflections are no longer observed. Since this phenomenon occurs for both the doped and un-doped samples, it cannot be caused by the presence of the amine dopant and is unlikely to affect comparison across these samples, however it should be considered when comparing activity to literature reports.

3.3.3 X-ray Photoemission Spectroscopy

X-ray photoemission spectroscopy was used to confirm the presence of nitrogen and determine the atomic percentage of nitrogen in the doped films. Depth profiling was used as the surface is often contaminated with environmental carbon and possibly other elements present in organic molecules which are on the surface as a result of handling the samples and being stored in air (i.e. not a clean room or glove box). Ten levels of the sample are interrogated, the surface and then nine lower levels within the film. The removal of material for the depth profiling is achieved by bombardment with argon ions. Depth profiling is important, not only to remove surface contamination, but also to determine whether the dopant is present throughout the material or purely at the surface as this may have consequences for the mobility of charge carriers in the films. There are significant changes in the data of the surface level compared to subsequent levels but after three etch levels the data becomes consistent, hence it is possible to assume the bulk of the material is being investigated The atomic percentage of titanium, oxygen, nitrogen and carbon for each sample are given in Table 3.

Sample	Titanium (atomic %)	Oxygen (atomic %)	Nitrogen (atomic %)	Carbon (atomic %)
Un-doped TiO_2	29.6	65.4	0.3	4.8
N-TiO_2-1	30.2	65.9	1.0	2.9
N-TiO_2-2	31.7	63.8	0.7	2.8

Table 3 Composition of un-doped TiO_2, N-TiO_2-1 and N-TiO_2-2.

The values in Table 3 are average percentages of the last seven levels in the depth profile. It is difficult to tell if the carbon that has been identified is in the TiO_2 film or on the surface of the substrate (glass) which is exposed by cracks in the film. Table 3 shows the level of nitrogen in the un-doped sample to be 0.3% however inspection of the spectra for the nitrogen 1s energy region does not show a significant peak below the first level. The spectra for each depth profiling level for all three samples in the nitrogen 1s energy region are shown in Figure 40.

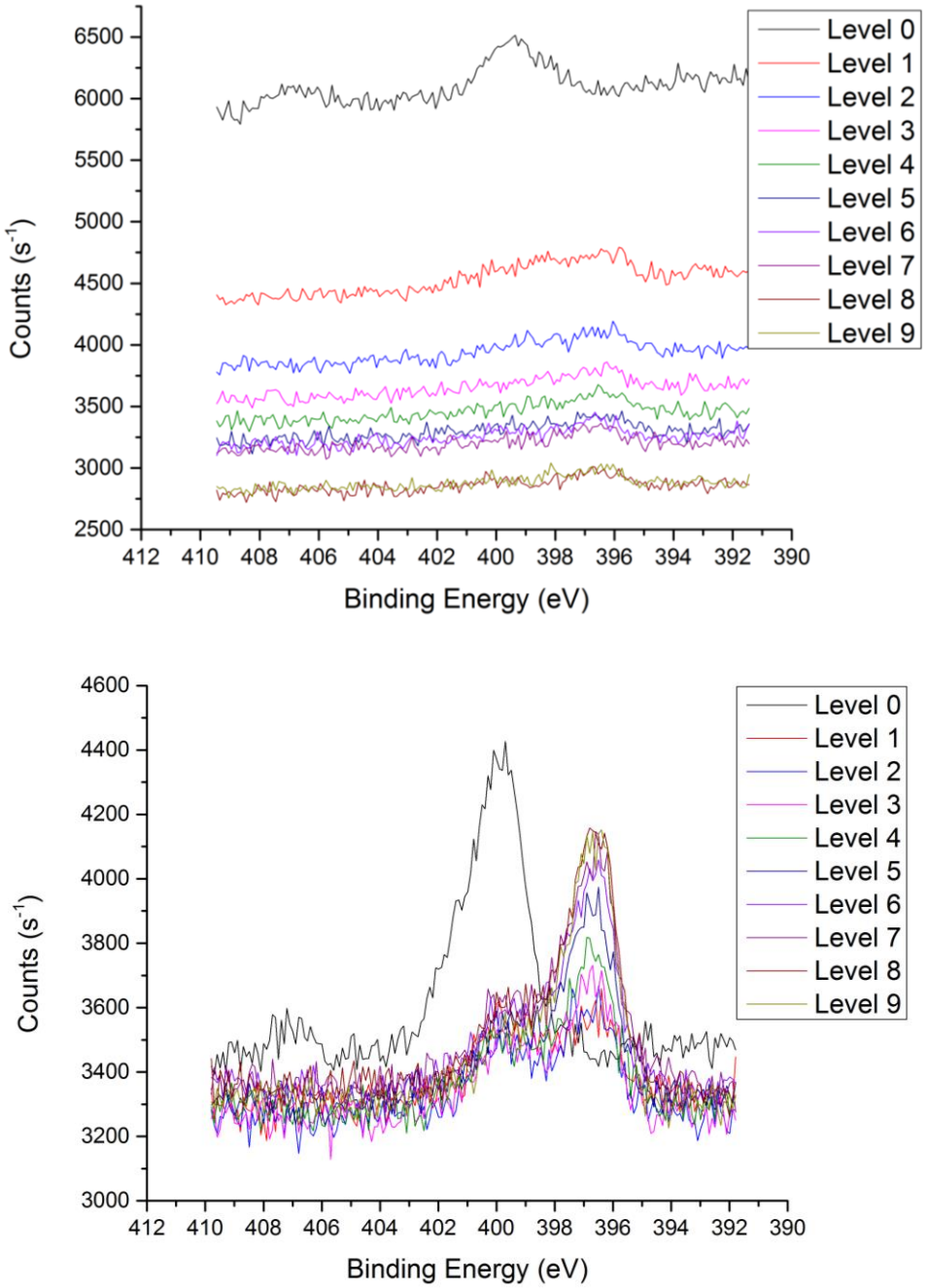

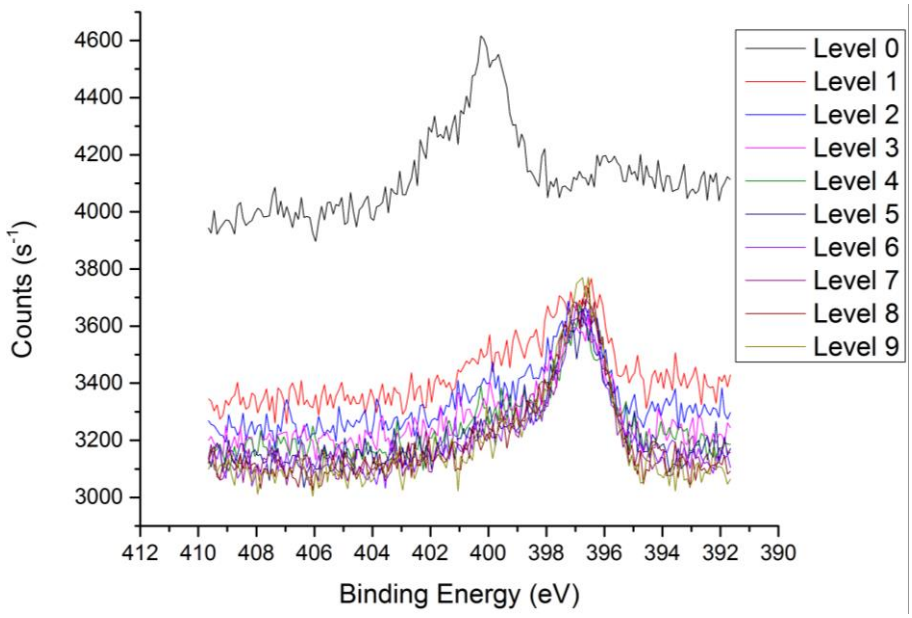

Figure 40 XPS data in the N 1s energy region for un-doped TiO_2 (top), N-TiO_2-1 (middle) and N-TiO_2-2 (bottom).

A peak at around 396 eV has been consensually assigned in the literature as substitutional nitrogen.[136] The peak at 400 eV is commonly assigned as interstitial nitrogen[137] and also to other species including surface adsorbed nitrogen,[138] and NH_x.[139] We can see that for all three samples there is a surface peak around 400 eV, which is most likely to be surface adsorbed nitrogen. For samples N-TiO_2-1 and N-TiO_2-2 there is also a peak at around 400 eV in the bulk which is most likely to be interstitial nitrogen.

The data in Figure 40 shows there is a difference in the nitrogen environment between samples N-TiO_2-1 and N-TiO_2-2 in the bulk. In both cases there appears to be two signals. Modelling of peaks at 400 and 396 eV allows the area to be determined for each contribution. The fitted peaks for level nine are shown as an example in Figure 41.

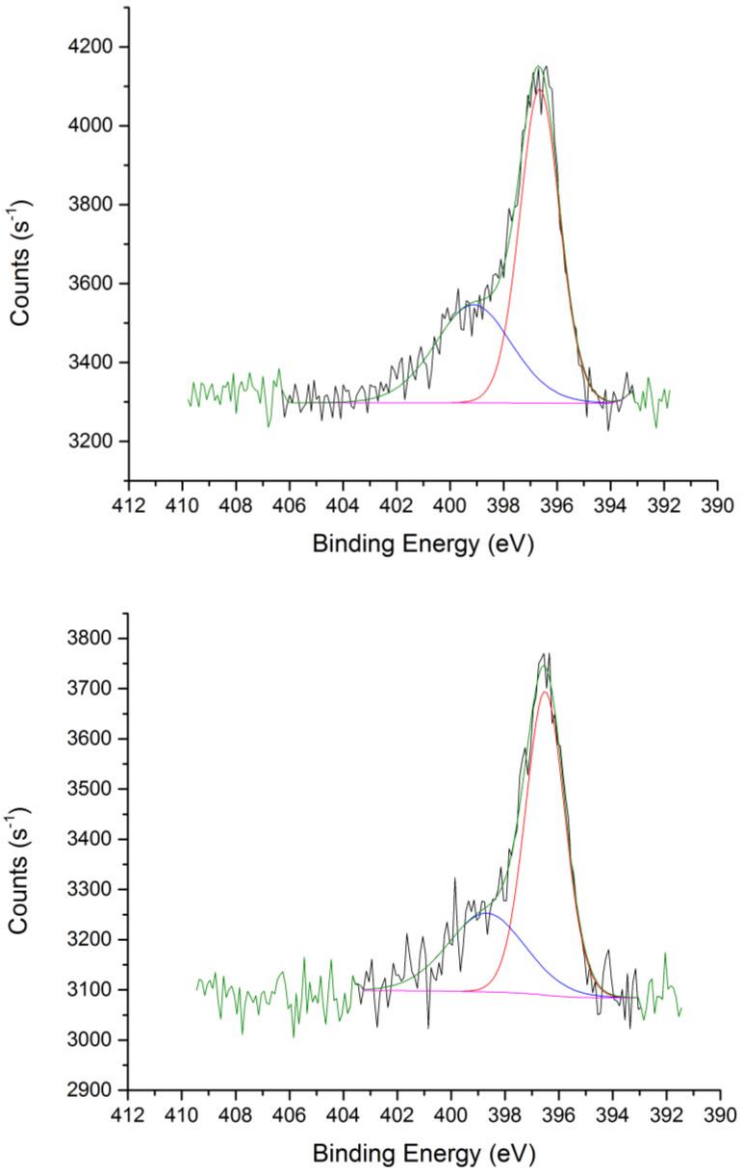

Figure 41 Fitted XPS peaks for nitrogen signals in samples N-TiO_2-1 (top) and N-TiO_2-2 (bottom).

The ratio of areas between the peak at 400 and the peak at 396 eV (averaged over the last seven levels) is 1 to 1.4 for sample N-TiO_2-1 and 1 to 1.9 for sample N-TiO_2-2. This indicates that there is a greater proportion of interstitial nitrogen in sample N-TiO_2-1, which had the higher flow rate of ethyl acetate. This would correspond with Di Valentin's hypothesis that interstitial nitrogen is preferred in conditions with an excess of oxygen. This also follows intuitively that titanium

oxygen bonds are formed in preference to titanium nitrogen bonds and that when the ratio of oxygen to nitrogen precursors is above a critical level, nitrogen cannot compete effectively for bond formation with titanium and is therefore forced into an interstitial position. However when there is less oxygen available the nitrogen is able to take its place within the lattice.

3.3.4 UV-vis Spectroscopy

From the yellow colour of the doped samples, it can be assumed they are absorbing visible light. To confirm this spectroscopically, UV-vis absorption spectra were recorded. In this instance, the exact area that was used for photocatalytic testing was not used. Instead a quartz piece that was placed on top of the glass (at the same position on the glass for all three samples) during the deposition was investigated. Using a quartz substrate for UV-vis measurements is advantageous since glass can absorb light in the region of interest and interfere with the analysis of the film itself, whereas the absorption edge of quartz is below 250 nm. Figure 42 shows the absorption spectra of an uncoated piece of quartz and un-doped TiO_2, N-TiO_2-1 and N-TiO_2-2.

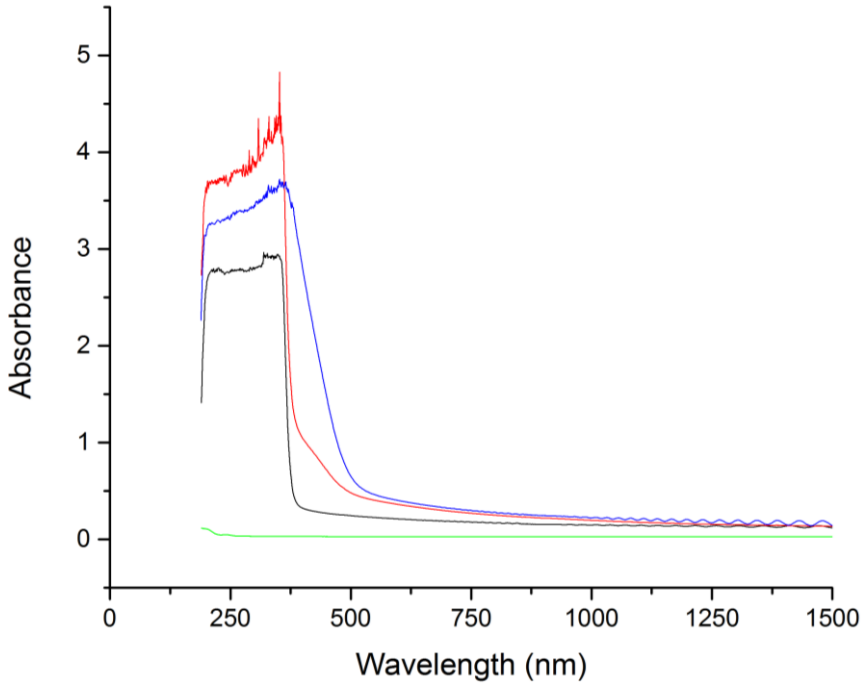

Figure 42 UV-vis spectra of un-doped TiO_2 (black), N-TiO_2-1 (red), N-TiO_2-2 (blue)and quartz (green).

Figure 42 shows a very clear shift in the absorption edge of the doped samples into the visible region. It is interesting to note that for sample N-TiO_2-2 the entire absorption edge appears to be shifted rather than just a shoulder as for sample N-TiO_2-1. This may be indicative of the effect on the band gap i.e. narrowing of the intrinsic band gap rather than the introduction of intra band gap sub levels, however this is debated in the literature.[140] From these data it is also possible to calculate an "apparent" band gap using a tauc plot, $(Ah\nu)^{1/2}$ against energy, (where A is absorbance) according to the tauc method[141] which is shown in Figure 43.

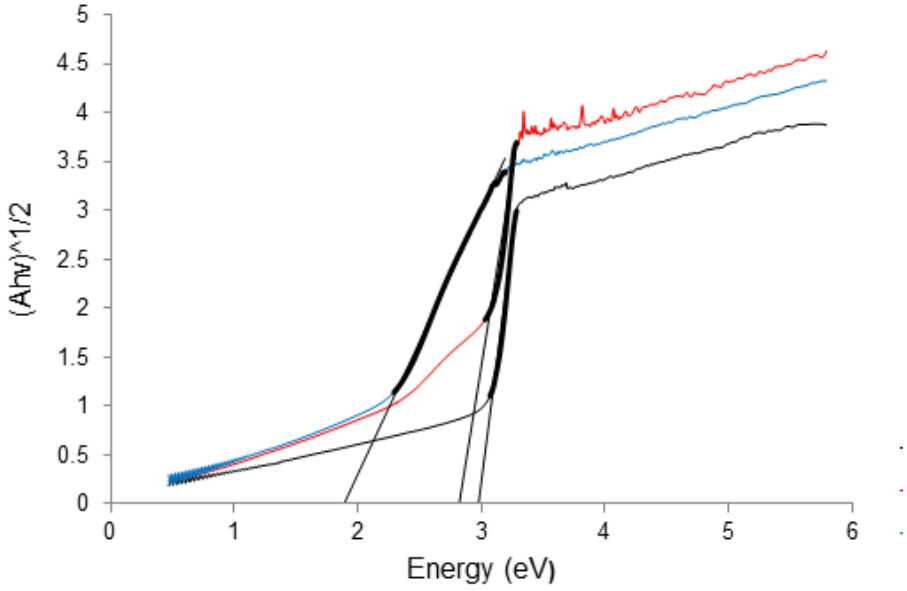

Figure 43 Tauc plot for un-doped TiO_2 (black), N-TiO_2-2 (red) and N-TiO_2-2 (blue).

Extrapolation of the linear section of each plot to the x axis gives values, to 1 dp, of 3.0, 2.8 and 1.9 eV for un-doped TiO_2, N-TiO_2-1 and N-TiO_2-2 respectively. Whilst these values are somewhat lower than may be expected (i.e. undoped anatase would be expected to have a band gap value of 3.2 eV) there is a significant difference between samples N-TiO_2-1 and N-TiO_2-2 which highlights the relative difference in the shape of the absorption edges.

3.3.5 Scanning Electron Microscopy

In order to assess the microstructure of the sample surface, SEM images of un-doped TiO_2, N-TiO_2-1 and N-TiO_2-2 were recorded and are shown in Figure 44.

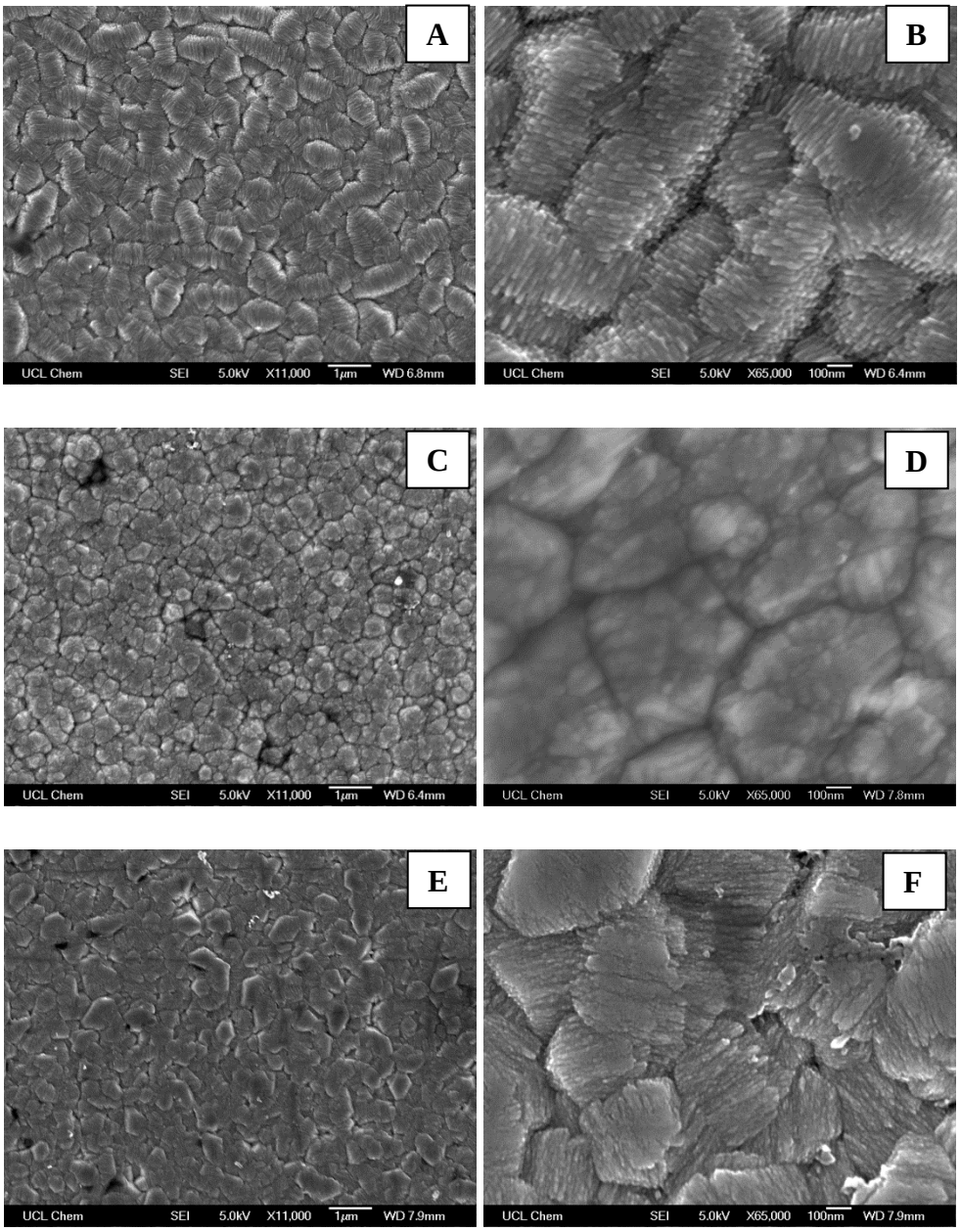

Figure 44 SEM micrographs of samples A) N-TiO_2-1 at low magnification, B) N-TiO_2-1 at high magnification and C) N-TiO_2-2 at low magnification, D) N-TiO_2-2 at high magnificent, E) un-doped TiO_2 at low magnification and F) un-doped TiO_2 at high magnification.

The images in Figure 44 show a difference in the surface morphology of doped samples, N-TiO_2-1 and N-TiO_2-2 which were shown to have similar crystallinity as shown by Raman spectroscopy and XRD. Sample N-TiO_2-1 has particles on the sub-micron size scale with a typical aspect ratio of 2:1 and a highly textured, stratified surface with angular facets. Sample N-TiO_2-2 has particles which are,

again, on the sub-micron size scale, but with an approximate aspect ratio of 1:1 and lack of well-defined texturing on the individual particles. Sample N-TiO_2-2 has a microstructure which is more similar to previously reported nitrogen doped APCVD films of TiO_2.[93] Given the similar scale of surface features, the surface area of these two types of samples is likely to be comparable. However, standard techniques for measuring specific surface area, such as nitrogen adsorption are not sensitive enough for these relatively smooth surfaces but these images do give a qualitative impression. The un-doped TiO_2 appears to have a morphology which is different to both of the doped samples and is more angular and less rounded than N-TiO_2-2 but does not have the stratified surface of sample N-TiO_2-1. These differences in morphology may be due to the type of dopant present, however it is difficult to establish a cause and effect relationship rather than purely a correlation. Additionally, since these samples have different thicknesses, which may also lead to differences in the surface morphology. Yates et al. have suggested the use of ammonia as a dopant detrimentally impacted the morphology of their samples leading to worse photocatalytic activity.[133] They described the morphology as less well defined and less structured however here for sample N-TiO_2-1 the opposite is true. Indeed, the opposite trend in activity is observed with sample N-TiO_2-1 being the most active. It may be that the deposition conditions, i.e. lower oxygen content, may be responsible for the well-defined, stratified surface, however this is difficult to explain intuitively.

3.3.6 Photocatalytic testing: Stearic Acid Degradation

The photocatalytic activity was assessed by the degradation of stearic acid. Stearic acid was chosen as a model organic pollutant as it is stable under UV and visible light in the absence of a photocatalyst. It is important to use a test method which is suitable for use with both UV and visible light to allow a meaningful comparison between results of the test when using a different light source. Since stearic acid is a solid at room temperature, it avoids many of the problems associated with solution or gas phase tests (i.e. variation in rates of adsorption and

desorption of probe molecules during the course of the reaction, difficulty with leaks in the gas phase).

The spectral output of the visible light source with and without the Optivex UV filter is shown in Figure 45.

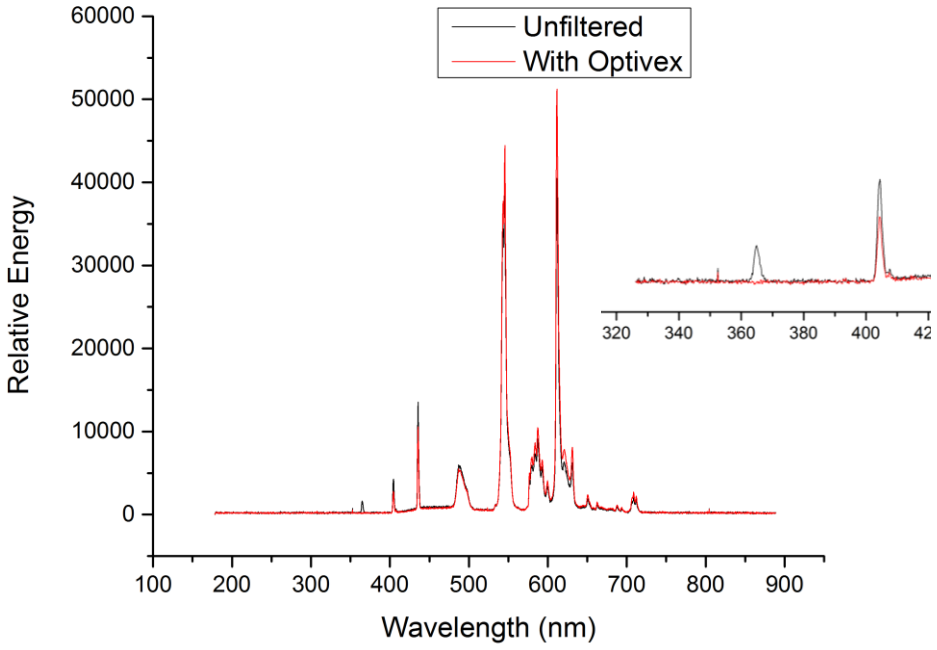

Figure 45 Spectral output of white light source unfiltered and with optivex filter. Inset is zoomed in on UV region.

It is clear that the small UV component of the light at 365 nm is removed when using the Optivex filter, so that it is possible to say that only visible light is incident on the photocatalyst.

The area of the stearic acid peak from IR is plotted against irradiation time for UV light in Figure 46 for un-doped TiO_2, N-TiO_2-1, N-TiO_2-2 and a piece of glass with a barrier layer i.e. the substrate used for un-doped TiO_2, N-TiO_2-1 and N-TiO_2-2. The un-doped TiO_2, was used as a comparison for the doped samples rather than a commercial photocatalyst film since, given the differences in thickness and morphology, a film made using the same deposition technique and deposition time seemed a more appropriate benchmark.

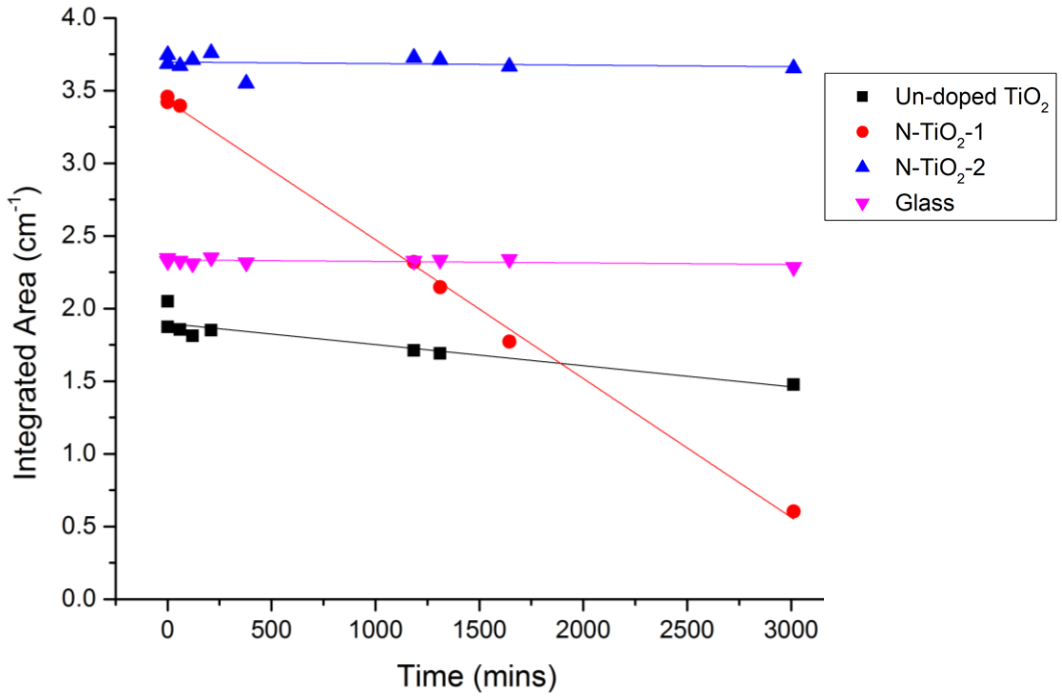

Figure 46 Degradation of stearic acid on un-doped TiO_2 (black), N-TiO_2-1 (red), N-TiO_2-2 (blue) and glass (pink) when irradiated with UV light.

As expected, the stearic acid layer on the glass shows no appreciable degradation over the course of the test. Sample N-TiO_2-2 also shows a negligible decrease such that it can be judged to be inactive in this test. There is a slight decrease for un-doped TiO_2, although it is perhaps less apparent than may have been expected for un-doped TiO_2. This could be due to the higher amount of carbon content in the un-doped TiO_2 compared to N-TiO_2-1 and N-TiO_2-2, preferential orientation or thickness of the film. Thick TiO_2 films produced by CVD previously have reported low activity,[142] however the fundamental reasons for this have not yet been investigated but could be related to the greater distance holes (or electrons in reductive processes) must travel to the surface in order to take part in a photocatalytic reaction. This could lead to high recombination rates of electrons and holes thus reducing activity. Sample N-TiO_2-1 shows a very clear decrease in the amount of stearic acid. The change in stearic acid with irradiation time under visible light is shown in Figure 47.

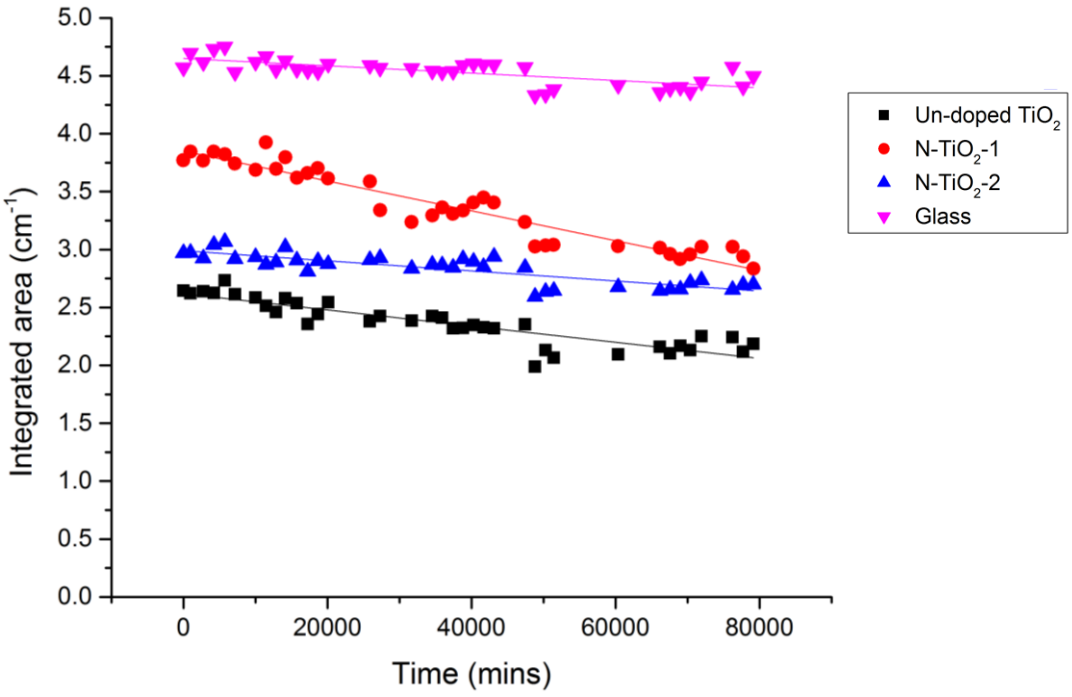

Figure 47 Degradation of stearic acid on un-doped TiO_2 (black), N-TiO_2-1 (red), N-TiO_2-2 (blue) and glass (pink) when irradiated with visible light.

Whilst it had been noted previously that stearic acid should be stable under visible light, a slight decrease can be observed even on the glass sample, which suggests that some change is occurring on the very long time scale of this experiment, which is not photocatalytic but most likely due to thermal degradation. The rates calculated for un-doped TiO_2 and N-TiO_2-2 (see Table 4) show similar values to the glass and therefore can also not be considered photocatalytic. This is to be expected since the un-doped TiO_2 does not absorb any visible light, and whilst the UV-vis spectrum of N-TiO_2-2 does indicate visible light absorption, the lack of activity under UV irradiation makes it unsurprising that there is still no activity under visible irradiation. This could be due to fast electron hole recombination kinetics, as has previously been observed with substitutional nitrogen doping.[143] Sample N-TiO_2-1 is the only sample which shows any appreciable decrease of stearic acid under visible illumination .

	Rate (cm^{-1} min^{-1})	
Sample	**UV**	**Visible**
Un-doped TiO_2	1.45E-04	6.98E-06
N-TiO_2-1	9.55E-04	1.29E-05
N-TiO_2-2	1.07E-05	4.35E-06
Glass	1.04E-05	3.17E-06

Table 4 Activity rates of un-doped TiO_2, N-TiO_2-1, N-TiO_2-2 and glass under UV and visible light irradiation.

The rates shown in Table 4 illustrate the, near order of magnitude, increase in activity of sample N-TiO_2-1. This shows a negative correlation to the amount of visible light absorption which is apparent from the UV-vis spectra (Figure 42). Sample N-TiO_2-2 appears to be absorbing more strongly at wavelengths below 400 nm and has a smaller calculated band gap, yet is almost totally inactive for stearic acid degradation under visible irradiation. This has been observed previously in the case of CVD with ammonia nitrogen source.[143] There could be several reasons to explain the higher activity of sample N-TiO_2-1: there is a higher total nitrogen content in sample N-TiO_2-1, a greater proportion of interstitial nitrogen or the well-defined surface morphology. Indeed, a combination of these factors could be influential. A further speculative consideration could be the formation of oxygen vacancies in the film synthesised with less oxygen precursor. Although no measurements have been performed in this work which can determine the presence of oxygen vacancies, this idea could provide an interesting avenue for future studies, which may support Serpone's interpretation of visible light activity.[130]

3.4 Conclusions

In summary, nitrogen doped films of TiO_2 were synthesised by APCVD with tert-butylamine as the nitrogen source and a varying amount of ethyl acetate. An un-doped film was also made using similar deposition conditions, (i.e. same deposition time and $TiCl_4$ flow but lower ethyl acetate flow rate). All films were shown by Raman spectroscopy and XRD to be the anatase phase, although the thicknesses of the films were different. Of two different N-doped samples, one contained a greater amount of interstitial nitrogen, at a ratio of 1:1.4, compared to the other which had a ratio of 1:1.9. This was achieved by a novel synthetic approach of altering the amount of oxygen precursor whilst keeping the amount of nitrogen precursor constant. Less oxygen precursor, led to a greater total amount of nitrogen. SEM investigations also revealed a difference in microstructure. The sample with more interstitial nitrogen and well-defined, stratified microstructure significantly out-performed the sample which had a greater proportion of substitutional nitrogen (and poor microstructure) in photocatalytic tests under both UV and visible light irradiation.

The results presented here have shown that variation in the flow of ethyl acetate can provide a method of influencing the position of nitrogen in the lattice of TiO_2 and the surface morphology. It is also further evidence to support the findings of others which have suggested that interstitial doping and a well-defined microstructure can contribute to visible light photocatalytic activity.

CHAPTER FOUR

FORMATION OF BROOKITE PHASE TiO_2 BY APCVD

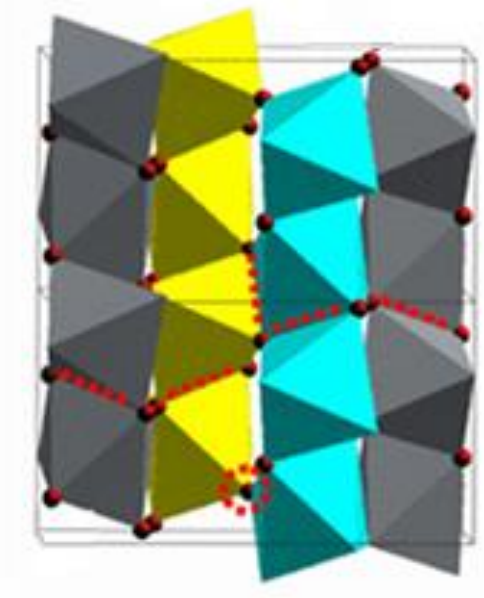

Chapter 4: Formation of brookite phase TiO_2 by APCVD

Abstract

Brookite, a metastable phase of TiO_2, has received relatively little attention by the photocatalysis community, largely due to the difficulty in establishing synthetic routes to the material. Here, it is shown that APCVD provides routes to the production of brookite which occur when the amount of oxygen precursor is lowered. Taking standard precursors for the atmospheric pressure CVD of TiO_2, ethyl acetate and $TiCl_4$, it is observed that when the flow rate of ethyl acetate is sufficiently low, brookite is formed in a mixture with anatase. Introduction of a dopant, specifically nitrogen via co-deposition with tert-butylamine is also shown to influence the resultant phase. It is proposed that the amine participates in an oxygen consuming reaction hence creating the low oxygen CVD environment which facilitates the formation of brookite. The phase is shown to be influenced by the substrate with pure brookite obtained on a steel substrate. A possible mechanism for brookite formation is discussed. Preliminary results of photocatalytic tests on pure brookite are presented.

4.1 Introduction

4.1.1 Structure and Stability of Brookite

As discussed in the introduction, the three crystalline polymorphs of titania have a different arrangement of atoms in space which dictate their properties. Whilst having broadly similar physical attributes (unlike, for example, the allotropes of carbon) in terms of appearance, chemically stability and low toxicity, the subtle differences in the crystal structure can enhance certain properties. Synthetic control over the phase therefore allows a means of tuning the reactivity of titania to a given application.

Both anatase and rutile have a tetragonal structure whereas brookite has an orthorhombic unit cell, this is shown in Figure 48.

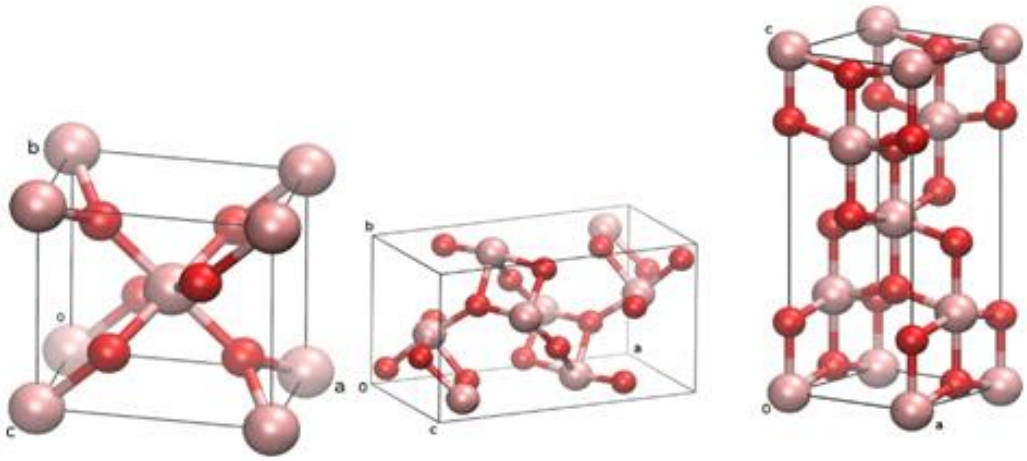

Figure 48 Unit cell diagrams of rutile (left), brookite (centre) and anatase (right). Titanium atoms are shown in pink and oxygen atoms are shown in red. Reproduced, with permission from reference [29].

Anatase and rutile each have two long bonds and four shorter bonds, 1.973 Å and 1.948 Å for anatase and 1.978 Å and 1.943 Å for rutile. In brookite, however, each bond is a different length ranging from 1.927 Å to 1.987 Å.[144]

Another way of visualising the structures is to consider the environment around each metal centre and how these relate to their neighbours. In all three cases the titanium metal ion is octahedrally coordinated, surrounded by six oxygen atoms. In the case of anatase and brookite the octahedron is distorted. These octahedra are linked together either by sharing a vertex (corner) or by sharing an edge. The rutile crystal structure is made up of chains of octahedra with shared vertices along the *a* and *b* axes and edge sharing along the *c* axis.[144] Anatase shares edges along all three axes. Brookite is more complicated with vertex and edge sharing along the *a* and *b* axes and edge sharing along the *c* axis. This is depicted in Figure 49.

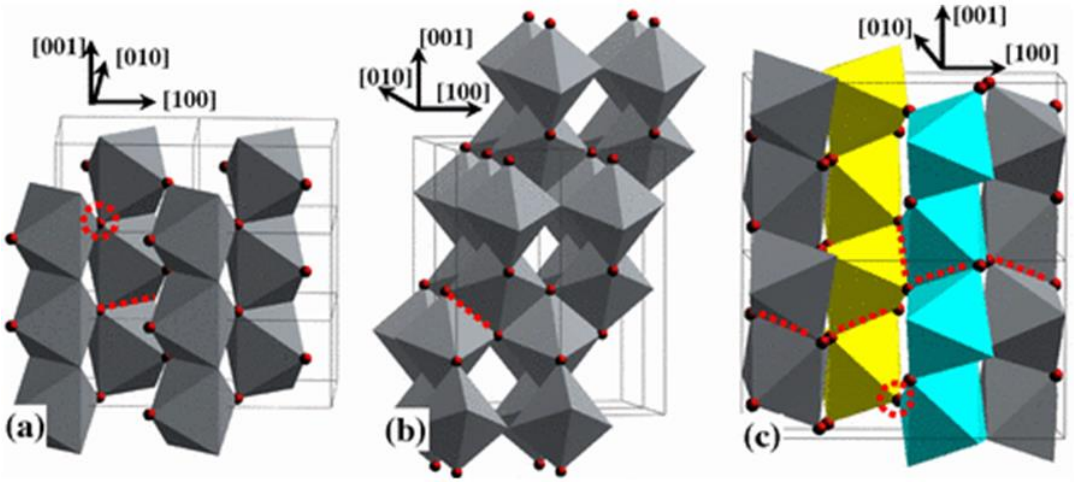

Figure 49 Octahedra in a) rutile, b) anatase and c) brookite. Reproduced with permission from reference [144].

In Figure 49 examples of the vertex and edge sharing interactions have been highlighted with a red dashed line or circle. The yellow and blue colours of the octahedra in brookite are used to clarify the vertex sharing (between the grey and yellow and also between the grey and blue) and the edge sharing (between the blue and yellow octahedra) along the *a* and *b* axes. Rutile has two shared edges per octahedra, anatase has four and brookite has three.[145] Gong and Selloni summarise this information regarding the interactions of the octahedra as "both rutile and anatase characteristics are present [in brookite]".[144]

Rutile is usually considered to be the most thermodynamically stable polymorph with both anatase and brookite as metastable phases. However Zhang and Banfield demonstrate the importance of particle size in the nanoscale regime.[146] They determined that for particles with a diameter greater than 35 nm, rutile is indeed the most stable phase, however for particles sized between 35 nm and 11 nm brookite is the most stable with anatase being the most stable below 11 nm. At 16 nm the stability of anatase and rutile is reversed. This information is summarised in Figure 50.

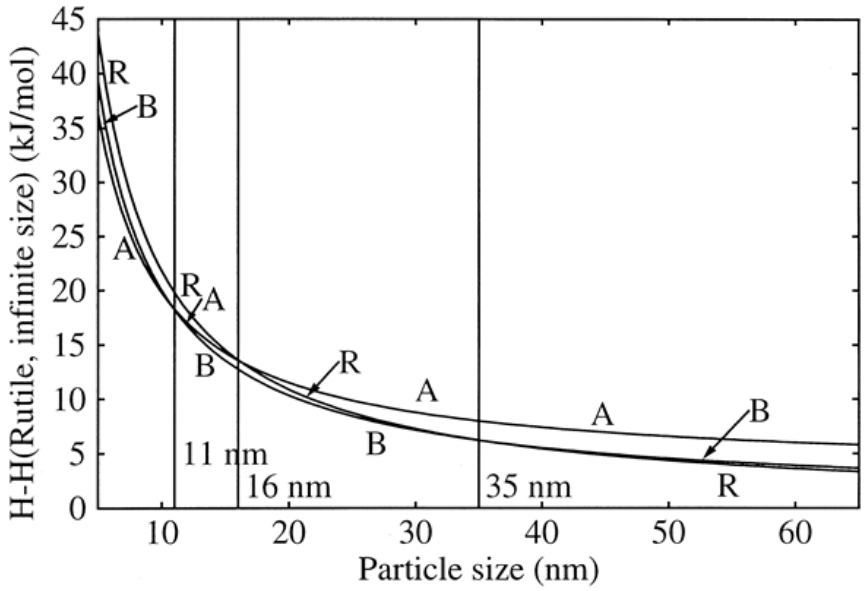

Figure 50 Enthalpies of nanoscale titania polymorphs. Reproduced with permission from reference [146].

The difference in surface energy for nanoparticles is sufficient to alter the overall stability of the particles. This insight resolved some of the previous contradictions in the literature which gave opposing results on the transformation sequence but had not fully considered the role of particle size.

Many groups have made efforts to understand the titania phase transformation sequence i.e. does anatase transform into brookite and then rutile or does brookite transform to anatase before rutile. A sample of natural brookite (mechanically powdered) was heated from 800-900°C to form rutile with no detection of anatase[147]. Recent work by Bahnemann et al. showed that pure brookite

nanoparticles and pure anatase nanoparticles both transformed directly into rutile. However, in a mixture of anatase and brookite, the anatase transforms first to brookite and then rutile.[148] These types of studies are complicated by the fact that as nanoparticles are heated they tend to aggregate and grow, and these rates may be different for the different phases. So for example it may be the case that anatase appears to transform to rutile at a lower temperature than brookite, but in actual fact it could be that the growth of the anatase particle is more rapid and it reaches a size at which rutile is favoured more quickly than brookite.

4.1.2 Synthetic methods for production of brookite

Brookite can often occur as a mixed phase with anatase but production of pure brookite is rather challenging. It has, however, been achieved by several different routes with many theories on which conditions lead to the formation of brookite. Some authors have argued that pH control is critical while others suggest that the presence of ions or surfactants can stabilise the brookite phase. There is very little consensus on general rules for brookite formation in the literature which is perhaps an indication of the sensitivity of each particular synthetic approach.

Hydrothermal synthesis has been studied by a number of groups with a range of reaction conditions and titanium sources. Wei and colleagues have demonstrated that brookite is only observed at pH 10.9 whereas in more acidic solution anatase is yielded.[149] These researchers used anatase powder as a starting material, converted it to sodium titanate by dispersion in NaOH(aq) then adjusted the pH with HCl to give a range of pHs before hydrothermal treatment. Zhang et al. also used a layered titanate precursor in aqueous ammonia to give anatase.[150] As NaCl is added, a mixture of brookite and anatase is obtained and pure brookite, with a nanoflower particle shape, is formed with 0.25 M NaCl. A later publication by Zhang and colleagues challenged the role of pH as the study varied the counter ions (CH_3COONa, KCl etc) and elucidated that it was in fact the presence of sodium ions rather than pH that was the key parameter.[151] They proposed that TiO_2 was formed by the closure of titanate layers leading to the formation of

anatase. Yet the presence of sodium can block full closure of the layers resulting in brookite. Nagase and co-workers have shown that both pH and amount of sodium, and indeed duration of reaction play a role.[152] Starting with amorphous titania in NaOH, they found that sufficiently high temperature (200 °C) and TiO_2:NaOH ratio resulted in an anatase/brookite mixture. Lower temperatures and TiO_2:NaOH ratios produced sodium titanate, whereas too high a temperature and reactant ratio gave a greater proportion of anatase. Pure brookite could be obtained with a TiO_2:Na ratio of 4:3 when the sodium source was NaOH. Varying the sodium source (Na_2CO_3, $Na_2B_4O_7$ and CH_3COONa) whilst maintaining the TiO_2:Na ratio resulted in a change in pH. Only the high pH (12.9) using NaOH gave pure brookite. It was suggested that crystallisation occurred more slowly in higher pH which led to brookite.

However, the situation is different when using a monometallic titanium complex precursor rather than a layered titanate. Pottier et al. used thermolysis of $TiCl_4$ to selectively form brookite by controlling the Ti:Cl ratio.[153] They suggested that the $[Ti(OH)_2Cl_2(OH_2)_2]^0$ complex is the precursor, formed in solution, which leads to brookite. Qi et al. demonstrated that pH also appears to have a critical influence on phase formation from a $TiCl_4$ precursor. They showed that, $TiCl_4$ in aqueous solution with KOH used to adjust the pH, anatase was formed at high pH, rutile at low pH and brookite was formed with an intermediate pH.[154] They proposed that the structure of the titanium complex in solution is determined by pH, and the structure of that complex, in turn, dictates the phase formation. At high pH there are more likely to be a greater number of hydroxyl, OH^-, ligands coordinated to the metal. The formation of Ti-O bonds for TiO_2 construction occurs by a dehydration mechanism through two OH^- ligands on different metals that are in close proximity. This would lead to a corner sharing type interaction. In order for edge sharing to occur there must be two adjacent OH^- ligands on two metal centres. The likelihood of this happening is greater in basic conditions. Therefore edge sharing interactions are formed at high pH and since anatase has the greatest number of edge sharing octahedra, it forms in basic conditions. Acidic conditions favour rutile since corner sharing octahedra form more readily. Brookite forms at

intermediate pH since it has an intermediate number of edge sharing octahedra relative to anatase and rutile.

Sun et al. also noticed the effect of pH on the resultant phase and in addition noted differences related to the concentration of the titanium precursor, $TiCl_3$ in this case.[145] They reported that brookite was formed at intermediate Ti concentrations but varying it either higher or lower resulted in anatase. They reasoned that at high concentrations of $TiCl_3$, the rate of reaction was so rapid that there was insufficient time for rearrangement to the brookite phase and anatase formed rapidly. Yet with low Ti concentration the particle size was limited to below 11 nm i.e. the size region in which anatase is more thermodynamically favourable.

Control of pH also gave control of phase formation when using titanium sulphate as a precursor for hydrothermal synthesis of titania.[155] However in this work, the researchers reported formation of brookite at high pH and anatase at lower pH. A comparison between $TiCl_4$ and $Ti(SO_4)_2$ has shown that brookite can be obtained at lower temperatures using $TiCl_4$ in a hydrothermal method.[156]

Kominami et al. demonstrated the importance of the presence of sodium with organometallic titanium sources.[157] They showed that using $TiO(acac)_2$, titanium acetylacetonate, with sodium laurate or sodium acetate at a 2:1 Na:Ti ratio in a solvothermal method produced pure brookite. However lowering the Na:Ti ratio or using a different alkali metal salt (e.g. potassium laurate and potassium acetate) gave a mixture of anatase and brookite. This system was also sensitive to the solvent, only the combination of ethylene glycol with a small amount of water resulted in pure brookite. This work serves to highlight each system has very specific and different conditions which lead to brookite.

Thin films of brookite have received even less attention than particles. Di Paola et al. formed a mixture of brookite and rutile nanoparticles by precipitation from $TiCl_4$ with HCl.[158] Brookite was isolated from the mixture by peptisation. The brookite nanoparticles were then deposited as a film by dip-coating a glass slide in a solution and then annealing at 573 K. A number of other groups have used their nanoparticles to make a paste to use in a technique such as doctor blading, but

from here on, methods for film fabrication where crystallisation take place in-situ, are presented. Mills et al. reported a correlation between brookite films and sodium ions.[159] Their study focussed on the incorporation of sodium in TiO_2 films that were produced by either dip-coating a substrate in a sol-gel or by spin-coating the sol-gel. They compared soda lime, borosilicate and quartz glass. When using the dip-coating method, brookite was observed on soda lime glass whereas anatase was produced on the other two substrates. Soda lime glass has the highest content of sodium ions, and whilst the authors noted the link with sodium content in hydrothermal methods, they did not offer any mechanism for the formation of brookite as a film.

There have been other reports of brookite formed by a sol-gel method, including both predominantly brookite[160] and pure brookite films.[161] The pure brookite film was obtained from a $TiCl_4$ precursor with cellulose and oxalic acid as complexing agents. It was found that sodium, which had diffused from the glass substrate, was present in the brookite film. These researchers concluded that a combination of factors including complexing agent, polymer additive, solution media and precursor concentration led to the formation of brookite.

Brookite has been obtained by sputtering from a titanium source onto a silicon wafer.[162] The as-deposited films contained a mixture of anatase and brookite. Two different annealing methods were tested; CTA, conventional thermal annealing (heating rate of 2 °C/min and held at the target temperature for two hours) and RTA, rapid thermal annealing, (heating the sample at the target temperature for 120 seconds). It was found that rutile was formed at temperatures of 800 °C or above with CTA whereas brookite was obtained at 800 °C with RTA. This was attributed to the lower amount of thermal energy applied to the sample during RTA which allowed metastable brookite to form.

The only publication found using chemical vapour deposition is a report by Basu and co-workers who employed a plasma enhanced CVD method.[163] They used titanium tetra-isopropoxide, TTIP, and oxygen gas (mixed with argon) as the precursors on a silicon (110) surface with an applied substrate bias of – 250 V d.c. The product was large pure brookite crystals approximately 500 x 1200 nm. They

have explained that the applied voltage can supply sufficient energy (as does heat in other variants of the CVD process) to achieve the required optimised energy that allows a certain crystal structure to form through reorganisation of the heavy ions. This explanation is rather vague and does not give any reason why these conditions should favour brookite over the other titania polymorphs.

Clearly, there is a great deal of work to be undertaken in order to elucidate the factors which lead to brookite formation in any thin film synthetic method but particularly from chemical vapour deposition.

4.1.3 Photocatalytic activity of brookite

Having reviewed synthetic strategies for brookite formation, the following section highlights selected reports of the photocatalytic properties of brookite in order to gain an appreciation for the potential applications of the material and understand the motivation for further investigation.

The physical properties of brookite are often considered to be between that of anatase and rutile. The band gap, for example, has been determined as 3.1 eV whereas anatase and rutile have a band gap of 3.2 eV and 3.0 eV respectively.[32] However, the photocatalytic activity is less well understood. Ohtani et al. in 1985 were the first to describe the photocatalytic activity of brookite.[164] They reported that (platinised) brookite was highly active in the degradation of propanol to acetone and hydrogen, demonstrating that the conduction band energy of brookite was sufficiently high to enable the hydrogen evolution, like anatase but unlike rutile. Photodeposition of silver from silver sulphate was also used as a test for photocatalytic activity. In both of these tests brookite was shown to be more active than anatase or rutile.

Koelsch identified brookite as a promising candidate material for use in DSSCs.[165] They used cyclic voltammetry to demonstrate that brookite is more electrochemically active than films of anatase.

The aforementioned study of TiO_2 on different glass substrates with varying levels of sodium assessed the photocatalytic activity of the film by resazurin ink bleaching and stearic acid degradation.[159] They reported the lowest activity for the brookite film in both tests. However in this case the presence of the sodium ion may be responsible for the low activity.

Another study by the group of Bahnemann used an aqueous solution of titanium bis(ammonium lactate) dihydroxide, TALH, and urea under hydrothermal conditions to form either anatase nanoparticles or brookite nanorods or a mixture of the two, depending on the concentration of urea.[166] Each of the pure phases and mixtures with a range of compositions were platinised and assessed for hydrogen evolution from a methanol/water solution. The pure brookite outperformed the pure anatase, the mixtures and even Degussa P25 (a commercially available mixture of anatase and rutile that is commonly used as a 'gold standard' in photocatalysis). This was despite the significantly lower surface area of the pure brookite. The authors attribute this to a slightly lower conduction band edge of brookite compared to anatase, making the production of hydrogen more favourable. This is also evidenced by measurement of the flat band potential of brookite and anatase. Degradation of dichloroacetic acid, DCA, was also used as a further examination of photocatalytic activity. The results of this test showed brookite and brookite containing mixtures to be less active than anatase. There was, however, a direct correlation between the surface area and activity, i.e. the anatase particles had the highest surface area and the highest activity, therefore it would be invalid to conclude that anatase is a better photocatalyst from these investigations.

Nanoflowers from a titanate precursor (discussed previously) showed activity for the degradation of methyl orange.[150] The most active sample tested was a mixture of anatase and brookite followed by pure brookite and then pure anatase. However it was noted that when accounting for difference in surface area, the pure brookite sample would be expected to give the highest activity.

Kominami et al., who used a $TiO(acac)_2$ precursor, demonstrated that their brookite nanoparticles had similar activity to Degussa P25 but worse activity

compared to pure anatase in the dehydrogenation of 2-propanol.[167] However these direct comparisons of activity may not be entirely fair since when comparing anatase and brookite particles with similar surface areas (i.e. samples calcined at 823 K in both cases), the authors note that a small amount of rutile appears in the brookite sample, which may have a detrimental effect on the photocatalytic activity.

Research by the same group (Kominami et al.) highlighted the different trends that can be observed when using different photocatalytic tests.[168] They used brookite particles that had been calcined at various temperatures between 400 K and 1200 K in three different photocatalytic tests. A higher calcination temperature gave larger particles and therefore a decreased surface area. Testing for CO_2 evolution from acetic acid, the rate decreased with increased annealing temperature implying that surface area is more important than crystallinity. The investigation of hydrogen evolution showed a (platinized) sample calcined at 823 K gave the best performance, suggesting a compromise between surface area and crystallinity gives the highest activity (this sample gave a similar rate to P25). Finally, for O_2 evolution from silver sulphate, the samples with the highest calcination temperatures were best. This was attributed to the requirement for four holes to be present for the generation of oxygen and therefore this test is more sensitive to the recombination of electrons and holes within the particles. Rates of recombination are generally lower in the samples that have been annealed at higher temperatures. These trends have also been shown to be the same for anatase.

Yu et al. have studied experimentally, the reactivity of different faces of the brookite crystal structure.[169] They report the synthesis of single crystal nanosheets, nanoflowers and nanospindles of brookite from $TiCl_4$, urea and sodium lactate, which acts as a surfactant and complexant, forming in-situ a $[Ti(C_3H_4O_3)_3]^{2-}$ precursor. The lactate ion absorbs onto specific faces of the brookite crystal causing kinetically selective growth of various faces of the grain seed. The lactate ion was necessary to form pure brookite as without which a different precursor $[Ti(OH)_2(OH_2)_4]^{2+}$ was generated which resulted in mostly anatase with only a little brookite and rutile. It was determined that the nanosheets

had four 210 two 101 and two 201 facets exposed. In contrast, the nanoflowers and nanospindles did not have any particular facets exposed and were described as irregularly faceted. Photocatalytic activity was assessed by the bleaching of methyl orange. The nanosheets showed higher activity than Degussa P25 whilst the nanoflowers and nanospindles were inactive. The authors attribute this to the high percentage of the exposed high energy 101 facet which is known to be highly catalytically active. Also, measurements of the production rate of ·OH radicals indicated that there is repressed recombination of electrons and holes in the nanosheets which would also give rise to a more active photocatalyst.

The aforementioned brookite films reported by Di Paolo et al. were shown to degrade 2-propanol under UV irradiation however no comparison of activity was made with either anatase films or an industry standard photocatalyst film.[158]

Some researchers have suggested there may be a synergistic interaction between anatase and brookite. Chen showed that nanoparticles synthesised hydrothermally from a titanate precursor could be either anatase or brookite depending on the NaOH concentration.[34] The pure brookite titania was more active for hydrogen evolution than pure anatase despite having lower surface area. Yet a mixture of anatase and brookite together gave the highest activity, which when normalised for surface area, was 220% higher than Degussa P25. They ascribed this to separation of electrons and holes at the phase interface by electrons in brookite transferring to the CB of anatase due to the more negative flat band potential of brookite. They also complimented these findings with femtosecond transient absorption spectroscopy (TAS) measurements which showed that the photoexcited electrons in brookite had the longest lifetimes.

4.2 Experimental

All depositions were carried out using the atmospheric pressure chemical vapour deposition reactor which is detailed in section 1.4. Titanium tetrachloride (ReagentPlus 99.9%) was obtained from Sigma Aldrich, ethyl acetate (laboratory

reagent grade) was obtained from Fischer Scientific, and tert-butylamine (99.5%) from Sigma Aldrich. A brookite crystal was purchased from Crystal Seen Trading Co. All precursors were used without further purification. Float glass with an SiO_2 barrier layer on one side was supplied by Pilkington and was cleaned with water and detergent, acetone and isopropanol then dried in an oven prior to use. Stainless steel coupons (25 x 25 x 0.1 mm), 304 grade, were purchased from Goodfellow. Characterisation by SEM, XRD and Raman spectroscopy were carried out using the instruments detailed in section 2.2. Photocatalytic activity for samples with a steel substrate was assessed using NO_x testing using the procedure outlined in section 1.5.3.

4.3 Results and Discussion

This section gives three examples of APCVD deposition conditions which lead to the formation of brookite, either as a pure phase or as a mixture with different TiO_2 polymorphs. The samples of pure brookite were further characterised and tested for photocatalytic activity.

4.3.1 Low ethyl acetate mass flow

Given the 1:2 ratio of titanium and oxygen in the structure of titanium dioxide it could be assumed that a 1:2 ratio of mass flows in the CVD process would be required to obtain the correct stoichiometry. However, practically, the ratio of flows is fairly insensitive and TiO_2 is strongly favoured above another titanium oxides such as TiO, Ti_2O_3, Ti_3O_5 or the Ti_nO_{2n-1} series (n = 4-10).[170] This is due to the greater thermodynamic stability (lowest Gibbs free energy) of the dioxide.. With this type of system (i.e. APCVD with $TiCl_4$ and ethyl acetate precursors) the phase is largely then dependent on the temperature of the substrate. Chapter two has shown that neither precursor nor substrate is the single determining factor, although both certainly do have an influence. Depositions were carried out with a

very high ratio of $TiCl_4$ to ethyl acetate. This led to the formation a mixture of anatase and brookite. The deposition parameters for samples 1, 2 and 3 are shown in Table 5.

Sample	**Time (mins, secs)**	**$TiCl_4$ flow rate (mol/min)**	**Ethyl acetate mass flow (mol/min)**	**$TiCl_4$: Ethyl acetate ratio**	**Plain lines total (L/min)**	**Thickness (nm) (at position 2b)**
Sample 1	14	0.0053	0.0034	1.6 : 1	4.6	2042
Sample 2	14, 53	0.0175	0.0011	16 : 1	4.6	637
Sample 3	14	0.0175	0.0011	16 : 1	4.6	486

Table 5 Deposition parameters for variation in ethyl acetate flow (all depositions at 500 °C).

As the table shows, the samples 2 and 3 vary from 1 in the ratio of ethyl acetate to $TiCl_4$. Upon visual inspection for all samples, the glass substrate was fully covered with an off-white film that is partially opaque. The interference fringes, typical of TiO_2 thin films, were also visible.

The most straight forward way of determining the phase is by using Raman spectroscopy. There are a large number of Raman active vibrations for brookite which can easily be identified within a mixture of anatase and brookite. A Raman spectrum for a commercially obtained brookite crystal (powdered with mortar and pestle) was recorded and is shown in Figure 51.

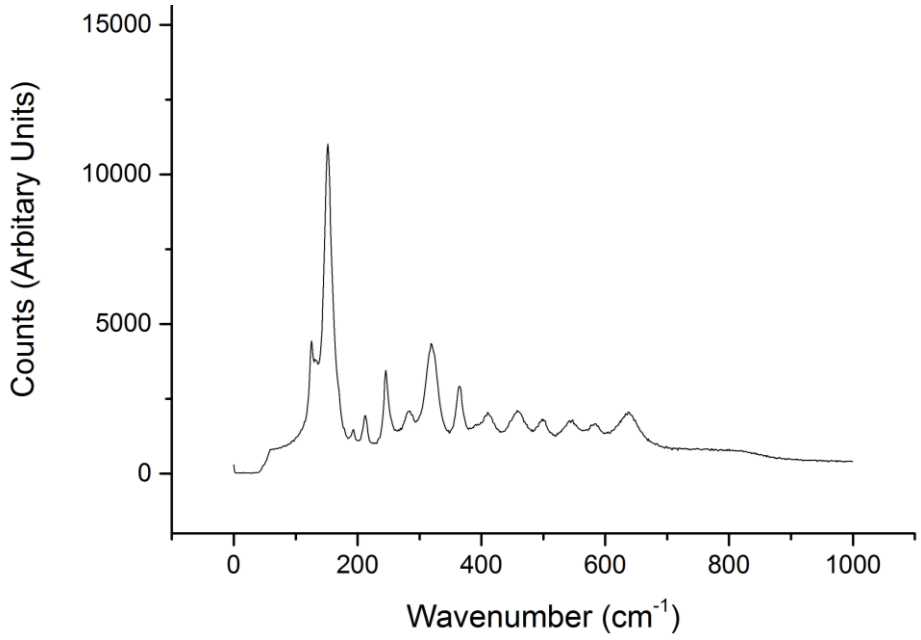

Figure 51 Reference Raman spectrum from commercially obtained brookite.

The peak positions observed in Figure 51 correlate with the reported Raman spectrum for brookite.[105] In contrast, XRD reveals only one peak for brookite which is not coincident (or very close to) an anatase peak and *vice-versa*. Furthermore, the short data collection time for high quality data in Raman spectroscopy, makes it a convenient tool for rapidly assessing many areas across a CVD substrate. For each of the samples, Raman spectra were recorded at a number of locations across the films. The positions are indicated by a number/letter code, which corresponds to a 10 x 20 square grid with letters A-J from left to right and numbers 1-20 from bottom (i.e. end closest to the gas inlet) to top (nearest to the exhaust). Figure 52 shows selected Raman spectra from specific regions of sample 2 exemplifying a region identified as pure rutile (position 2i), pure anatase (position 4b) and an anatase/brookite mixture (position 2b).

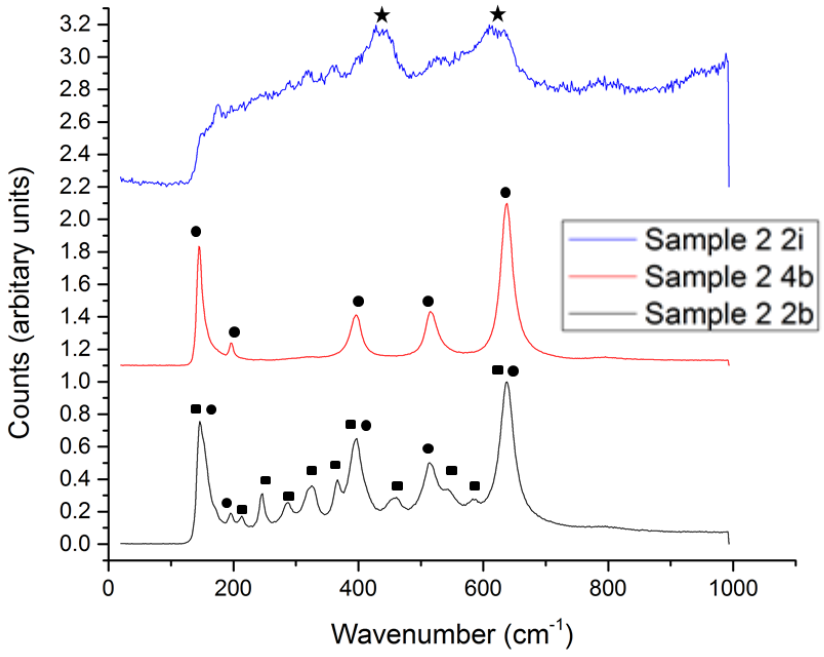

Figure 52 Raman spectra of selected positions on sample 2. Circles indicate anatase, squares indicate brookite and stars indicate rutile.

There are a number of peaks which occur very close to one another (for example the E_g mode of anatase at 144 cm^{-1} and the A_{1g} mode at 153 cm^{-1} brookite), however the presence of a peak at 516 cm^{-1} is used to confirm the presence of anatase whilst brookite has several peaks in the region of 200-380 cm^{-1} for identification of brookite. Note that the region below ca. 150 cm^{-1} does not show peaks with the expected intensity due to degradation of the notch filter within the Raman instrument, however unambiguous assignment of the phases present is still possible. The effect of the notch filter is also seen in the decrease in background noise hence it is possible to establish that the reduced intensity of peaks below 150 cm^{-1} is due to an instrument artefact rather than a peculiarity of the sample. In Figure 53 colour is used to indicate the phase of the TiO_2 in each of the positions analysed.

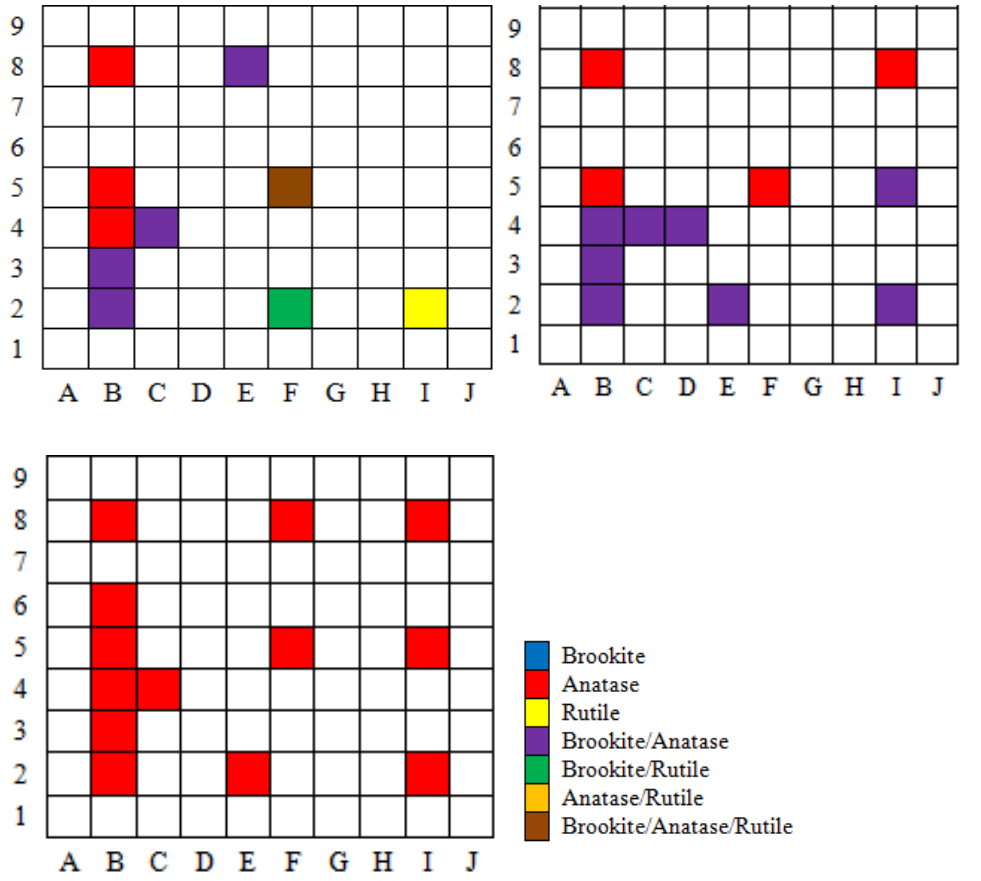

Figure 53 Map of phase distribution for samples 2 (top left) and 3 (top right) and 1 (bottom left).

Inspection of the phase maps reveals that the films formed under low ethyl acetate conditions do not have a homogenous phase. Brookite tends to be present near to the gas inlet on the left-hand side of the glass substrate. The TiO_2 precursors entered the reactor on the right-hand side. Only nitrogen gas entered through the inlet on the left-hand side of the reactor. Sample 3 was made with a slightly shorter deposition time and showed a similar trend with anatase and brookite mixtures on the left hand side of the reactor, however there was no discernible rutile present on the right hand side. It could be presumed that rutile was formed as a result of a longer reaction time however a deposition for 1 minute 15 seconds (with the same flow rates as 2 and 3) shows the presence of rutile in the centre and right-hand side of the substrate and a mixture of anatase and brookite on the left-hand side in a similar manner to 2. It may be the case that rutile is present in sample 3 but it not detectable by Raman or that variation in the substrate

temperature have led to rutile formation in sample 2. CVD reactors of this nature are known to give a variation in conditions. Previous work has investigated the variation in phase across a TiO_2 film formed under similar reaction conditions.[104] These researchers found that at 450 °C anatase was found across the substrate but at 600 °C anatase was formed nearer the front and rutile was incorporated toward the back of the reactor. This was attributed to changes in temperature of the gaseous precursors when entering the hot reactor environment and heating up as they pass through the reactor, as well as subtle changes in reactant concentration through the reactor. It is also difficult to say with confidence that the temperature of the carbon block is uniform across its whole area. There are two Whatman heater cartridges within the carbon block which are approximately 2 cm in diameter placed in the centre of the block, hence it is likely that the edges of the block are somewhat cooler, particularly given that the quartz surrounding the reactor zone is not heated, i.e. it is a cold walled type reactor. Once the reactor has reached its temperature set point, it is allowed to equilibrate for a minimum of 45 mins before the deposition to minimise the temperature gradient across the carbon block. Variations in precursor concentration within the reactor can be caused by dispersion of the gas as it moves from the pipework into the much larger volume of the reactor and also by depletion of the precursors due to their reaction at the front region of the reactor. These are innate features of CVD and very difficult to avoid and also extremely challenging to measure or monitor in-situ. It is highly likely, however, that these variations in concentration may affect the chemistry of the deposition reaction and in turn influence the phase of the material. As discussed in the introduction of this chapter, concentration of solution phase reactants can have a critical effect on polymorphic phase, hence it is reasonable to suggest it is also a relevant parameter in APCVD. Given that all other parameters (temperature, plain flow rates, substrate etc) have been kept constant between samples 2/3 and 1, other than the $TiCl_4$ to ethyl acetate flow rate (note that this consequently increases the total flow rate since plain flow lines were not adjusted) the amount of the oxygen precursor present in the reactor can be identified as a critical parameter in the formation of the brookite polymorph. Brookite is observed when the flow rate of ethyl acetate is very low.

In order to gain further insight into the conditions and mechanism for brookite formation, two further systems were studied.

4.3.2 Brookite formation in the presence of an amine

Depositions were carried out in the presence of an additional chemical species, namely tert-butylamine. Here, depositions were performed on glass with identical parameters except for changed amount of tert-butylamine and ethyl acetate used (note that this does have the effect of altering the total gas flow since the plain flow lines were not adjusted). The films formed in the presence of amine are yellow in colour, indicating incorporation of nitrogen into the TiO_2 structure. The deposition parameters are shown in Table 6.

Sample	$TiCl_4$ mass flow	Ethyl acetate mass flow	Plain lines	Amine mass flow	Phase	Thickness (µm) (range)
Sample 1	0.0053	0.0034	4.6	0	Anatase	6.4 (6.1 - 6.7)
Sample 4	0.0053	0.0034	4.6	0.0013	Anatase/Brookite mix	2.4 (2.1 - 2.6)
Sample 5	0.0053	0.0104	4.6	0.0013	Anatase/Brookite mix	2.4 (2.1 - 2.7)
Sample 6	0.0053	0.0142	4.6	0.0013	Anatase	8.0 (7.3 - 8.5)
Sample 7	0.0053	0.0034	4.6	0.0007	Anatase	4.0 (3.8 - 4.1)

Table 6 Deposition parameters of TiO_2 varying amine and ethyl acetate flow rates (all deposition at 500 °C for 14 mins).

For all samples in Table 6 an area in the centre of the glass (approximately 12 cm^2 was investigated. At least four Raman spectra and three thickness measurements were recorded in this area for each sample. The phase designation (i.e. either anatase or anatase/brookite mixture) was the same for each of the four spectra from one sample. The thickness varied in different positions as shown in Table 6. It was found that without the amine, pure anatase is formed (sample 1) on the glass substrate and when the amine is introduced (sample 4), an anatase/brookite mixture is formed. From this starting point the amount of ethyl acetate was increased. Increasing to a ratio of approximately 1:2 $TiCl_4$:ethyl acetate an anatase/brookite mixture was observed again (sample 5), but then increasing the ethyl acetate flow rate still further to 1:2.7 $TiCl_4$:ethyl acetate ratio yielded pure anatase (sample 6). Similarly, reverting to initial ethyl acetate flow rate, used in sample 1 and sample 4, and introducing a very small amount of amine (lower flow than sample 4) resulted in pure anatase (sample 7).

Looking at the phase of the sample 4 film alone, one could infer that the presence of the amine causes the formation of brookite. However, with the same amount of amine, but sufficiently increased ethyl acetate, pure anatase is observed. From these observations it is possible to conclude that introduction of the amine above a critical amount will cause brookite formation unless the flow rate of ethyl acetate is increased. The proposed explanation is that the amine reacts with ethyl acetate with the effect of lowering the overall ethyl acetate concentration. This then results in a situation such as in the previous section which results in brookite formation mixed with anatase.

4.3.3 Substrate dependant brookite formation

An investigation was carried out to determine if substrates other than glass can support the formation brookite titania, and if so, what effect the substrate has on the phase composition. Steel (304 grade) was an appropriate choice of alternative substrate given the industrial interest in photocatalytic coatings on architectural materials, as outlined in section 2.1.1. Four pieces of steel were placed directly on

top of a sheet of SiO_2 barrier coated glass, with gaps of approximately 4 mm between each steel piece. This was to allow the glass between the steel pieces to be coated and compare the phase of the coating on the steel and the surrounding glass. The deposition parameters used are shown in Table 7.

Sample	**Temp (°C)**	**Time (mins, secs)**	**$TiCl_4$ mass flow rate (mol/min)**	**Ethyl acetate mass flow rate (mol/min)**	**Plain lines (L/min)**
Sample 8	500	1, 15	0.008	0.004	4.6

Table 7 Deposition parameters for TiO_2 on steel and glass, simultaneously.

Each piece of steel was analysed by Raman spectroscopy in three different positions. It was found that all the pieces of steel except the one from the bottom left corner was pure brookite, in all areas analysed. The piece of steel from the bottom left corner of the reactor had pure brookite in one of the three areas tested and an anatase/brookite mixture in the other two areas. As mentioned previously there are a number of coincident Raman peaks in the brookite and anatase spectra, however for this analysis it has been judged to be pure brookite if the peaks at 128 cm^{-1}, 153 cm^{-1} with a shoulder at 135 cm^{-1} are discernible. This is used to discount the presence of anatase as it is presumed that the very strong intensity of the anatase Eg mode at 144 cm^{-1} would obscure this shoulder even with a very small amount of anatase present. An example of a pure brookite on steel Raman spectrum is given in Figure 54.

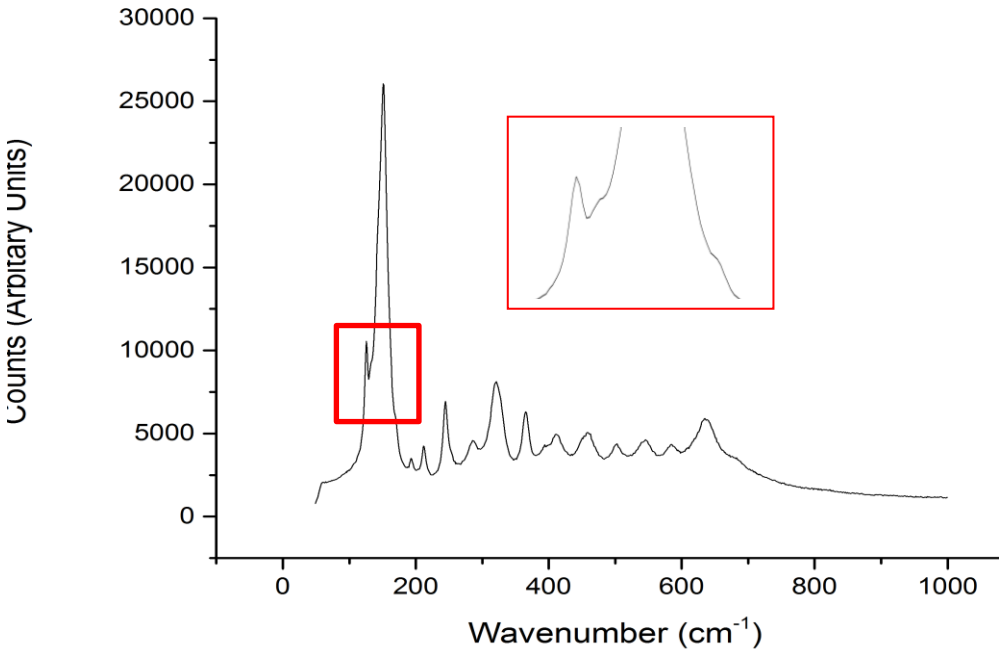

Figure 54 Raman spectrum of pure brookite, sample 8 with inset illustration of shoulder at 135 cm^{-1}.

Pure anatase was found on the glass in every area tested including around the positions where the steel had been. This demonstrates that a steel substrate can induce formation of an entirely different polymorph even under identical flow and heating conditions (i.e. simultaneous deposition on glass and steel). The reasons for this could be physical, i.e. a templating effect due to the nature of the surface on steel, or chemical. Given that Chapter 2 presents results demonstrating the formation of anatase on a 304 steel substrate, the nature of the steel surface cannot be the dominating factor. The conditions used to produce brookite on steel had lower ethyl acetate flow rate than was used in Chapter 2 where anatase was formed. However, the low ethyl acetate flow rate also cannot be the determining factor since the identical flow rates produce anatase on the glass surrounding the steel. Given that the previous sections have suggested low ethyl acetate concentration as a condition for brookite formation, one could consider whether the ethyl acetate could be depleted or removed in some way at the steel surface. A possibility could be that the steel surface is not fully oxidised (unlike the SiO_2

surface of the glass) and is chemically reacting with the ethyl acetate and lowering the amount available for TiO_2 formation. However, with this theory, one would expect the oxide layer to be formed quickly and the continuous flow of ethyl acetate to be sufficient to replace any that has reacted with the steel surface. Further work is required to establish what the critical difference between the glass and steel substrate is, see Chapter 5 for possible strategies.

4.3.4 Mechanism of brookite formation

These results presented in the previous three sections give three sets of conditions in which the formation of brookite is observed. In the first case, low ethyl acetate flow rate is clearly identified as the variable which results in brookite formation. It is proposed that in the presence of amine the ethyl acetate concentration is also depleted, however this is speculative since no direct measurements have been carried out. However, these observations do not establish a cause and effect relationship. The question remains as to why this condition, of low ethyl acetate concentration, would favour brookite over anatase or rutile. The answer to this is not immediately obvious since the stoichiometry of all three polymorphs is, by definition, the same, so lowering the amount of oxygen precursor available is not an intuitive explanation for the formation of brookite. In contrast to solution based methods of TiO_2 formation, no published work has been found on the mechanism of brookite formation from vapour deposition. It is interesting to note that the only other paper which reports brookite formation by a CVD process, plasma enhanced CVD, comments on the chemical reaction of O^+ ions, suggesting that hydroxyl and carboxyl groups are not able to bond with Ti but are instead oxidised into gaseous products and removed via the exhaust (i.e. lowering the amount of reactive oxygen). This has not been proven experimentally and again why this should lead to brookite is not explained.

It is necessary to consider the chemical species which are involved in the reaction which forms the bonds in TiO_2. No reports were found in the literature of either experimental work or theoretical modelling on the decomposition pathway of

$TiCl_4$ and ethyl acetate or of the mechanism for TiO_2 formation. A speculative mechanism was proposed by Parkin et al. which involved a three step process.[171] Equation 4 shows the degradation of ethyl acetate into ethenone and ethanol.

$$CH_3CO_2CH_2CH_3 \rightarrow C_2H_2O + CH_3CH_2OH$$

Equation 4

The ethanol can then further break down into water and ethane, as shown in Equation 5.

$$CH_3CH_2OH \rightarrow H_2O + C_2H_4$$

Equation 5

The water can then react with the titanium chloride and form the titanium dioxide, as shown in Equation 6.

$$TiCl_4 + 2H_2O \rightarrow TiO_2 + 4HCl$$

Equation 6

The exact processes which take place in this final step are not detailed, however it is reasonable to assume that all four chloride ions do not simultaneously dissociate, but rather that it is a step by step process in which each Cl^- is replaced with a OH^- resulting in a $Ti(OH)_4$ complex. This would then give rise to a situation whereby the TiO_2 bonds are formed by a dehydration step between two hydroxide ligands.

An alternative degradation pathway of the ethyl acetate could be nucleophilic-type attack of the ester bond to form acetyl chloride and an ethoxide ligand on the titanium centre, as shown in Equation 7. This seems reasonable as the ethenone product proposed in Equation 4 is highly reactive and susceptible to nucleophilic attack.

$$CH_3CO_2CH_2CH_3 + TiCl_4 \rightarrow CH_3COCl + Ti(Cl)_3(OCH_2CH_3)$$

Equation 7

Both of these approaches have been proposed as possible reaction pathways by Sheel et al.[72] It is interesting to note that a titanium centre with four ethoxide ligands would closely resemble titanium tetra-isopropoxide, TTIP, which is another common precursor used in CVD for the deposition of TiO_2.

With either scenario for ethyl acetate decomposition it seems likely that there is a stage at which the titanium metal is coordinated to an oxygen containing ligand. This oxygen containing ligand would then be able to react with another ligand on a nearby metal centre, with the elimination of water, ethanol or HCl, forming a Ti-O-Ti bond. This then leads to a circumstance in which one could apply the same logic to explain brookite formation as for solution based processes. That is, for edge sharing octahedra to form there must be two adjacent oxygen containing ligands on a metal centre. When only one OH group is present on each metal centre a vertex sharing interaction would form. This is depicted in Figure 55.

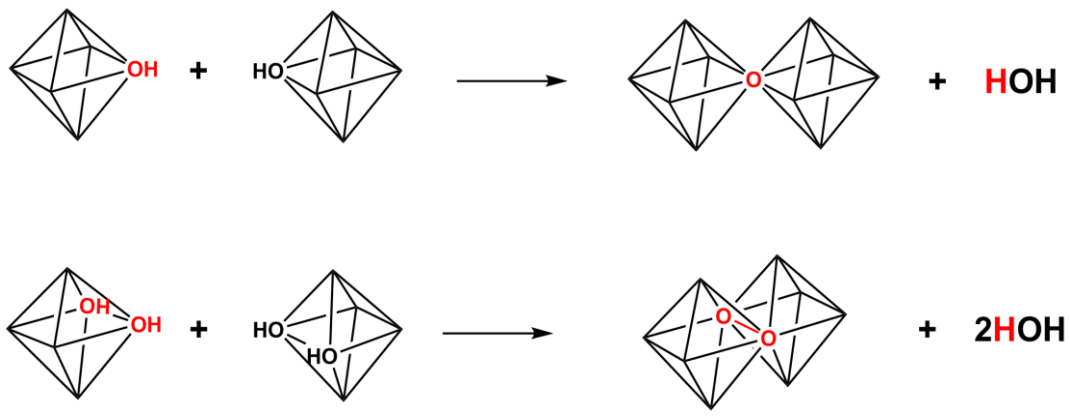

Figure 55 Formation of vertex sharing octahedra (top) and edge sharing octahedra (bottom).

There would be a higher chance of edge sharing interaction occurring with more ethyl acetate present. Since anatase has four edge sharing octahedra, its formation is favoured with higher levels of ethyl acetate but with low ethyl acetate

concentration, the chloride ligand are less likely to be replaced with an oxygen containing ligand. This rationale would suggest anatase is always favoured with a single source precursor such as TTIP as all four ligands would contain oxygen and may explain why brookite formation has not been reported by other groups since TTIP is usually the preferred precursor.

4.3.5 Characterisation and photocatalytic activity of pure brookite

In order to investigate the morphology of pure brookite, the surface was investigated using scanning electron microscopy. The images below show pure brookite on steel (sample 8) at three different magnifications.

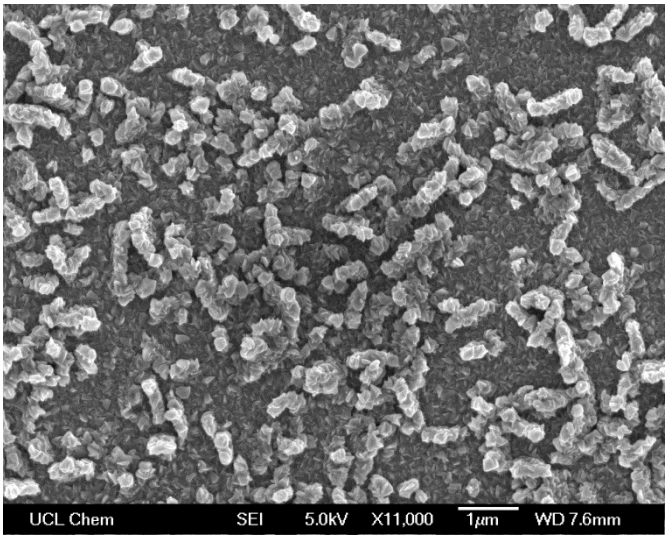

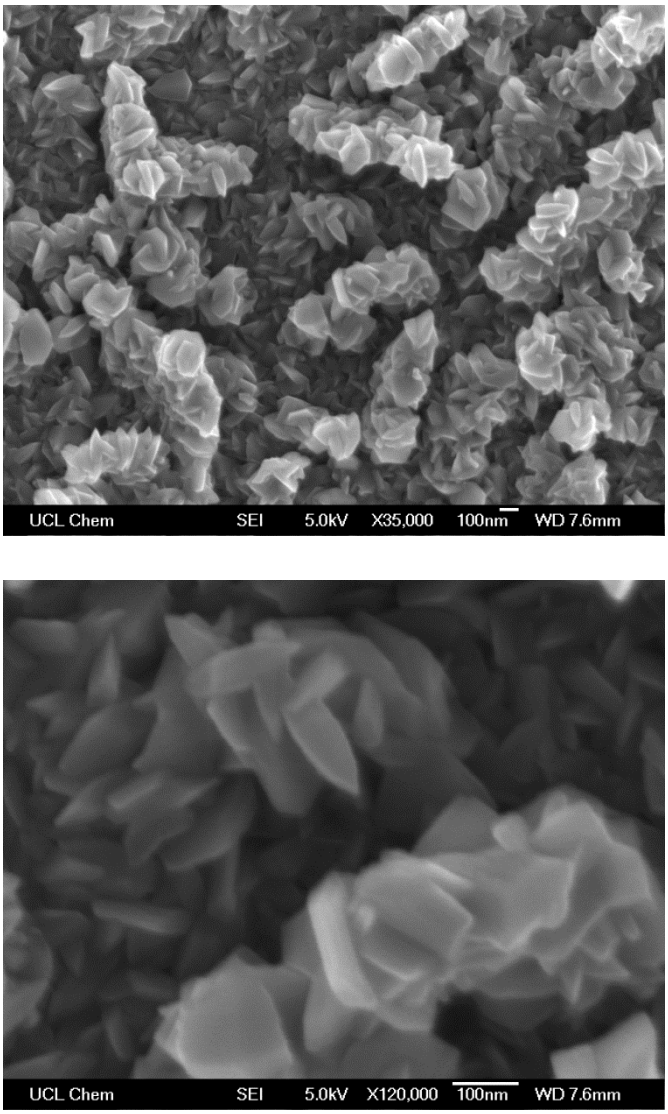

Figure 56 SEM images of brookite on steel substrate at differing magnifications.

These images illustrate that the particle size of brookite is comparable to that of anatase and rutile (as shown in Chapter 2). However there appears to be pillars or columns consisting of many stacked plate-like particles, which results in a more textured surface at the micron scale than is typically seen for anatase films. This would indicate that these films would be of interest for future studies of photocatalysis as an increased surface area would be predicted to give high photocatalytic performance.

Plate type morphology of brookite has been observed by others.[145] This may suggest that the growth mechanism is similar, adding weight to the hypothesis that

the brookite, here, is formed by linking of Ti octahedra in a similar manner to solution based processes.

Given that no studies into the photocatalytic properties of brookite CVD films were found in the literature, a sample of pure brookite sample 8 on steel was selected for testing and compared to a standard of Pilkington Activ glass in addition to a blank of uncoated steel. NO_x destruction was selected as a test method given that other standard photocatalytic tests such as stearic acid and dye degradation usually require a transparent substrate for transmission measurements of IR or UV-vis. The results shown in Figure 57 plot the change of NO concentration in the dark and under UVA irradiation for sample 8, blank uncoated steel and a piece of Activ glass (25 mm x 25 mm).

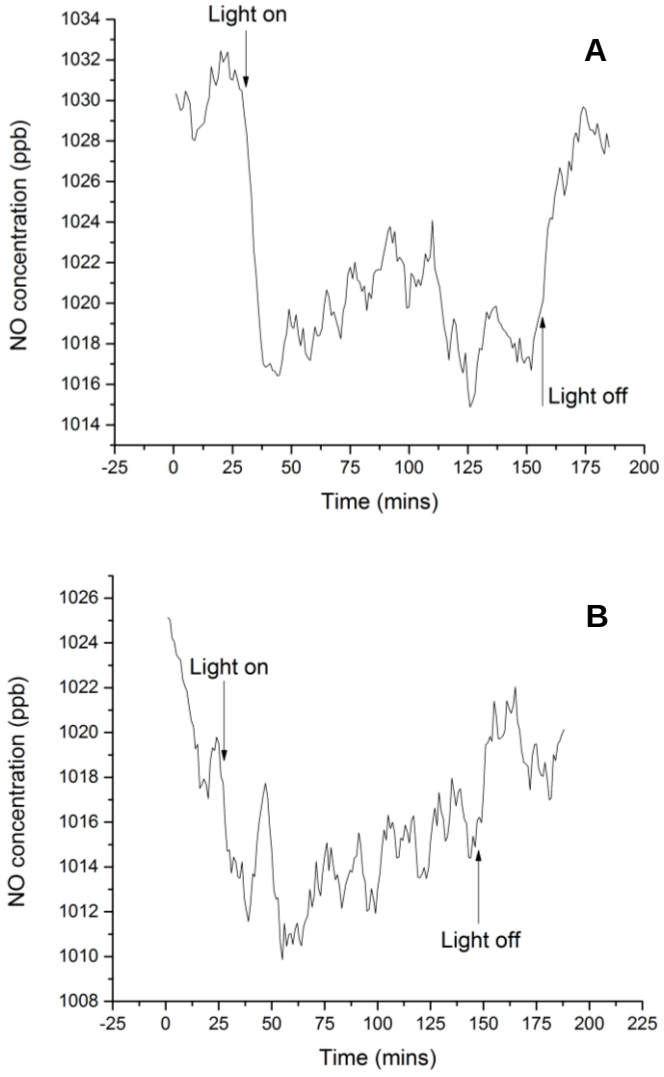

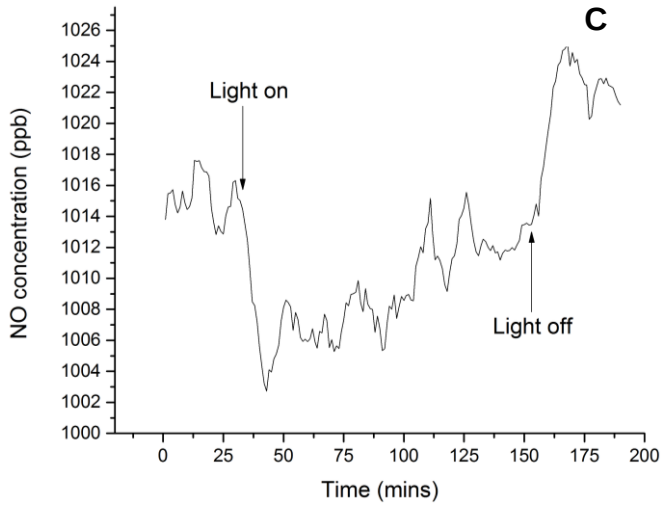

Figure 57 Change in NO concentration during irradiation of A) sample 8 B) Uncoated steel C) Activ glass.

As can be seen from the graphs in Figure 57, sample 8 clearly shows a response to illumination, as does the Activ glass whereas for the uncoated steel this is not obvious. Unfortunately the baseline for the steel test was not steady before the light was switched on so it is difficult to determine if the continuing decrease in NO concentration after switching the lamp on is due to the illumination or a continuation of the shifting baselines. The percentage loss of NO was 0.97% for sample 8 and 0.93% for Activ glass. Although it would appear that the pure brookite sample is more active than Activ glass, it is also difficult to determine the relative activity from these results. The high level of noise observed in the test means that the results should be treated with caution. Under ISO conditions for this test a sample size of 100 mm x 50 mm is used which has an area eight times greater than these 25 mm x 25 mm samples, hence approximately only one eighth of the response would be expected compared to a typical thin film tested under ISO conditions. However less than half the expected response, since a 100 mm x 50 mm piece of Activ glass, which was used to check the validity of the test method, gave 19.2% loss of NO. Therefore these results only serve to indicate that brookite on steel does have a photocatalytic response but further testing would be required, with a larger sample to confidently compare activity with other standards.

4.4 Conclusions

The results in this chapter have demonstrated a simple route to brookite formation using atmospheric pressure CVD. Three different systems were investigated and a correlation was found that suggested low gas phase ethyl acetate concentration was a key factor in the phase determination. It was proposed that brookite formation is due to fewer oxygen containing ligands around the metal centre during elimination reactions which form the titania bonds. Photocatalytic results presented here and evidence from the literature suggest that brookite is a promising photocatalyst which could potentially overtake anatase in popularity. This simple synthetic procedure could allow a great deal of further research into the properties of brookite thin films and further progress toward to the wider goal of developing efficient photocatalysts.

CHAPTER FIVE

CONCLUSIONS AND FURTHER WORK

Chapter 5: Conclusions and further work

The work presented in this thesis has demonstrated how the variation in parameters of chemical vapour deposition can affect the properties of the resultant film. Some novel properties have been demonstrated and a new application in the biomedical field has been investigated.

The investigation into films deposited from $TiCl_4$ and ethyl acetate onto different grades of stainless steel (presented in Chapter 2) has shown that anatase is the predominant phase in the vast majority of areas analysed for each type of steel. These findings provided evidence to show that a previously proposed mechanism in the literature for precursor directed phase control in TiO_2 deposition on steel is incomplete and more complex than previously thought. Based on the data presented in this thesis it is difficult to rule out a link between film thickness and phase. This could be studied using grazing incident angle XRD (GIXRD). The angle at which x-rays hit the sample can be accurately controlled so as to vary the penetration depth of the x-rays, thus allowing phase determination at different depths in one area of the film. This would reveal any changes in phase as the film increases in thickness.

Titanium dioxide films have been produced on aluminium foil, a flexible, light-weight, corrosion resistant and inexpensive substrate. The film remains adherent after repeated bending and folding. The coating has also demonstrated photocatalytic properties in contrast to several previous literature reports of titania coated aluminium. These results have highlighted the possibility of flexible photocatalytic films but a great deal of further work could be undertaken to realise its full potential such as anti-bacterial testing, water purification studies and corrosion resistance in sea water.

Titanium dioxide coatings were deposited on a CoCrMo alloy. The development of human mesenchymal stem cells was studied by investigating the cell morphology, hydroxyapatite and collagen formation and calcium deposition. The results revealed improved osteogenic differentiation of hMSCs on CoCrMo alloy when coated with TiO_2. This opens many attractive avenues of future work.

Studies are currently in progress to assess the adhesion of cells to the titania coating, ion release in biological media and wear resistance properties. If successful, in-vivo studies could be considered to determine how the titania coated CoCrMo material could translate to a clinical environment.

A study on nitrogen doped TiO_2 investigated the effect of variation in oxygen precursor concentration on nitrogen incorporation in the TiO_2 lattice, optical properties, morphology and photocatalytic activity of the film. It was found that a sample synthesised with lower amount of oxygen precursor was photocatalytically active under both UV and visible light illumination. However, there could be several explanations for this and a range of samples would need to be synthesised to understand the effect of all these variables in the films' properties on photocatalytic activity. A further possible variable that has not been investigated in this work, is the concentration of oxygen vacancies. Since the most active film was produced with a lower amount of oxygen precursor, it is conceivable that the number of oxygen vacancies could be higher. There are suggestions in the literature which indicate oxygen vacancies are responsible for visible light activity so this would be an intriguing possibility worthy of further investigation.

Finally, the fourth chapter reports the first known example of brookite formation by APCVD. Brookite was observed in three separate systems, i) under low ethyl acetate flow conditions, ii) in the presence of an amine and iii) on a steel substrate. In the case of the steel substrate pure brookite was obtained. It has been proposed that the mechanism for brookite formation is related to the amount of ethyl acetate that is available, however in the case of the amine and steel studies that has not been proven experimentally. An insightful progression to this work could be a study of the gas phase reactions occurring in these systems by a technique such as mass spectrometry. IR spectroscopy could be used to study the species present at the surface of the substrate during a deposition, however specialist equipment would be required for these studies. Elucidation of the reactive species in the CVD reactor could help to explain why brookite has been observed under these conditions. Furthermore, since a simple and easily scalable method for pure brookite formation has been developed, this allows extensive further research into the properties and applications of brookite. The work here has only given an

indication of the photocatalytic properties of brookite films but a broad investigation could identify optimum conditions in order to maximise photocatalytic properties. The resazurin ink test could be used to test samples on glass with a mixture of anatase/brookite compositions to rapidly investigate the link between phase and photocatalytic activity. As many literature reports have suggested brookite can be a more active photocatalyst than anatase, there is great potential to investigate this further and explore the possibility of brookite based commercial products.

References

1. Lademann, J., et al., *TiO2 nanoparticles as an effective UV-B radiation skin-protective compound in sunscreens.* Journal of physics. D, Applied physics, 2005. **38**(15): p. 2564-2570.
2. Yang, W. and C.A. Wolden, *Plasma-enhanced chemical vapor deposition of TiO2 thin films for dielectric applications.* Thin Solid Films, 2006. **515**(4): p. 1708-1713.
3. Kim, S.K., et al., *Titanium dioxide thin films for next-generation memory devices.* Journal of Materials Research, 2013. **28**(03): p. 313-325.
4. Tang, H., et al., *TiO2 anatase thin films as gas sensors.* Sensors and actuators. B, Chemical, 1995. **26**(1-3): p. 71-75.
5. Garzella, C., et al., *TiO2 thin films by a novel sol–gel processing for gas sensor applications.* Sensors and actuators. B, Chemical, 2000. **68**(1-3): p. 189-196.
6. Fujishima, A. and K. Honda, *Electrochemical photolysis of water at a semiconductor electrode.* Nature, 1972. **238**(5358): p. 37-8.
7. Wang, Q., et al., *Characteristics of high efficiency dye-sensitized solar cells.* The journal of physical chemistry. B, 2006. **110**(50): p. 25210-21.
8. Inoue, T., et al., *Photoelectrocatalytic reduction of carbon dioxide in aqueous suspensions of semiconductor powders.* Nature, 1979. **277**(5698): p. 637-638.
9. Minabe, T., et al., *TiO2-mediated photodegradation of liquid and solid organic compounds.* Journal of photochemistry and photobiology. A, Chemistry, 2000. **137**(1): p. 53-62.
10. Paz, Y., et al., *Photooxidative self-cleaning transparent titanium dioxide films on glass.* Journal of materials research, 1995. **10**(11): p. 2842-2848.
11. Parkin, I.P. and R.G. Palgrave, *Self-cleaning coatings.* Journal of Materials Chemistry, 2005. **15**(17): p. 1689-1695.
12. Howarter, J. and J. Youngblood, *Self-Cleaning and Next Generation Anti-Fog Surfaces and Coatings.* Macromolecular rapid communications, 2008. **29**(6): p. 455-466.
13. Dunlop, P.S.M., et al., *The photocatalytic removal of bacterial pollutants from drinking water.* Journal of Photochemistry and Photobiology A: Chemistry, 2002. **148**(1–3): p. 355-363.

14. Watts, R.J., et al., *Photocatalytic inactivation of coliform bacteria and viruses in secondary wastewater effluent.* Water Research, 1995. **29**(1): p. 95-100.
15. Seven, O., et al., *Solar photocatalytic disinfection of a group of bacteria and fungi aqueous suspensions with TiO2, ZnO and Sahara desert dust.* Journal of photochemistry and photobiology. A, Chemistry, 2004. **165**(1-3): p. 103-107.
16. Page, K., M. Wilson, and I.P. Parkin, *Antimicrobial surfaces and their potential in reducing the role of the inanimate environment in the incidence of hospital-acquired infections.* Journal of materials chemistry, 2009. **19**(23): p. 3819-3831.
17. Cai, R., et al., *Induction of cytotoxicity by photoexcited TiO2 particles.* Cancer research, 1992. **52**(8): p. 2346-8.
18. Atkins, P., et al., *Shriver and Atkins Inorganic Chemistry p.106*. Fourth ed. 2006: Oxford University Press.
19. Atkins, P., et al., *Shriver and Atkins Inorganic Chemistry p.103-4*. Fourth ed. 2006: Oxford University Press.
20. Atkins, P. and J. de Paula, *Elements of Physical Chemistry*. Fourth ed. 2005: Oxford Univeristy Press.
21. Atkins, P., et al., *Shriver and Atkins Inorganic Chemistry p.107*. 2006: Oxford University Press.
22. Atkins, P. and J. de Paula, *Elements of Physical Chemistry p.612*. 2005: Oxford University Press.
23. Ni, M., M.K.H. Leung, and K. Sumathy, *A review and recent developments in photocatalytic water-splitting using TiO2 for hydrogen production.* Renewable & sustainable energy reviews, 2007. **11**(3): p. 401-425.
24. Wang, R., et al., *Light-induced amphiphilic surfaces.* Nature, 1997. **388**(6641): p. 431-432.
25. Carp, O., C.L. Huisman, and A. Reller, *Photoinduced reactivity of titanium dioxide.* Progress in solid state chemistry, 2004. **32**(1-2): p. 33-177.
26. Nelson, J., A. Eppler, and I. Ballard, *Photoconductivity and charge trapping in porous nanocrystalline titanium dioxide.* Journal of photochemistry and photobiology. A, Chemistry, 2002. **148**(1-3): p. 25-31.
27. Mills, A. and S. Le Hunte, *An overview of semiconductor photocatalysis.* Journal of Photochemistry and Photobiology A: Chemistry, 1997. **108**(1): p. 1-35.
28. Moiseev, A., et al., *Analysis of photocatalytic performance of nanostructured pyrogenic titanium dioxide powders in view of their polydispersity and phase transition: Critical anatase particle size as a factor for suppression of charge recombination.* Chemical engineering journal, 2013. **228**: p. 614-621.

29. Moellmann, J., et al., *A DFT-D study of structural and energetic properties of TiO2 modifications.* Journal of physics. Condensed matter, 2012. **24**(42): p. 424206.
30. Herrington, K. and D. Cromer, *The Structures of Anatase and Rutile.* Journal of the American Chemical Society, 1955. **77**(18): p. 4708-4709.
31. Wyckoff, *Crystal structures / R. W. G. Wyckoff Vol. 1*.
32. Grätzel, M. and F. Rotzinger, *The influence of the crystal lattice structure on the conduction band energy of oxides of titanium(IV).* Chemical Physics Letters, 1985. **118**(5): p. 474-477.
33. Kruczynski, L., et al., *Porous titania glass as a photocatalyst for hydrogen production from water.* Nature, 1981. **291**(5814): p. 399-401.
34. Tay, Q., et al., *Enhanced Photocatalytic Hydrogen Production with Synergistic Two-Phase Anatase/Brookite TiO2Nanostructures.* The journal of physical chemistry. C, 2013. **117**(29): p. 14973-14982.
35. Tang, H., et al., *ELECTRICAL AND OPTICAL-PROPERTIES OF TIO2 ANATASE THIN-FILMS.* Journal of Applied Physics, 1994. **75**(4): p. 2042-2047.
36. Macwan, D.P., P. Dave, and S. Chaturvedi, *A review on nano-TiO2 sol–gel type syntheses and its applications.* Journal of materials science, 2011. **46**(11): p. 3669-3686.
37. Patil, K.R., et al., *Preparation of TiO2 thin films by modified spin-coating method using an aqueous precursor.* Materials letters, 2003. **57**(12): p. 1775-1780.
38. Dreesen, L., et al., *Synthesis of titanium dioxide nanoparticles by reactive DC magnetron sputtering.* Thin solid films, 2009. **518**(1): p. 112-115.
39. O'Neill, S.A., et al., *Novel TiO2 CVD films for semiconductor photocatalysis.* Journal of photochemistry and photobiology. A, Chemistry, 2002. **151**(1-3): p. 171-179.
40. Pore, V., et al., *Atomic Layer Deposition of Photocatalytic TiO2 Thin Films from Titanium Tetramethoxide and Water.* Chemical vapor deposition, 2004. **10**(3): p. 143-148.
41. Abou Helal, M.O. and W.T. Seeber, *Preparation of TiO2 thin films by spray pyrolysis to be used as a photocatalyst.* Applied surface science, 2002. **195**(1-4): p. 53-62.
42. Tuan, A., et al., *Interface control in the chemical vapor deposition of titanium dioxide on silicon(100).* Thin solid films, 2000. **377**: p. 766-771.

43. Clark, R.J.H., et al., *Anatase Thin Films on Glass from the Chemical Vapor Deposition of Titanium(IV) Chloride and Ethyl Acetate.* Chemistry of materials, 2003. **15**(1): p. 46-50.
44. Krumdieck, S. and R. Raj, *Conversion efficiency or alkoxide precursor to oxide films grown by an ultrasonic-assisted, pulsed liquid injection, metalorganic chemical vapor deposition (pulsed-CVD) process.* Journal of the American Ceramic Society, 1999. **82**(6): p. 1605-1607.
45. Evans, P. and D.W. Sheel, *Photoactive and antibacterial TiO2 thin films on stainless steel.* Surface & coatings technology, 2007. **201**(22-23): p. 9319-9324.
46. Huang, S., et al., *Morphology of and surface modification by TiO2 deposits on a porous ceramic substrate.* Journal of materials science, 1999. **34**(17): p. 4293-4304.
47. Khalilian, M., Y. Abdi, and E. Arzi, *Formation of well-packed TiO2 nanoparticles on multiwall carbon nanotubes using CVD method to fabricate high sensitive gas sensors.* Journal of nanoparticle research, 2011. **13**(10): p. 5257-5264.
48. Devi, A., *'Old Chemistries' for new applications: Perspectives for development of precursors for MOCVD and ALD applications.* Coordination chemistry reviews, 2013. **257**(23-24): p. 3332-3384.
49. Clark, R.J.H., et al., *Atmospheric pressure chemical vapour deposition of titanium dioxide coatings on glass.* Journal of materials chemistry, 2003. **13**(1): p. 56-60.
50. Hou, X. and K.-L. Choy, *Processing and Applications of Aerosol-Assisted Chemical Vapor Deposition.* Chemical vapor deposition, 2006. **12**(10): p. 583-596.
51. Huang, S.S. and J.S. Chen, *Comparison of the characteristics of TiO2 films prepared by low-pressure and plasma-enhanced chemical vapor deposition.* Journal of materials science. Materials in electronics, 2002. **13**(2): p. 77-81.
52. Babelon, P., et al., *SEM and XPS studies of titanium dioxide thin films grown by MOCVD.* Thin solid films, 1998. **322**(1-2): p. 63-67.
53. Boyd, D.A., et al., *Plasmon-Assisted Chemical Vapor Deposition.* Nano Letters, 2006. **6**(11): p. 2592-2597.
54. Gerbasi, R., et al., *PECVD of amorphous TiO2 thin films: effect of growth temperature and plasma gas composition.* Thin solid films, 2000. **371**(1-2): p. 126-131.

55. Palgrave, R. and I.P. Parkin, *Aerosol assisted chemical vapor deposition using nanoparticle precursors: a route to nanocomposite thin films.* Journal of the American Chemical Society, 2006. **128**(5): p. 1587-97.
56. Choy, K.L., *Chemical vapour deposition of coatings.* Progress in Materials Science, 2003. **48**(2): p. 57-170.
57. Sawunyama, P., et al., *Photodecomposition of a Langmuir−Blodgett Film of Stearic Acid on TiO2Film Observed by in Situ Atomic Force Microscopy and FT-IR.* The journal of physical chemistry. B, 1997. **101**(51): p. 11000-11003.
58. Mills, A. and J. Wang, *Simultaneous monitoring of the destruction of stearic acid and generation of carbon dioxide by self-cleaning semiconductor photocatalytic films.* Journal of photochemistry and photobiology. A, Chemistry, 2006. **182**(2): p. 181-186.
59. Krysa, J., et al., *Correlation of oxidative and reductive dye bleaching on TiO2 photocatalyst films.* Journal of photochemistry and photobiology. A, Chemistry, 2009. **203**(2-3): p. 119-124.
60. Mills, A., J. Wang, and M. McGrady, *Method of rapid assessment of photocatalytic activities of self-cleaning films.* The journal of physical chemistry. B, 2006. **110**(37): p. 18324-31.
61. Kafizas, A., A. Mills, and I.P. Parkin, *A comprehensive aerosol spray method for the rapid photocatalytic grid area analysis of semiconductor photocatalyst thin films.* Analytica Chimica Acta, 2010. **663**(1): p. 69-76.
62. Evans, P., et al., *A comparative study of three techniques for determining photocatalytic activity.* Journal of photochemistry and photobiology. A, Chemistry, 2007. **188**(2-3): p. 387-391.
63. Mills, A. and C. Hill, *Overview of the current ISO tests for photocatalytic materials.* Journal of photochemistry and photobiology. A, Chemistry, 2012. **237**: p. 7-23.
64. Ohko, Y., et al., *Photocatalytic oxidation of nitrogen monoxide using TiO2 thin films under continuous UV light illumination.* Journal of photochemistry and photobiology. A, Chemistry, 2009. **205**(1): p. 28-33.
65. *http://www.pilkingtonselfcleaningglass.co.uk/*. Accessed 19/3/14.
66. *http://uk.saint-gobain-glass.com/product/670/sgg-bioclean*. Accessed 19/3/2014.
67. Hyett, G., et al., *An Investigation into the Optimum Thickness of Titanium Dioxide Thin Films Synthesized by Using Atmospheric Pressure Chemical Vapour Deposition for Use in Photocatalytic Water Oxidation.* Chemistry – A European Journal, 2010. **16**(34): p. 10546-10552.

68. Hyett, G., et al., *Substrate-Dependant Ability of Titanium(IV) Oxide Photocatalytic Thin Films Prepared by Thermal CVD to Generate Hydrogen Gas from a Sacrificial Reaction.* Chemical vapor deposition, 2010. **16**(10-12): p. 301-304.

69. Edusi, C., et al., *Aerosol-Assisted CVD of Titanium Dioxide Thin Films from Methanolic Solutions of Titanium Tetraisopropoxide; Substrate and Aerosol-Selective Deposition of Rutile or Anatase.* Chemical vapor deposition, 2011. **17**(1-3): p. 30-36.

70. Zhao, J. and M.L. Hitchman, *The LPCVD of rutile at low temperatures.* Le Journal de Physique IV, 1999. **9**(P8): p. Pr8-Pr8-364.

71. Battiston, G., et al., *Influence of substrate on structural properties of TiO2 thin films obtained via MOCVD.* Thin solid films, 1994. **239**(2): p. 186-191.

72. Evans, P., M. Pemble, and D. Sheel, *Precursor-Directed Control of Crystalline Type in Atmospheric Pressure CVD Growth of TiO2on Stainless Steel.* Chemistry of materials, 2006. **18**(24): p. 5750-5755.

73. Jeong, H., et al., *Role of Interface Reaction on Resistive Switching of Metal/Amorphous TiO2/Al RRAM Devices.* Journal of the Electrochemical Society, 2011. **158**(10): p. H979-H982.

74. Liu, T., et al., *Structure stability and corrosion resistance of nano-TiO2 coatings on aluminum in seawater by a vacuum dip-coating method.* Surface & coatings technology, 2010. **205**(7): p. 2335-2339.

75. Sun, Y., *Tribological rutile-TiO2 coating on aluminium alloy.* Applied surface science, 2004. **233**(1-4): p. 328-335.

76. Zhu, Y., et al., *Interface diffusion and reaction between TiO2 film photocatalyst and aluminium alloy substrate.* Surface and interface analysis, 2001. **32**(1): p. 218-223.

77. Chen, S.-Z., et al., *Deactivation of TiO2 photocatalytic films loaded on aluminium: XPS and AFM analyses.* Applied Surface Science, 2006. **252**(20): p. 7532-7538.

78. Ho, W., J. Yu, and S. Lee, *Photocatalytic activity and photo-induced hydrophilicity of mesoporous TiO2 thin films coated on aluminum substrate.* Applied catalysis. B, Environmental, 2007. **73**(1-2): p. 135-143.

79. Kang, S.Z., et al., *Immobilization and photocatalytic activity of TiO2 nanoparticles on porous aluminium foil.* Journal of dispersion science and technology, 2005. **26**(2): p. 169-171.

80. Chen, D.Y., C.C. Tsao, and C.Y. Hsu, *Photocatalytic TiO2 thin films deposited on flexible substrates by radio frequency (RF) reactive magnetron sputtering.* Current applied physics, 2012. **12**(1): p. 179-183.
81. Kuang, D., et al., *Application of highly ordered TiO2 nanotube arrays in flexible dye-sensitized solar cells.* ACS nano, 2008. **2**(6): p. 1113-6.
82. Kurtz, S., et al., *Projections of primary and revision hip and knee arthroplasty in the United States from 2005 to 2030.* Journal of Bone and Joint Surgery; American volume, 2007. **89**(4): p. 780-5.
83. Kurtz, S., et al., *Future clinical and economic impact of revision total hip and knee arthroplasty.* Journal of Bone and Joint Surgery; American volume, 2007. **89 Suppl 3**: p. 144-51.
84. Geetha, M., et al., *Ti based biomaterials, the ultimate choice for orthopaedic implants - A review.* Progress in Materials Science, 2009. **54**(3): p. 397-425.
85. McGee, M.A., et al., *Implant retrieval studies of the wear and loosening of prosthetic joints: a review.* Wear, 2000. **241**(2): p. 158-165.
86. Branemark, P.I., *Osseointegration and its experimental background.* The Journal of prosthetic dentistry, 1983. **50**(3): p. 399-410.
87. Long, M. and H.J. Rack, *Titanium alloys in total joint replacement--a materials science perspective.* Biomaterials, 1998. **19**(18): p. 1621-39.
88. Hinueber, C., et al., *Biocompatibility and mechanical properties of diamond-like coatings on cobalt-chromium-molybdenum steel and titanium-aluminum-vanadium biomedical alloys.* Journal of biomedical materials research. Part A, 2010. **95**(2): p. 388-400.
89. Jakobsen, S., et al., *Acid etching does not improve CoCrMo implant osseointegration in a canine implant model.* Hip International, 2010. **20**(2): p. 171-8.
90. Wisbey, A., M. Tuke, and P.J. Gregson, *Application of PVD TiN coating to Co-Cr-Mo based surgical implants.* Biomaterials, 1987. **8**(6): p. 477-80.
91. Webster, T. and J. Ejiofor, *Increased osteoblast adhesion on nanophase metals: Ti, Ti6Al4V, and CoCrMo.* Biomaterials, 2004. **25**(19): p. 4731-9.
92. Tsaryk, R., et al., *Improving cytocompatibility of Co28Cr6Mo by TiO2 coating: gene expression study in human endothelial cells.* Journal of The Royal Society Interface, 2013. **10**(86): p. 20130428.
93. Kafizas, A. and I.P. Parkin, *The combinatorial atmospheric pressure chemical vapour deposition (cAPCVD) of a gradating N-doped mixed phase titania thin film.* Journal of materials chemistry, 2010. **20**(11): p. 2157-2169.

94. Swanepoel, R., *Determination of the thickness and optical constants of amorphous silicon.* Journal of physics. E, Scientific instruments, 1983. **16**(12): p. 1214-1222.

95. *http://www.spiusa.com/Ref001/austenitic.html*. Accessed 21/3/2014.

96. Betsch, R., *Parametric analysis of control parameters in MOCVD.* Journal of Crystal Growth, 1986. **77**(1-3): p. 210-218.

97. Oh, S., D.C. Cook, and H.E. Townsend, *Characterization of iron oxides commonly formed as corrosion products on steel.* Hyperfine interactions, 1998. **112**(1-4): p. 59-66.

98. Hyett, G., M. Green, and I.P. Parkin, *X-ray diffraction area mapping of preferred orientation and phase change in TiO2 thin films deposited by chemical vapor deposition.* Journal of the American Chemical Society, 2006. **128**(37): p. 12147-55.

99. Simoes, A.M.P., et al., *The role of Mo in the chemical composition and semiconductive behaviour of oxide films formed on stainless steels.* Corrosion science, 1999. **41**(1): p. 17-34.

100. Wu, M., et al., *Sol-Hydrothermal Synthesis and Hydrothermally Structural Evolution of Nanocrystal Titanium Dioxide.* Chemistry of materials, 2002. **14**(5): p. 1974-1980.

101. Ohsaka, T., F. Izumi, and Y. Fujiki, *RAMAN-SPECTRUM OF ANATASE, TIO2.* Journal of Raman Spectroscopy, 1978. **7**(6): p. 321-324.

102. Evans, P., et al., *The role of SiO2 barrier layers in determining the structure and photocatalytic activity of TiO2 films deposited on stainless steel.* Applied catalysis. A, General, 2007. **321**(2): p. 140-146.

103. Mills, A., et al., *Characterisation of the photocatalyst Pilkington Activ (TM): a reference film photocatalyst?* Journal of photochemistry and photobiology. A, Chemistry, 2003. **160**(3): p. 213-224.

104. Hyett, G., M. Green, and I.P. Parkin, *X-ray diffraction area mapping of preferred orientation and phase change in TiO(2) thin films deposited by chemical vapor deposition.* Journal of the American Chemical Society, 2006. **128**(37): p. 12147-12155.

105. Tompsett, G.A., et al., *The Raman spectrum of brookite, TiO2 (Pbca, Z = 8).* Journal of Raman spectroscopy, 1995. **26**(1): p. 57-62.

106. Alam, M.J. and D.C. Cameron, *Preparation and characterization of TiO2 thin films by sol-gel method.* Journal of sol-gel science and technology, 2002. **25**(2): p. 137-145.

107. Sanjines, R., et al., *ELECTRONIC-STRUCTURE OF ANATASE TIO2 OXIDE.* Journal of applied physics, 1994. **75**(6): p. 2945-2951.

108. Pittenger, M.F., et al., *Multilineage potential of adult human mesenchymal stem cells.* Science, 1999. **284**(5411): p. 143-147.

109. Davies, J.E., *Understanding peri-implant endosseous healing.* J Dent Educ, 2003. **67**(8): p. 932-49.

110. Puleo, D.A. and A. Nanci, *Understanding and controlling the bone-implant interface.* Biomaterials, 1999. **20**(23-24): p. 2311-2321.

111. Rodriguez, J.P., et al., *Cytoskeletal organization of human mesenchymal stem cells (MSC) changes during their osteogenic differentiation.* Journal of cellular biochemistry, 2004. **93**(4): p. 721-31.

112. Khan, M.R., et al., *The enhanced modulation of key bone matrix components by modified Titanium implant surfaces.* Bone, 2012. **50**(1): p. 1-8.

113. *http://rredc.nrel.gov/solar/spectra/am1.5/*. 19/1/2014]; Available from: http://rredc.nrel.gov/solar/spectra/am1.5/.

114. Hagfeldt, A., et al., *Dye-Sensitized Solar Cells.* Chemical Reviews, 2010. **110**(11): p. 6595-6663.

115. Kamat, P.V., *Quantum Dot Solar Cells. Semiconductor Nanocrystals as Light Harvesters†.* The Journal of Physical Chemistry C, 2008. **112**(48): p. 18737-18753.

116. Awazu, K., et al., *A plasmonic photocatalyst consisting of sliver nanoparticles embedded in titanium dioxide.* Journal of the American Chemical Society, 2008. **130**(5): p. 1676-1680.

117. Liu, Z.W., et al., *Plasmon Resonant Enhancement of Photocatalytic Water Splitting Under Visible Illumination.* Nano Letters, 2011. **11**(3): p. 1111-1116.

118. Liu, G., et al., *Titania-based photocatalysts-crystal growth, doping and heterostructuring.* Journal of Materials Chemistry, 2010. **20**(5): p. 831-843.

119. Acket, G.A. and J. Volger, *ON ELECTRON MOBILITY AND DONOR CENTRES IN REDUCED AND LITHIUM-DOPED RUTILE (TIO2).* Physica, 1966. **32**(10): p. 1680-&.

120. Baumard, J.F. and E. Tani, *ELECTRICAL-CONDUCTIVITY AND CHARGE COMPENSATION IN NB DOPED TIO2 RUTILE.* Journal of Chemical Physics, 1977. **67**(3): p. 857-860.

121. Anpo, M., *Preparation, Characterization, and Reactivities of Highly Functional Titanium Oxide-Based Photocatalysts Able to Operate under UV–Visible Light*

Irradiation: Approaches in Realizing High Efficiency in the Use of Visible Light. Bulletin of the Chemical Society of Japan, 2004. **77**(8): p. 1427-1442.

122. Asahi, R., et al., *Visible-light photocatalysis in nitrogen-doped titanium oxides.* Science, 2001. **293**(5528): p. 269-271.
123. Avendano, E., et al., *Photoelectrochemical and Optical Properties of Nitrogen Doped Titanium Dioxide Films Prepared by Reactive DC Magnetron Sputtering.* The journal of physical chemistry. B, 2003. **107**(24): p. 5709-5716.
124. Ihara, T., et al., *Visible-light-active titanium oxide photocatalyst realized by an oxygen-deficient structure and by nitrogen doping.* Applied catalysis. B, Environmental, 2003. **42**(4): p. 403-409.
125. Sakthivel, S. and H. Kisch, *Photocatalytic and photoelectrochemical properties of nitrogen-doped titanium dioxide.* ChemPhysChem, 2003. **4**(5): p. 487-90.
126. Yin, S., et al., *Preparation of nitrogen-doped titania with high visible light induced photocatalytic activity by mechanochemical reaction of titania and hexamethylenetetramine.* Journal of materials chemistry, 2003. **13**(12): p. 2996-3001.
127. Pore, V., et al., *Atomic layer deposition of TiO2−xNx thin films for photocatalytic applications.* Journal of photochemistry and photobiology. A, Chemistry, 2006. **177**(1): p. 68-75.
128. Di Valentin, C., G. Pacchioni, and A. Selloni, *Origin of the different photoactivity of N-doped anatase and rutile TiO2.* Physical review. B, Condensed matter and materials physics, 2004. **70**(8).
129. Di Valentin, C., et al., *Characterization of paramagnetic species in N-doped TiO2 powders by EPR spectroscopy and DFT calculations.* The journal of physical chemistry. B, 2005. **109**(23): p. 11414-9.
130. Serpone, N., *Is the band gap of pristine TiO(2) narrowed by anion- and cation-doping of titanium dioxide in second-generation photocatalysts?* The journal of physical chemistry. B, 2006. **110**(48): p. 24287-93.
131. Lee, D., et al., *Metalorganic chemical vapor deposition of TiO2:N anatase thin film on Si substrate.* Applied physics letters, 1995. **66**(7): p. 815-816.
132. Pradhan, S.K. and P.J. Reucroft, *A study of growth and morphological features of TiOxNy thin films prepared by MOCVD.* Journal of Crystal Growth, 2003. **250**(3–4): p. 588-594.
133. Yates, H.M., et al., *The role of nitrogen doping on the development of visible light-induced photocatalytic activity in thin TiO2 films grown on glass by*

chemical vapour deposition. Journal of photochemistry and photobiology. A, Chemistry, 2006. **179**(1-2): p. 213-223.

134. Kafizas, A., C. Crick, and I. Parkin, *The combinatorial atmospheric pressure chemical vapour deposition (cAPCVD) of a gradating substitutional/interstitial N-doped anatase TiO2 thin-film; UVA and visible light photocatalytic activities.* Journal of photochemistry and photobiology. A, Chemistry, 2010. **216**(2-3): p. 156-166.
135. Dunnill, C. and I.P. Parkin, *N-Doped Titania Thin Films Prepared by Atmospheric Pressure CVD usingt-Butylamine as the Nitrogen Source: Enhanced Photocatalytic Activity under Visible Light.* Chemical vapor deposition, 2009. **15**(7-9): p. 171-174.
136. Morikawa, T., et al., *Band-Gap Narrowing of Titanium Dioxide by Nitrogen Doping.* Japanese journal of applied physics, 2001. **40**(6A): p. L561-L563.
137. Peng, F., et al., *Synthesis and characterization of substitutional and interstitial nitrogen-doped titanium dioxides with visible light photocatalytic activity*. Journal of Solid State Chemistry, 2008. **181**(1): p. 130-136.
138. Saha, N. and H. Tompkins, *Titanium nitride oxidation chemistry: An x-ray photoelectron spectroscopy study.* Journal of applied physics, 1992. **72**(7): p. 3072-3079.
139. Goralski, E.G., et al., *Photochemical Activity of Nitrogen-Doped Rutile TiO2(110) in Visible Light.* The journal of physical chemistry. B, 2004. **108**(19): p. 6004-6008.
140. Emeline, A., et al., *Visible-Light-Active Titania Photocatalysts: The Case of N-Doped TiO2s—Properties and Some Fundamental Issues.* International Journal of Photoenergy, 2008. **2008**: p. 1-19.
141. Tauc, J., *Optical properties and electronic structure of amorphous Ge and Si.* Materials research bulletin, 1968. **3**(1): p. 37-46.
142. Quesada-Cabrera, R., et al., *Photocatalytic Evidence of the Rutile-to-Anatase Electron Transfer in Titania.* Advanced Materials Interfaces, 2014: p. n/a-n/a.
143. Kafizas, A., C. Crick, and I.P. Parkin, *The combinatorial atmospheric pressure chemical vapour deposition (cAPCVD) of a gradating substitutional/interstitial N-doped anatase TiO2 thin-film; UVA and visible light photocatalytic activities.* Journal of Photochemistry and Photobiology a-Chemistry, 2010. **216**(2-3): p. 156-166.

144. Gong, X.-Q. and A. Selloni, *First-principles study of the structures and energetics of stoichiometric brookite TiO2 surfaces.* Physical review. B, Condensed matter and materials physics, 2007. **76**(23).

145. Li, J.-G., T. Ishigaki, and X. Sun, *Anatase, Brookite, and Rutile Nanocrystals via Redox Reactions under Mild Hydrothermal Conditions: Phase-Selective Synthesis and Physicochemical Properties.* The journal of physical chemistry. C, 2007. **111**(13): p. 4969-4976.

146. Zhang, H. and J.F. Banfield, *Understanding Polymorphic Phase Transformation Behavior during Growth of Nanocrystalline Aggregates: Insights from TiO2.* The Journal of Physical Chemistry B, 2000. **104**(15): p. 3481-3487.

147. Huberty, J. and H. Xu, *Kinetics study on phase transformation from titania polymorph brookite to rutile.* Journal of Solid State Chemistry, 2008. **181**(3): p. 508-514.

148. Kandiel, T., et al., *Brookite versus anatase TiO2 photocatalysts: phase transformations and photocatalytic activities.* Photochemical & photobiological sciences, 2013. **12**(4): p. 602-609.

149. Deng, Q., et al., *Brookite-type TiO2nanotubes.* Chemical Communications, 2008(31): p. 3657-3659.

150. Zhao, B., et al., *Brookite TiO2 nanoflowers.* Chemical Communications, 2009(34): p. 5115-5117.

151. Jiao, Y., et al., *Insight into the crystal lattice formation of brookite in aqueous ammonia media: the electrolyte effect.* CrystEngComm, 2011. **13**(12): p. 4167-4173.

152. Nagase, T., et al., *Hydrothermal Synthesis of Brookite.* Chemistry Letters, 1999. **28**(9): p. 911-912.

153. Chaneac, C., et al., *Synthesis of brookite TiO2 nanoparticles by thermolysis of TiCl4 in strongly acidic aqueous media.* Journal of materials chemistry, 2001. **11**(4): p. 1116-1121.

154. Cheng, H., et al., *Hydrothermal Preparation of Uniform Nanosize Rutile and Anatase Particles.* Chemistry of materials, 1995. **7**(4): p. 663-671.

155. Lu, X., et al., *Tunable synthesis of enhanced photodegradation activity of brookite/anatase mixed-phase titanium dioxide.* Journal of materials research, 2013. **28**(3): p. 400-404.

156. Zheng, Y.Q., et al., *Hydrothermal preparation and characterization of brookite-type TiO2 nanocrystallites.* Journal of materials science letters, 2000. **19**(16): p. 1445-1448.

157. Kominami, H., M. Kohno, and Y. Kera, *Synthesis of brookite-type titanium oxide nano-crystals in organic media.* Journal of materials chemistry, 2000. **10**(5): p. 1151-1156.

158. Di Paola, A., et al., *Preparation of photocatalytic brookite thin films.* Thin solid films, 2007. **515**(7-8): p. 3527-3529.

159. Krysa, J., et al., *Effect of glass substrate and deposition technique on the properties of sol gel TiO2 thin films.* Journal of photochemistry and photobiology. A, Chemistry, 2011. **222**(1): p. 81-86.

160. Djaoued, Y., et al., *Sol–gel nanocrystalline brookite-rich titania films.* Materials letters, 2004. **58**(21): p. 2618-2622.

161. Blaskov, V., et al., *TiO2 pure phase brookite with preferred orientation, synthesized as a spin-coated film.* Materials letters, 2005. **59**(29-30): p. 3820-3823.

162. Yoo, D., et al., *Effects of annealing temperature and method on structural and optical properties of TiO2 films prepared by RF magnetron sputtering at room temperature.* Applied Surface Science, 2007. **253**(8): p. 3888-3892.

163. Srivatsa, K.M.K., et al., *Pure brookite titania crystals with large surface area deposited by Plasma Enhanced Chemical Vapour Deposition technique.* Thin solid films, 2008. **516**(21): p. 7443-7446.

164. Ohtani, B., et al., *Highly active semiconductor photocatalyst: Extra-fine crystallite of brookite TiO2 for redox reaction in aqueous propan-2-ol and / or silver sulfate solution.* Chemical Physics Letters, 1985. **120**(3): p. 292-294.

165. Koelsch, M., et al., *Comparison of optical and electrochemical properties of anatase and brookite TiO2 synthesized by the sol–gel method.* Thin solid films, 2002. **403**: p. 312-319.

166. Kandiel, T., et al., *Tailored Titanium Dioxide Nanomaterials: Anatase Nanoparticles and Brookite Nanorods as Highly Active Photocatalysts.* Chemistry of materials, 2010. **22**(6): p. 2050-2060.

167. Kominami, H., et al., *Solvothermal syntheses of semiconductor photocatalysts of ultra-high activities.* Catalysis today, 2003. **84**(3-4): p. 181-189.

168. Kominami, H., et al., *Nanocrystalline Brookite-Type Titanium(IV) Oxide Photocatalysts Prepared by a Solvothermal Method: Correlation Between Their Physical Properties and Photocatalytic Activities.* Catalysis letters, 2003. **91**(1-2): p. 41-47.

169. Lin, H., et al., *Synthesis of High-Quality Brookite TiO2 Single-Crystalline Nanosheets with Specific Facets Exposed: Tuning Catalysts from Inert to Highly*

Reactive. Journal of the American Chemical Society, 2012. **134**(20): p. 8328-8331.

170. Podshivalova, A.K. and I.K. Karpov, *Thermodynamic analysis of the stability of titanium oxides in the TiO-TiO2 range.* Russian journal of inorganic chemistry, 2007. **52**(7): p. 1147-1150.

171. Kafizas, A. and I.P. Parkin, *Combinatorial Atmospheric Pressure Chemical Vapor Deposition (cAPCVD): A Route to Functional Property Optimization.* Journal of the American Chemical Society, 2011. **133**(50): p. 20458-20467.

Appendix One

Experimental details for CoCrMo functional testing.

Sample preparation

CoCrMo discs (Cr 26-30, Mo 5-7) provided by Corin Group (Cirencester, UK) of 15 mm Ø, 1 mm thickness, were supplied with a machined finish. To remove this topography, individual discs were mounted on resin bases (SpeciFix-20, Struers, 40200048) and fixed in place using araldite rapid for 30 minutes. Once the discs were securely fixed, using a LaboForce-1 grinding machine (Struers) the surface of the discs were manually ground with SiC #1000 grit paper (Struers, 40400011) to remove any visible appearance of the machined topography. Following this, discs were transferred to a RotoForce-1 polishing machine (Struers) and polished for 4.5 minutes at 150rpm using MD-Dac (Struers, 40500071) with DP-Suspension P 3µm (Struers, 40600251) while lubricating the samples with DP-Lubricant Blue (Struers, 40700006). To prepare CoCrMo, CoCrMo-TiO_2 and Ti discs for cell culture experiments, discs were put in nitric acid (0.1 M, BDH, 19088 5E) for 10 minutes, washed thoroughly in $_{dd}H_2O$ and allowed to air dry before being UV irradiated for 20 minutes on each side (BONMAY, BR-506).

Cell culture

Human MSCs were obtained from the Institute for Regenerative Medicine, Texas A&M Health Science Center College of Medicine, USA. Pre-characterisation of the MSCs had been performed which included the expression of stem cell surface markers, and osteogenic, adipogenic and chondrogenic differentiation. Cells were seeded on tissue culture plastic at a density of 740 cells cm^{-2} and expanded in complete growth medium (CGM) that comprised of Minimum Essential Medium α (Gibco, 22571-020) containing 10% fetal bovine serum (PAA Laboratories, A15-151) and 1% penicillin/streptomycin (PAA Laboratories, P11-010). MSCs

were incubated at standard culture conditions of 37 °C/5%CO2 in a humidified atmosphere with media changed every 3 or 4 days. When cells reached 80% confluence they were harvested by treatment of Trypsin (0.05%)/EDTA(0.002%)(PAA Laboratories, L11-004). Only cells of low passage (<5) were used to ensure integrity of the results. When osteogenic media (OM) was implemented, it consisted of Dulbecco's Modified Eagle's Medium (DMEM) low glucose pyruvate (Gibco, 31885-023), containing 10% fetal bovine serum, 1% penicillin/streptomycin and further supplemented with β-glycerol phosphate (Sigma-Aldrich, G9891), L-ascorbic acid (Sigma-Aldrich, A8960-5G) and dexamethasone.

Cell morphology

To analyse cell morphology, f-actin and the nuclei of MSCs were fluorescently labelled to undergo confocal laser microscopy. MSCs were seeded at $12.5x10^3$ cells per well in OM (n=3) with media changes every 3-4 days. After 1 and 7 days in culture MSCs were fixed using 4% paraformaldehyde (PFA) for 15 minutes then treated with 0.15% Triton X-100 (BDH, 30632 4N) in PBS for 4 minutes to permeabilise the cellular membrane. Actin was labelled using Alexa fluor 488 phalloidin in PBS (Molecular probes, A12379, 2.5:100) for 20 minutes at room temperature, then counterstained to label the nuclei using propidium iodide for 10 minutes (Molecular probes, P3566) (4 µg/ml). Cells were washed three times in PBS and suspended in 3 ml of PBS in for viewing. MSCs were analysed at X40, using a Radiance 2100 Laser Scanning System.

Osteogenic fluorescent markers

To obtain a measure of the level of osteogenic differentiation occurring in MSCs on the three surfaces, type 1 collagen (COL) and hydroxyapatite (HA) expression were examined using fluorescent microscopy techniques. MSCs were seeded at 12.5×10^3 cells per well in OM (n = 3) with media changes every 3-4 days. COL

was analysed after 7 and 14 days, with HA being studied after 7, 14 and 21 days. Succeeding culture, cells were fixed as previously described and blocked using 10% goat serum in PBS for 30 minutes to prevent any unspecific binding. Primary antibody incubation was performed overnight at 4 °C with anti-type-1 collagen antibody (Sigma, C2456, 1:1000). Alexa fluor 488 goat anti-mouse (Molecular probes, A11001, 2.5:100) was used as a secondary antibody to label COL with all primary and secondary antibodies diluted in 1.5% skim milk in PBS. Lastly, cultures were counterstained with 4′,6-Diamidino-2-phenylindole dihydrochloride (DAPI) for 40 minutes (Sigma-aldrich, D9542, 10 µg/ml). HA staining was performed using the OsteoImage kit (Lonza, PA-1503) as per the manufacturer's instructions. Images were taken using a fluorescent microscope fitted with the appropriate filters (Leica DMIRB) and then quantifiable analysis was performed via a pixel based method using ImageJ software.

Calcium ion content

MSCs were seeded at a density of 12.5 x 10^3 cells per well in osteogenic media and examined at 7, 14 and 21 days. Prior to performing assays, the amount of cells were assessed using AlamarBlue (AbD Serotec); oxidised dye was added to each well containing media and cells were incubated for 3 hours at standard culture conditions before having two aliquots of supernatant removed from each well for analysis. The fluorescent intensity of the dye was measured (Excitation λ = 530 nm, emission λ = 590 nm, Floroskan Fluorometer) and cell numbers calculated via interpolation through use of a seven point standard curve, ranging to a maximum of 16 x 10^4 cells per well. Calcium content was measured using the QuantiChrom assay (Bio Assay systems, DICA-500) as per the manufacturer's instructions. The cell monolayer was homogenised by incubation with 1M hydrochloric acid (HCL) for 60 minutes at room temperature on a rocking plate. Aliquots were then taken from each sample and transferred to a clear 96 well plate and combined with assay reagent. Calcium levels were then measured (λ = 620 nm, Tecan M200) and concentrations calculated with use of known concentration standards.

Appendix Two

Publications Resulting From This Work

Cross A.J., et al., *Production of Predominantly Anatase Thin Films on Various Grades of Steel and Other Metallic Substrates From $TiCl_4$ and Ethyl Acetate by Atmospheric Pressure CVD*. Chemical Vapour Deposition, 2012. **18** (4-6): p. 133-139.

Logan N., et al., *TiO_2 coated CoCrMo; Improving the osteogenic differentiation and adhesion of mesenchymal stem cells in vitro.* Journal of Biomedical Materials Part A, 2014. (Published online July 2014)

Cross A.J. et al., A Review of Synthetic Routes to Brookite TiO_2. In preparation.

Cross A.J. et al., Production of Brookite TiO_2 by APCVD. In preparation.

Cross A.J. et al., Flexible Titania Thin Films on Aluminium Foil With Photocatalytic Ability. In preparation.